POROUS CERAMIC AND METALLIC MICROREACTORS

Tuning interfaces for multiphase processes

The research presented in this thesis was financially supported by Stichting voor de Technische Wetenschappen (STW, Project 07569).

Promotion committee

Prof. Dr.ir. R.G.H. Lammertink (promotor)	University of Twente
Prof. Dr.-Ing. M. Wessling (co-promotor)	University of Twente
Prof. Dr.ir. L. Lefferts	University of Twente
Prof. Dr. G. Mul	University of Twente
Prof. Dr. J.G.E. Gardeniers	University of Twente
Prof. Dr.ir. M.T. Kreutzer	Delft University of Technology
Prof. Dr. V. Hessel	Eindhoven University of Technology
Prof. Dr. S.R.A. Kersten (chairman)	University of Twente

Cover design:

Silhouette of Istanbul, representing a multiphase process.

Photograph by *Taner Dortunc*, Design by *Cenk Aytekin* (http://www.cenkaytekin.com/)

Porous Ceramic and Metallic Microreactors: Tuning interfaces for multiphase processes

ISBN: 978-90-365-3268-6

DOI: 10.3990/1.9789036532686

URL: http://dx.doi.org/10.3990/1.9789036532686

Printed by Gildeprint, Enschede, The Netherlands

POROUS CERAMIC AND METALLIC MICROREACTORS

Tuning interfaces for multiphase processes

DISSERTATION

to obtain
the degree of doctor at the University of Twente,
on the authority of the rector magnificus,
Prof. Dr. H. Brinksma,
on account of the decision of the graduation committee,
to be publicly defended on
Friday the 4^{th} of November, 2011 at 16:45

by

Halil Can Aran

born on February 21^{st}, 1982
in Istanbul, Turkey

This thesis has been approved by:

Prof. Dr. ir. R.G.H. Lammertink (promotor)

Prof. Dr.-Ing. M. Wessling (co-promotor)

dedicated to my parents *Ahmet* and *Necla Aran*

for all the support, love and encouragement...

Contents

Chapter 1

General Introduction

The aim of this research is to explore new concepts for multiphase gas-liquid-solid reactions within microreactors, using membrane technology. This chapter provides a general view about microreactors and already existing concepts for multiphase reactions in these devices. Furthermore, an overview of conventional membrane reactors is presented, followed by some background information on model reactions, which were performed in this study. Lastly, the scope and outline of this thesis are given.

1.1 Microreactors

Microreactors are devices with reduced characteristic dimensions for performing chemical reactions. Their dimensions are much lower than conventional reactors in process engineering, classically in the sub-millimeter range [1–3]. Typical examples of microreactors are shown in Figure 1.1.

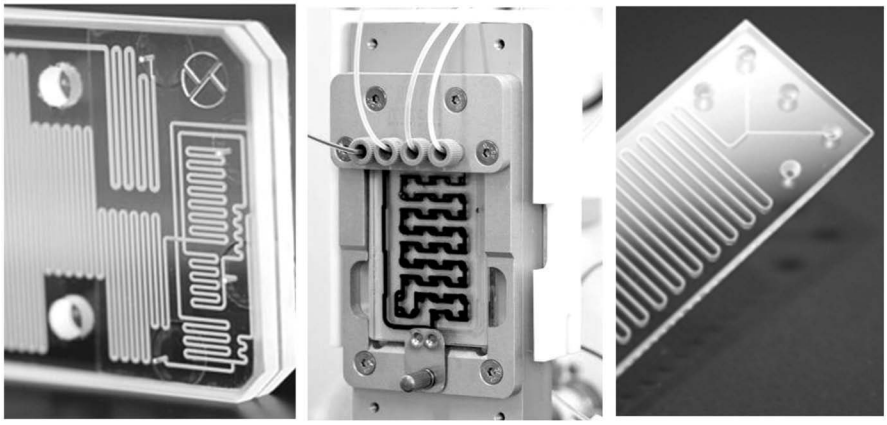

Figure 1.1: Examples of microreactors: *(left)* FRX (Syrris), *(center)* FlowSyn (Future Chemistry), *(right)* Micronit Microfluidics.

Microreactors occupy less space and enable much more controlled processes than conventional macro-scale reactors. Due to their small characteristic length, the flow inside microreactors is typically laminar, which makes the hydrodynamic characteristics well defined and controllable. Using these devices, high quality and accurate experimental information can be gathered very quickly within a small volume. Reactant costs and waste streams are reduced and safe operation can be performed thanks to the small volume of these reactors [3,4].

The microchannels in these reactors have a large surface to volume ratio (typically 10000 - 50000 m^2/m^3), which is much higher than in conventional chemical reactors (100 - 1000 m^2/m^3) [1,3]. This ratio leads to excellent heat and mass transfer properties (Figure 1.2), which make them very suitable for exploring and performing fast and exothermic reactions [5]. These properties enable high productivity

rates, energy efficiency, sustainability and operational safety for a given process in microreactors[2–4,6].

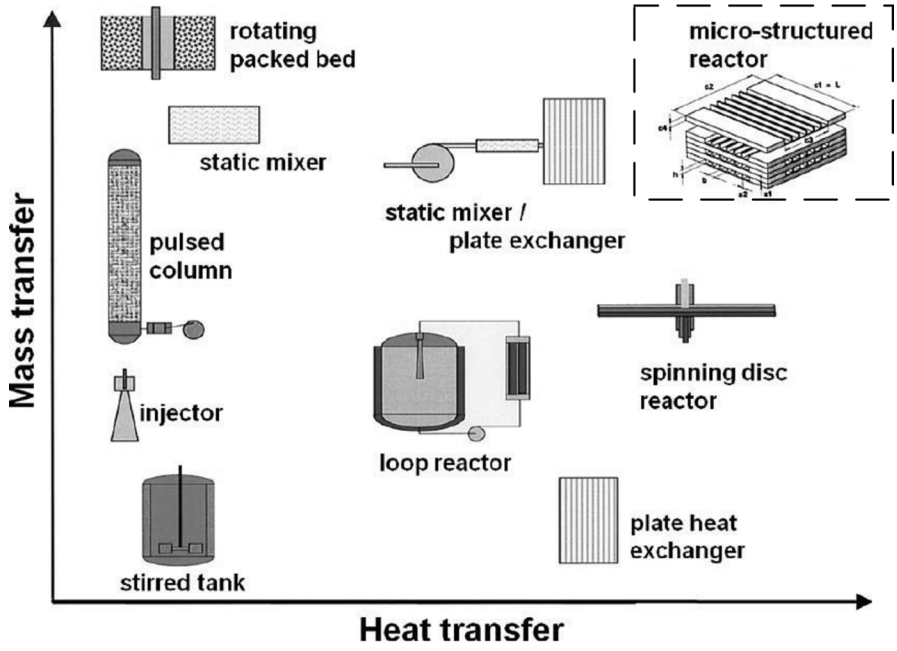

Figure 1.2: Benchmarking of microreactors with conventional reactors (adapted from[5]).

The small volumes and improved heat transfer characteristics of microreactors allow the safe operation of chemical reactions, which would otherwise be risky to carry out in conventional macro-scale reactors. Reactions such as direct fluorinations, with a high exothermic nature, explosion risks and hazardous/toxic chemicals can be performed in microreactors. Hence, the use of microreaction technology opens new opportunities for novel chemical routes, which are of high importance for the chemical process industry[2,3].

Besides laboratory scale, microreactors can also be applied for small- or large-scale production in process engineering. The strategy to increase the production capacity of microreactors is typically the "numbering-up" of microchannels[3,4]. Schenk et al.[7] classified numbering-up in two main types (Figure 1.3): external and internal

numbering-up. External numbering-up is carried out by simply connecting the desired amount of microreactor modules in a parallel fashion. The internal numbering-up is referred as the parallel connection of microchannels within only one microreactor device.

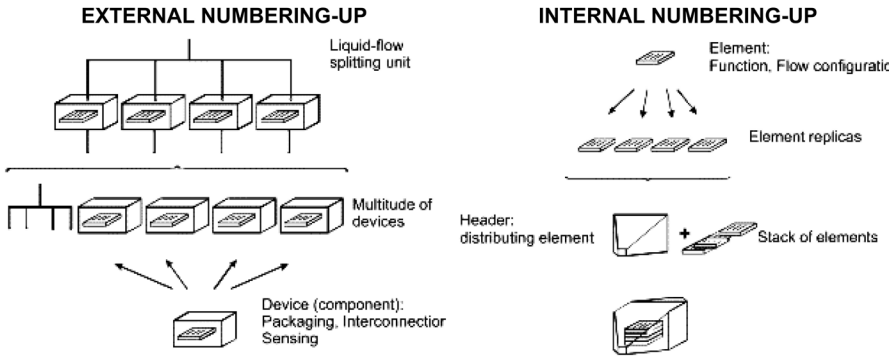

Figure 1.3: Schematic representation of external and internal numbering-up for microreactors (adapted from[7,10]).

By numbering-up, production volumes can be increased while keeping the process in each microchannel unaffected. In this way, redesign and pilot-scale production steps for conventional scale-up in chemical engineering can be by-passed. With internal numbering-up a higher degree of parallelism can be achieved within a smaller volume. This type of scaling-out is more suitable for standard reactions and safe processes and it requires lower equipment costs than the external numbering-up. External numbering-up is advantageous for complex and hazardous processes. In externally numbered-up systems, in case of malfunction or an accident within one microreactor module, the other modules can still continue the production and the consequences are less devastating than in a conventional chemical production process. A further advantage is that the production capacity can easily be adjusted according to demand. This would be a great advantage for small-scale, local production sites[4,7].

To sum up, all the above-mentioned properties make microreactors attractive tools for many applications in chemical technology, such as laboratory-scale research, industrial

process development and intensification, and on-site production of chemicals in small-scale[2,4].

The aim of the research in this thesis is to explore multiphase processes, such as gas-liquid-solid reactions, within microreactors. Following, a brief overview of existing microreactor concepts for these processes is given.

1.2 Gas-liquid-solid microreactors

Multiphase gas-liquid (G-L) and gas-liquid-solid (G-L-S) reactions are of great interest to the industry; therefore, intensive research is being carried out on these reactions including microreactors[5,8,9]. In G-L-S processes, besides the gas and liquid (G-L) reactants, an additional solid catalyst (S) is required, which catalyzes the reaction between both reactants.

Hessel et al.[9,10] classified multiphase microreactors into two main types: *Dispersed* and *Continuous Phase* microreactors. In the dispersed phase reactors, one phase is dispersed into the other one, so that both gas and liquid flow in the same microchannel. In the continuous phase reactors, both phases are separately fed to and withdrawn from the reactor without being dispersed into each other.

1.2.1 Dispersed phase microreactors

In these devices, gas and liquid are merged inside the same microchannel. Both streams are fed into the reactor using a dual- or multiple-feed arrangement, in order to obtain a G-L dispersion in the microchannel. The gas to liquid (G/L) flow ratio and the inlet conditions of both phases are very critical because they determine the flow pattern in the microchannel. At low G/L flow ratios, bubbly flow (very small bubbles) is observed. At intermediate low G/L flow ratios slug flow (segmented-Taylor flow) and at very large ratios annular flow is predominant[11] (Figure 1.4).

The concept of these systems is relatively simple. Slug flow (Figure 1.4 *left*-(c,d), Figure 1.4 *right*) can improve liquid mixing properties inside the microchannel thanks to the toroidal vortices, which is a great advantage especially in the case of fast

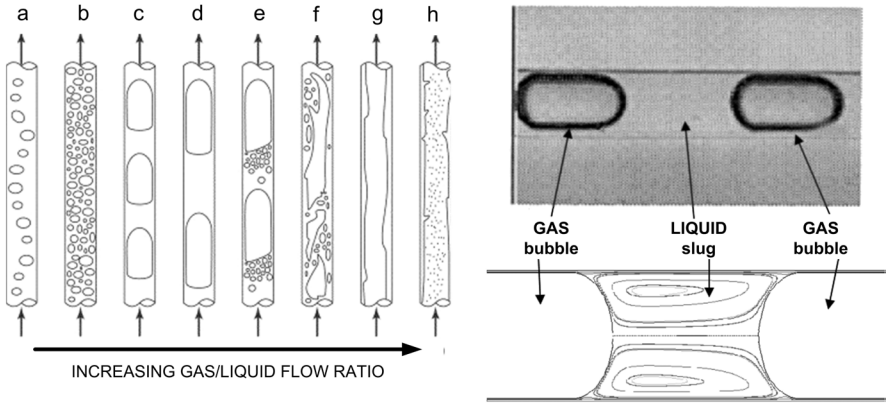

Figure 1.4: *(left)* Schematic representation of flow patterns in dispersed phase microreactors (adapted from [11]), *(right)* slug flow and streamlines within the liquid slug (adapted from [9]).

chemical reactions [9,11]. Dispersed phase microreactors are applied in various areas of chemical reaction engineering, such as direct fluorination [12], hydrogenation [11] and photocatalytic reactions [13–15].

Next to its simplicity and improved mass transfer properties, this principle also has some drawbacks. Gas and liquid separation is needed at the reactor outlet, since both streams are inter-mixed. The slugs might coalesce and this situation creates uncertainty about the actual flow patterns and interfaces in these devices [9,10]. Another disadvantage is that the presence of a gas phase in the microchannel decreases the residence time of the liquid reactant in the reactor.

1.2.2 Continuous phase microreactors

In these microreactors, liquid and gas streams flow separately in their own ports, do not intermix, but are in contact through the whole reactor length. Some advantages of these types of reactors are that no phase separation is needed at the outlet of the reactor, the gas-liquid interface is well-defined and internal numbering-up is relatively easy. A general drawback is that some additional technical precautions in reactor design need to be taken to avoid the inter-mixing of the gas and liquid

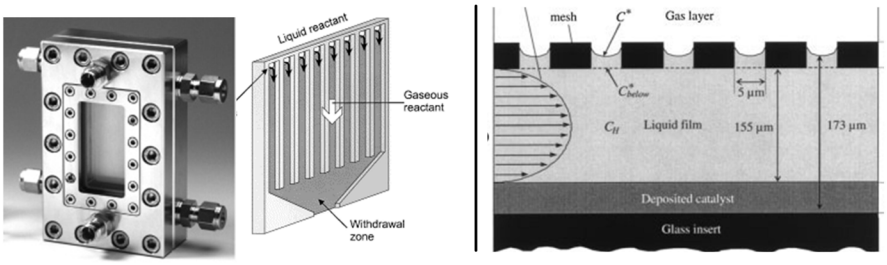

Figure 1.5: *(left)* Falling film microreactor (adapted from [9]), *(right)* Mesh microreactor (adapted from [19]) for gas-liquid-solid reactions.

streams. Common examples of continuous phase microreactors include the falling film microreactors, mesh microreactors and overlapping channel microreactors [9,11]. Continuous phase reactors can be further categorized according to the stabilization of the G–L interface. In some reactor designs the G–L interface is stabilized by a physical structure (i.e. meshes, membranes), while in others the gas and liquid coflow without any interface stabilizing structure.

Continuous phase microreactors without stabilizing structures:

Among these, falling film microreactors are the most commonly used reactors. In falling film microreactors, a thin falling liquid film (few tens of micrometers) flows by gravitational force along a surface and is exposed to the co-flowing gas throughout the whole reactor length [16]. These reactors are commercially available (IMM Mainz) and were already applied for various reactions (hydrogenations, fluorinations, chlorinations, photochemical reactions) [17,18]. They are well suited for G-L reactions. For G-L-S reactions, these reactors may suffer from mass transfer limitations, as the gas has to diffuse through the liquid film to reach an immobilized solid catalyst on the microstructured surface.

In overlapping channel microreactors, gas and liquid phases flow in separate microchannels (each open on one side) and these channels overlap at defined areas in the reactor module, where the contacting occurs. These reactors have small G-L interfacial areas and limited interface stability [9,10].

Continuous phase microreactors with stabilizing structures:

In these reactors, typically, a physical structure with defined openings (pores) is placed between the gas and liquid phases in order to stabilize the G-L interface. The position of the G-L interface is defined by the wetting properties of the liquid phase on the physical structure. The G-L interface will be in the liquid side, if the pressure difference over the stabilizing structure is lower than the Laplace pressure (Δp):

$$\Delta p = -\frac{2 \cdot \gamma_{\mathrm{L}} \cdot \cos(\theta)}{r_{\max}} \tag{1.1}$$

where γ_{L} is the surface tension of the liquid, θ contact angle of the liquid on the material of the stabilizing structure and $r_{\max}$ the maximum pore radius of this structure. When θ is below 90°, the liquid will wet the stabilizing structure and no stable interface can be formed under flow conditions. In this case, an additional gas pressure needs to be applied to stabilize the G-L interface. When θ is above 90°, no additional gas pressure is required, but in that case, the pore size of the stabilizing structure becomes crucial. Structures with large openings will face wetting even at low-pressure values in the liquid side.

Mesh microreactors are a common example of continuous microreactors with a stabilizing interface. In these reactors, the gas and the liquid ports are separated with a planar mesh structure. Both phases are in contact through the openings (diameter≈5 μm) of the mesh (e.g. nickel)[1,19,20]. For G-L-S reactions, the solid catalyst can be immobilized either on the outer side of the liquid port (Figure 1.5) or directly on the mesh material itself. In the first case, mass transfer limitations might occur, because the gaseous reactant would have to travel through the liquid film to reach the solid catalyst.

In these reactors, the meniscus stability at the G-L interface is an important aspect. Typically, the interface is stabilized by pressure difference between both phases, which makes the operation technically demanding. The interface can also be stabilized by hydrophobizing the mesh contactor (for aqueous processes), which can prevent the leakage of the liquid reactant to the gas port[21]. However, no high pressures can be

applied in the liquid stream due the relatively large pore diameter of the mesh (low Laplace pressure).

De Jong et al. investigated G-L contacting in microfluidic devices using polymeric membranes. In their work, porous hydrophobic membranes were used as a stabilizing interface between the gas and liquid phases[22–24]. They demonstrated the applicability of membranes for the local control of liquid composition within a microchannel, by using various gaseous reactants on the opposite sides of the membrane (Figure 1.6)[24]. In addition, they performed catalytic oxidation of glucose as a model reaction, though very low activity and rapid deactivation was observed. The polymeric membrane itself was used as catalyst support, which is not well suited for heterogeneously catalyzed reactions[22].

The dual channel microreactor is a new continuous microreactor concept for G-L-S chemistry that has recently been published by Park et al.[25]. In these microreactors, the gas and the liquid are flowing in their own microchannels and they are contacted

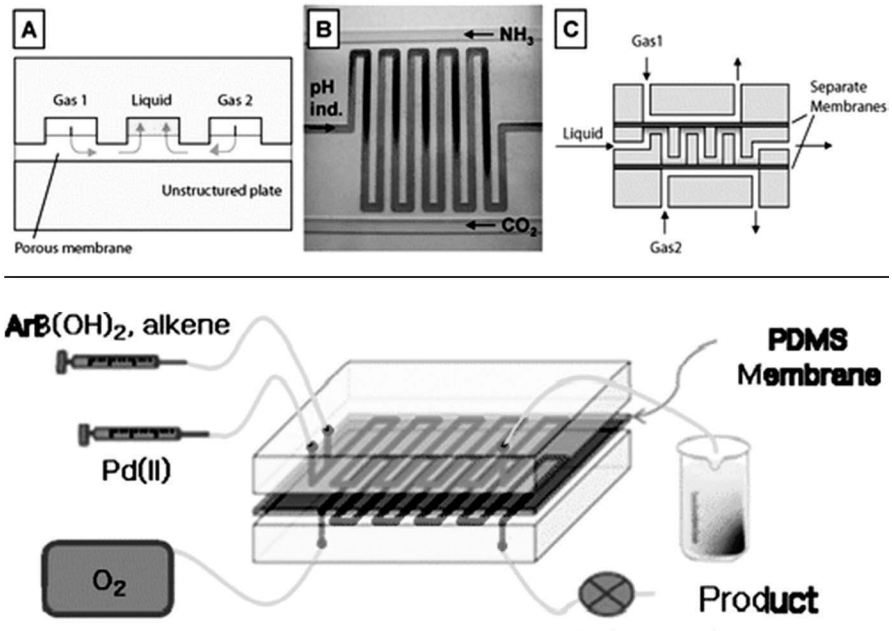

Figure 1.6: (*top*) generation of local concentration gradients by gas-liquid contacting (adapted from[24]), (*bottom*) Dual channel microreactor (adapted from[25]).

with a gas permeable PDMS membrane (Figure 1.6). Continuous contacting between both phases can be carried out with a stable membrane interface. However, the membrane does not act as a support for the catalyst. In this concept, the metal catalyst is suspended inside the liquid phase and needs to be separated from the liquid product at the reactor outlet. Separation of catalyst particles adds complications to the process, especially in a continuous operation mode.

De Jong[22] and Park et al.[25] demonstrated that membranes have a great potential in microsystems, by providing stable interfaces in multiphase reactions. Even though there are only very few examples of membrane assisted G-L-S contacting in microreactor technology, in the past decades intensive research was carried out on conventional membrane reactors (with higher characteristic dimensions). Membrane reactors for G-L-S reactions are described in the following section.

1.3 Membrane reactors

Multiphase reactions for gas-liquid (G-L) and heterogeneously catalyzed gas-liquid-solid (G-L-S) systems are conventionally performed in various types of reactors. The most widespread types include agitated tanks, slurry reactors, bubble or spray columns, and trickle-bed reactors. Membrane reactors have also been intensively investigated due to their various advantages.

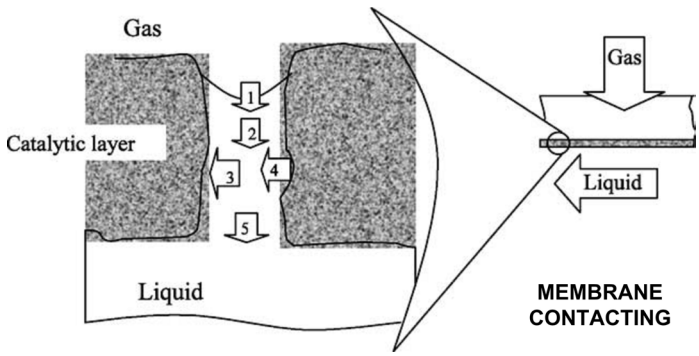

Figure 1.7: Gas-liquid-solid contacting concept in membrane reactors (adapted from[26]).

Membrane reactors offer a stable and controlled G-L interface with a simple reactor design (Figure 1.7). The gas and liquid phases are added to the reaction zone from opposite sides of a membrane and meet precisely where the solid (S) catalyst is located. In these reactors, the gas/liquid flow ratios can be independently varied[26–32]. Moreover, the gaseous reactant is distributed homogeneously over to the catalytic area, along the full reactor length. This makes these reactors advantageous for processes with low gaseous reactant solubility and/or high gas consumption, preventing a possible depletion of this reactant in the reactor. Using membrane reactors, high-pressure operation can be avoided because of the improved three-phase contacting[32,33].

For this concept, porous membranes are preferred over dense membranes because of their high gas permeability. The porosity of the membrane offers easy access of the gaseous reactant to the catalytic layer. Typical membrane materials are polymeric or inorganic membranes. Polymeric membranes are cheap and are available in various geometries and properties. However, at high temperatures and under chemically harsh conditions their use is limited. Moreover, the bonding of a metal catalyst particle to the polymeric surface is weak and the regeneration of the polymer embedded catalyst is not an easy task. Inorganic materials, such as ceramics, are very favorable to G-L-S reactions because of their high chemical, thermal and structural stability. Conventional catalyst immobilization techniques (e.g. wet impregnation, incipient wetness) with high temperature post-processing can be applied on these materials. In addition, the regeneration of the catalyst can easily be conducted by calcination and reduction steps[33].

For porous inorganic membrane reactors the G-L interface is typically stabilized by a pressure difference (trans-membrane pressure), because of the hydrophilic nature of the membrane materials. An excess pressure (see Equation 1.1) is applied from the gas side of the reactor and the G-L interface can be positioned on the porous membrane at the desired location. The stabilization of the interface was intensively investigated by Vospernik et al.[27] and Bercic et al.[34] and they demonstrated that the mass transfer of the gaseous reactant is strongly dependent on the position of the G-L

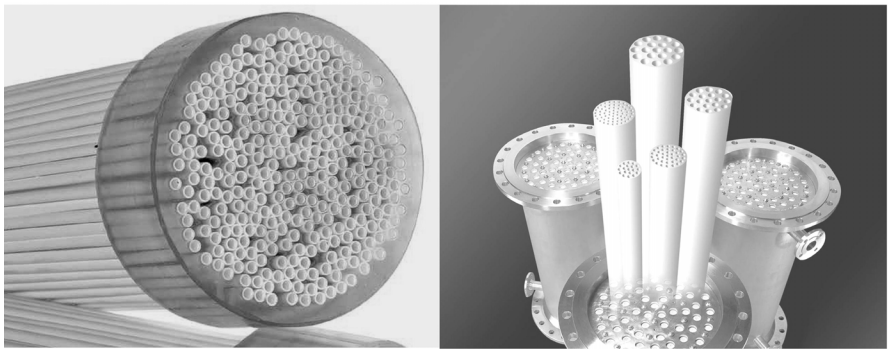

Figure 1.8: Examples of numbering-up in membrane technology: *(left)* Hyflux Inocep, *(right)* GEA membrane modules.

interface in the membrane. Even though accurate interface control can be obtained by trans-membrane pressure, this method can be considered technically demanding due to the necessity of additional equipment (e.g. pressure regulators, sensors).

Catalytic membrane reactors were already applied for various chemical reactions such as hydrogenation[27,29] and oxidation[28,34] reactions. Large-scale operation with membrane reactors can be conducted very easily, especially in tubular geometry (Figure 1.8). Membrane modules with high packing density are already available on the market; this provides a simple way of channel numbering-up of a developed reactor.

An important aspect of these reactors is the mass transport in the liquid phase due to the laminar flow profile. In membrane reactors, the mass transport of the reactant in the liquid phase from the liquid bulk to the catalytic surface on the wall is mainly carried out by radial diffusion, which is a relatively slow process. In order to improve the mass transfer, Vospernik et al.[28] and Pashkova et al.[35] used static mixers and glass beads, respectively, inside the membrane channel and observed significant improvement in the reactor performance. Despite the improved reactor performance, both methods add operational complications to the process.

A practical way to overcome mass transfer limitations in a process with a wall reaction is miniaturizing the characteristic length of the reactor channel, as described above for microreactors. The small characteristic length increases the surface area (catalytic

wall) per reactor volume and reduces the diffusion path for the reactant to the reactor wall. The aim of the present study is to apply the above-mentioned advantages of membrane reactors for G-L-S reactions in microreactors and merge the advantages of both reactor designs. In order to test the performances of our microreactors, two model reactions were performed. These reactions are described below.

1.4 Model gas-liquid-solid reactions

1.4.1 Catalytic hydrogenation of nitrite ions in water

Increasing concentrations of the harmful nitrite (NO_2^-) and nitrate (NO_3^-) ions in ground waters throughout the world is a critical environmental problem. Therefore, various processes are being developed to tackle this problem, such as biological processes, physicochemical techniques and catalytic hydrogenation. Biological processes are reported to have low conversion rates and to be slow. Physicochemical techniques (ion exchange, reverse osmosis, electrodialysis) remove these compounds efficiently, but they require regeneration; since they accumulate these compounds in secondary streams at high concentrations. The catalytic hydrogenation process is mentioned as the most promising solution for nitrite removal[36–38].

$$2NO_2^- + 3H_2 \xrightarrow{Pd} N_2 + 2OH^- + 2H_2O \tag{1.2}$$

$$2NO_2^- + 6H_2 \xrightarrow{Pd} 2NH_4^+ + 4OH^- \tag{1.3}$$

In this reaction, NO_2^- ions in aqueous solution (L-reactant) react with hydrogen (H_2; G-reactant) on the solid catalyst (e.g. palladium (Pd); S-catalyst) surface and form the desired product nitrogen (N_2) and the undesired product ammonia (NH_4^+). Hydrogenation of nitrite is known to be a very fast reaction inducing mass transfer limitations, which makes it very suitable to study as a model reaction in microreactors[39].

1.4.2 Photocatalytic degradation of organic compounds in water

A photochemical reaction is a chemical reaction that takes place in the presence of light. A photocatalytic reaction is a photochemical reaction, which takes place only in the presence of a photocatalyst. Photocatalysis is applied in numerous disciplines, such as water and air treatment, organic synthesis, hydrogen (H_2) production from water and reduction of carbon dioxide (CO_2)[40,41].

In a photocatalytic reaction, a photon reaches the surface of the photocatalyst leading to molecular excitation (Figure 1.9). To realize this excitation, the photon needs to be at the appropriate wavelength and to have energy equal to or higher than the band gap energy (E_{bg}) of the photocatalyst. With the molecular excitation, electrons (e^-) and holes (h^+) are formed and they promote the formation of hydroxyl radicals (OH), superoxide radicals ($O_2{}^-$) and hydrogen peroxide (H_2O_2)[42].

Electrons and holes can also recombine competitively, which would lead to process inefficiencies[42]. The presence of oxygen (O_2) is known to be very crucial for photocatalytic degradation processes. It is an electron acceptor in the photocatalytic degradation and prevents the recombination of electron (e^-) and hole (h^+) pairs. Additional oxygen supply was reported to enhance efficiency of photocatalytic degradation processes (e.g, methylene blue, phenol degradation)[13,43,44].

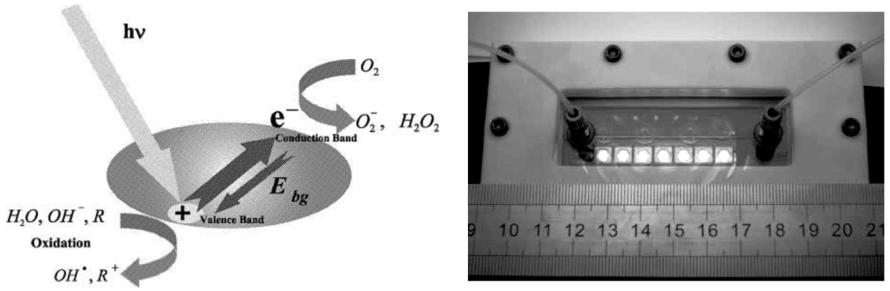

Figure 1.9: *(left)* Schematic representation of a photocatalytic reaction (adapted from[42]), *(right)* microreactor chip for photocatalytic reactions (adapted from[43]).

1.5 Scope of the thesis

The aim of this study is to introduce a membrane reactor concept for G-L-S microreaction technology. In this concept, the contact between gas and liquid for reaction purposes is achieved using membrane technology and selective wetting of porous ceramic and metallic membranes.

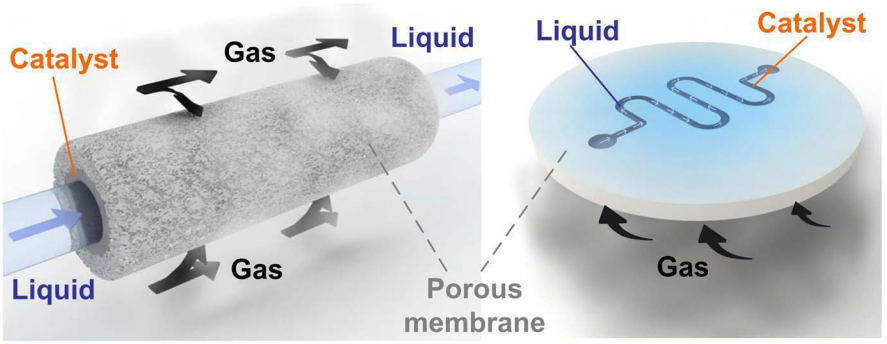

Figure 1.10: Contacting concept of the porous meso- and microreactors for G-L-S reaction systems in *(left)* tubular and *(right)* planar geometry.

The contact of gas and liquid occurs precisely on the membrane surface, where the solid catalyst is deposited. For ceramic membrane reactors, the G-L interface is positioned by controlling the wetting properties of the porous reactor wall, as opposed to trans-membrane pressure in conventional membrane reactors. For metallic membrane reactors, a gas-permeable polymeric layer was integrated on the outer surface to confine the liquid phase.

Fabrication, catalyst deposition, selective surface modification steps and module preparation were carried out for reactor development. We developed reactors with tubular (hollow fiber) and planar (chip) geometry and tested them for two model reactions in water: catalytic hydrogenation of nitrite ions and photocatalytic degradation of organic compounds. Tubular reactors were applied for the catalytic hydrogenation in Chapters 2, 3 and 4 and the planar reactor the photocatalytic reaction in Chapter 5.

Chapter 2 introduces the contacting concept of gas and liquid phases in a membrane using surface modification techniques. Preparation, characterization and operation of the reactors are described. In this study, we investigated the influences of the surface properties and catalyst (palladium) loading on the reactor performance. Furthermore, we studied the effects of the gas phase composition on the overall productivity of the reactor. It was observed that reactor performance could be significantly improved by controlling its surface properties. In addition, even at dilute concentrations of the gaseous reactant, the reaction rates remained constant, which is of great advantage for multiphase reactions.

Chapter 3 focuses on improving the understanding of the concept developed in Chapter 2. Tubular reactors with various thicknesses of catalyst supports and internal hydraulic diameters were prepared and characterized. The influences of these geometrical parameters on the reactor performance were tested. Results indicated increasing internal mass transfer limitations with increasing thickness of the catalyst support. We also observed that the reactor productivity of the hollow fibers with smaller internal diameter was considerably improved, indicating external mass transfer limitations in these reactors. Furthermore, to enhance the mixing in the membrane channel, slug flow operation (see Figure 1.4) was studied using an inert gas. With the induced mixing of the inert slug flow, the nitrite conversion values increased significantly.

Chapter 4 demonstrates the development and application of porous metallic membrane reactors with carbon nanofibers catalyst supports. We prepared these reactors by porous stainless steel hollow fiber fabrication, carbon nanofiber growth and catalyst immobilization steps. Reactors with high mechanical strength and catalytic surface area were obtained. With the operation of these reactors, we observed high conversion values for nitrite reduction, even without the presence of hydrogen or palladium. These results suggest reductive properties of the reactor material itself and prove their promising potential for chemical reduction processes.

Chapter 5 describes the preparation of porous ceramic microreactors in planar (chip) geometry and their utilization in photocatalytic processes. Microfabrication, photo-

catalyst (titanium dioxide-TiO_2) immobilization and selective surface modification steps for the reactor preparation are explained. The developed reactors showed high photocatalytic activity in the photocatalytic degradation of phenol and methylene blue in water. Furthermore, membrane-assisted supply of oxygen improved the reactor performance.

Chapter 6 summarizes the results obtained in the scope of this work. It gives recommendations for future research, together with concluding remarks.

Bibliography

[1] L. Kiwi-Minsker and A. Renken. Microstructured reactors for catalytic reactions. *Catalysis Today*, 110(1-2):2 – 14, 2005. 2, 8

[2] A. Gavriilidis, P. Angeli, E. Cao, K. K. Yeong, and Y. S. S. Wan. Technology and applications of microengineered reactors. *Chemical Engineering Research and Design*, 80(1):3 – 30, 2002. 3, 5

[3] K. Jahnisch, V. Hessel, H. Lowe, and M. Baerns. Chemistry in microstructured reactors. *Angewandte Chemie International Edition*, 43(4):406–446, 2004. 2, 3

[4] V. Hessel, S. Hardt, and H. Lowe. *Chemical Micro Process Engineering: Fundamentals, Modelling and Reactions, Sections 1.1-1.5*, pages 1–66. Wiley-VCH Verlag GmbH & Co. KGaA, 2005. 2, 3, 4, 5

[5] M. N. Kashid and L. Kiwi-Minsker. Microstructured reactors for multiphase reactions: State of the art. *Industrial & Engineering Chemistry Research*, 48(14):6465–6485, 2009. 2, 3, 5

[6] V. Hessel, S. Hardt, and H. Lowe. *Chemical Micro Process Engineering: Fundamentals, Modelling and Reactions, Sections 1.6-1.9*, pages 66–124. Wiley-VCH Verlag GmbH & Co. KGaA, 2005. 3

[7] R. Schenk, V. Hessel, C. Hofmann, J. Kiss, H. Lowe, and A. Ziogas. Numbering-up of micro devices: a first liquid-flow splitting unit. *Chemical Engineering Journal*, 101(1-3):421 – 429, 2004. 3, 4

[8] G. Chen, J. Yue, and Q. Yuan. Gas-liquid microreaction technology: Recent developments and future challenges. *Chinese Journal of Chemical Engineering*, 16(5):663 – 669, 2008. 5

[9] V. Hessel, P. Angeli, A. Gavriilidis, and H. Lowe. Gas-liquid and gas-liquid-solid microstructured reactors: Contacting principles and applications. *Industrial & Engineering Chemistry Research*, 44(25):9750–9769, 2005. 5, 6, 7

[10] V. Hessel, S. Hardt, and H. Lowe. *Chemical Micro Process Engineering: Fundamentals, Modelling and Reactions, Sections 5.1-5.3*, pages 577–619. Wiley-VCH Verlag GmbH & Co. KGaA, 2005. 4, 5, 6, 7

[11] M. T. Kreutzer, F. Kapteijn, J. A. Moulijn, and J. J. Heiszwolf. Multiphase monolith reactors: Chemical reaction engineering of segmented flow in microchannels. *Chemical Engineering Science*, 60(22):5895 – 5916, 2005. 5, 6, 7

[12] K. Jahnisch, M. Baerns, V. Hessel, W. Ehrfeld, V. Haverkamp, H. Lowe, Ch. Wille, and A. Guber. Direct fluorination of toluene using elemental fluorine in gas/liquid microreactors. *Journal of Fluorine Chemistry*, 105(1):117 – 128, 2000. 6

[13] H. Lindstrom, R. Wootton, and A. Iles. High surface area titania photocatalytic microfluidic reactors. *AIChE Journal*, 53(3):695–702, 2007. 6, 14

[14] Y. Matsushita, M. Iwasawa, T. Suzuki, and T. Ichimura. Multiphase photocatalytic oxidation in a microreactor. *Chemistry Letters*, 38(8):846–847, 2009.

[15] R. Gorges, S. Meyer, and G. Kreisel. Photocatalysis in microreactors. *Journal of Photochemistry and Photobiology A: Chemistry*, 167(2-3):95–99, 2004. 6

[16] B. K. Vankayala, P. Lob, V. Hessel, G. Menges, C. Hofmann, D. Metzke, U. Krtschil, and H. J. Kost. Scale-up of process intensifying falling film microreactors to pilot production scale. *International Journal of Chemical Reactor Engineering*, 5:A91, 2007. 7

[17] P. Lob, H. Lowe, and V. Hessel. Fluorinations, chlorinations and brominations of organic compounds in micro reactors. *Journal of Fluorine Chemistry*, 125(11):1677–1694, 2004. 7

[18] K. K. Yeong, A. Gavriilidis, R. Zapf, and V. Hessel. Experimental studies of nitrobenzene hydrogenation in a microstructured falling film reactor. *Chemical Engineering Science*, 59(16):3491 – 3494, 2004. 7

[19] R. Abdallah, P. Magnico, B. Fumey, and C. de Bellefon. Cfd and kinetic methods for mass transfer determination in a mesh microreactor. *AIChE Journal*, 52(6):2230–2237, 2006. 7, 8

[20] C. Amador, D. Wenn, J. Shaw, A. Gavriilidis, and P. Angeli. Design of a mesh microreactor for even flow distribution and narrow residence time distribution. *Chemical Engineering Journal*, 135(Supplement 1):S259 – S269, 2008. 8

[21] T. R. Henriksen. *Silicon Microreactors for Measurements of Catalytic Activity*. PhD thesis, Lyngby, Technical University of Denmark, April 2010. 8

[22] J. de Jong. *Application of membrane technology in microfluidic devices*. PhD thesis, Enschede, University of Twente, April 2008. 9, 10

[23] J. de Jong, B. Ankone, R. G. H. Lammertink, and M. Wessling. New replication technique for the fabrication of thin polymeric microfluidic devices with tunable porosity. *Lab on a Chip*, 5:1240–1247, 2005.

[24] J. de Jong, P. W. Verheijden, R. G. H. Lammertink, and M. Wessling. Generation of local concentration gradients by gas-liquid contacting. *Analytical Chemistry*, 80(9):3190–3197, 2008. 9

[25] C. P. Park and D.-P. Kim. Dual-channel microreactor for gas-liquid syntheses. *Journal of the American Chemical Society*, 132(29):10102–10106, 2010. 9, 10

[26] A. Bottino, G. Capannelli, A. Comite, A. Del Borghi, and R. Di Felice. Catalytic ceramic membrane in a three-phase reactor for the competitive hydrogenation-isomerisation of methylenecyclohexane. *Separation and Purification Technology*, 34(1-3):239 – 246, 2004. 10, 11

[27] M. Vospernik, A. Pintar, G. Bercic, and J. Levec. Experimental verification of ceramic membrane potentials for supporting three-phase catalytic reactions. *Journal of Membrane Science*, 223(1-2):157 – 169, 2003. 11, 12

[28] M. Vospernik, A. Pintar, G. Bercic, J. Batista, and J. Levec. Potentials of ceramic membranes as catalytic three-phase reactors. *Chemical Engineering Research and Design*, 82(5):659 – 666, 2004. 12

[29] J. Peureux, M. Torres, H. Mozzanega, A. Giroir-Fendler, and J-A. Dalmon. Nitrobenzene liquid-phase hydrogenation in a membrane reactor. *Catalysis Today*, 25(3-4):409 – 415, 1995. 12

[30] R. Dittmeyer, V. Hollein, and K. Daub. Membrane reactors for hydrogenation and dehydrogenation processes based on supported palladium. *Journal of Molecular Catalysis A: Chemical*, 173(1-2):135 – 184, 2001.

[31] R. Dittmeyer, K. Svajda, and M. Reif. A review of catalytic membrane layers for gas/liquid reactions. *Topics in Catalysis*, 29:3–27, 2004.

[32] H. C. Aran, J. K. Chinthaginjala, R. Groote, T. Roelofs, L. Lefferts, M. Wessling, and R. G. H. Lammertink. Porous ceramic mesoreactors: A new approach for gas-liquid contacting in multiphase microreaction technology. *Chemical Engineering Journal*, 169(1-3):239 – 246, 2011. 11

[33] G. Centi, R. Dittmeyer, S. Perathoner, and M. Reif. Tubular inorganic catalytic membrane reactors: advantages and performance in multiphase hydrogenation reactions. *Catalysis Today*, 79-80:139 – 149, 2003. Catalysis in Multiphase Reactors. 11

[34] G. Bercic, A. Pintar, and J. Levec. Positioning of the reaction zone for gas-liquid reactions in catalytic membrane reactor by coupling results of mass transport and chemical reaction study. *Catalysis Today*, 105(3-4):589 – 597, 2005. 11, 12

[35] A. Pashkova, R. Dittmeyer, N. Kaltenborn, and H. Richter. Experimental study of porous tubular catalytic membranes for direct synthesis of hydrogen peroxide. *Chemical Engineering Journal*, 165(3):924 – 933, 2010. 12

[36] J. K. Chinthaginjala, J. H. Bitter, and L. Lefferts. Thin layer of carbon-nano-fibers (cnfs) as catalyst support for fast mass transfer in hydrogenation of nitrite. *Applied Catalysis A: General*, 383(1-2):24 – 32, 2010. 13

[37] J.K. Chinthaginjala and L. Lefferts. Support effect on selectivity of nitrite reduction in water. *Applied Catalysis B: Environmental*, 101(1-2):144 – 149, 2010.

[38] A. Pintar, G. Bercic, and J. Levec. Catalytic liquid-phase nitrite reduction: Kinetics and catalyst deactivation. *AIChE Journal*, 44(10):2280–2292, 1998. 13

[39] J. K. Chinthaginjala. *Hairy foam : thin layers of carbon nanofibers as catalyst support for liquid phase reactions*. PhD thesis, Enschede, University of Twente, June 2010. 13

[40] O. Carp, C. L. Huisman, and A. Reller. Photoinduced reactivity of titanium dioxide. *Progress in Solid State Chemistry*, 32(1-2):33 – 177, 2004. 14

[41] T. van Gerven, G. Mul, J. Moulijn, and A. Stankiewicz. A review of intensification of photocatalytic processes. *Chemical Engineering and Processing*, 46(9):781–789, 2007. 14

[42] Serrano B. de Lasa, H. and M. Salaices. *Photocatalytic reaction engineering*. Springer, 2005. 14

[43] Y. Matsushita, N. Ohba, S. Kumada, K. Sakeda, T. Suzuki, and T. Ichimura. Photocatalytic reactions in microreactors. *Chemical Engineering Journal*, 135(Supplement 1):S303–S308, 2008. 14

[44] C.-H. Wu and J.-M. Chern. Kinetics of photocatalytic decomposition of methylene blue. *Industrial & Engineering Chemistry Research*, 45(19):6450–6457, 2006. 14

Chapter 2

Porous Ceramic Mesoreactors: A new approach for gas-liquid contacting in multiphase microreactor technology

A REVISED VERSION OF THIS CHAPTER HAS BEEN PUBLISHED:

H.C. Aran, J.K. Chinthaginjala, R. Groote, T. Roelofs, L. Lefferts, M. Wessling, R.G.H. Lammertink, Porous ceramic membrane mesoreactors: A new approach for gas-liquid contacting in multiphase microreaction technology, *Chemical Engineering Journal*, 169(1-3)239–246, 2011 *(featured on the journal cover)*.

ABSTRACT

In this study a concept for gas-liquid-solid (G-L-S) microreactor technology was developed and optimized which ensures that the gaseous and liquid reactants directly meet at the solid catalyst surface with a simple contacting approach. Fabrication, catalyst deposition and surface modification steps were carried out to develop porous ceramic (alumina-Al_2O_3) mesoreactors. In order to realize liquid flow inside the intrinsically hydrophilic porous reactor channel and to obtain a stabilized gas-liquid-solid interface different surface modification (hydrophobization) strategies were successfully implemented. Catalytically active reactors with varying surface properties along the cross-section were obtained and their performance was tested for nitrite hydrogenation as a G-L-S model reaction. Results showed that the performance of the reactor could be drastically enhanced by tuning the surface properties. With the proposed concept, even at dilute concentrations of the gaseous reactant, the reactor performance remained constant.

2.1 Introduction

The development of miniaturized devices (in micro– and mesoscale) for carrying out chemical analysis and chemical reactions has shown a rapid improvement in the past years. A micro– or mesoreactor is a chemical reactor with a reduced dimensional scale (hydraulic diameter), which results in a very large surface to volume ratio. This large ratio provides enhanced heat and mass transfer enabling the development of more efficient processes (process intensification). Micro– and mesofluidic devices allow new chemical processes that were previously not applied in conventional systems. In addition, they are sustainable by creating less waste, occupying less space, and enabling safer operation due to their small volume[1–5].

Multiphase reactions for gas–liquid (G–L) and heterogeneously catalyzed gas-liquid-solid (G–L–S) systems are conventionally performed in various types of reactors. The most widespread types include agitated tanks, slurry reactors, bubble or spray columns, and trickle-bed reactors[6]. Also membrane reactors have been intensively investigated due to their various advantages including well-defined contact regions and simple reactor design. In these types of reactors, the G–L interface is generally stabilized by the use of a pressure difference across the membrane (trans–membrane pressure)[7–14].

With the rapid developments in microreaction technology, some analogues of the macro-scale reactors became available for G–L and G–L–S reaction systems in the microscale[3,4,6,15,16]. Multiphase microreactors for these systems were classified by Hessel et al.[6] in two main types: Continuous and Dispersed Phase microreactors. In the continuous phase reactors, both phases are separately fed to and withdrawn from the reactor without being dispersed into each other (e.g. the falling film microreactor). In the dispersed phase reactors, one phase is dispersed into the other one. Various flow patterns (e.g. Taylor flow and annular flow) are obtained in these microchannels. In these microreactors the G/L flow ratios have to be well controlled to create a stable interface between both phases[6]. In most of the existing continuous and dispersed

phase reactor designs, the gaseous reactant usually has to diffuse through a liquid film to reach the solid catalyst that can be immobilized on the microchannel wall.
The aim of the present work is to introduce a membrane reactor concept for G–L–S microreaction technology. The contact between gas and liquid for reaction purposes is achieved using membrane technology and selective wetting of porous ceramic membranes (Figure 2.1).

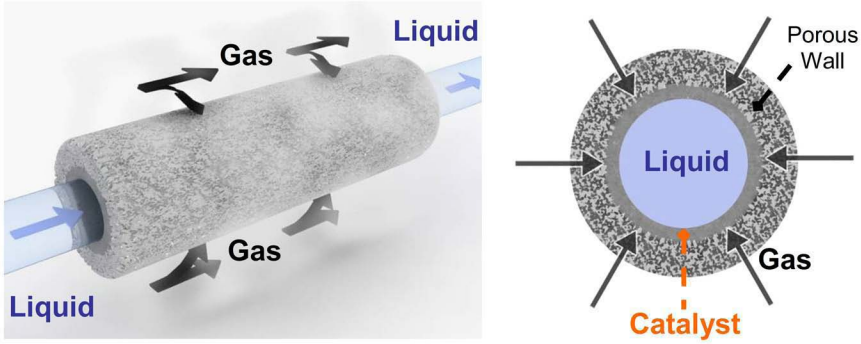

Figure 2.1: Contacting concept of the porous ceramic mesoreactor for G-L-S reaction systems.

The contacting between both phases takes place directly at the inner membrane surface, where the catalyst is immobilized. Using this continuous process concept, the gas phase composition can be kept constant along the full length of the reactor. Furthermore, no separation of gas and liquid reactants is necessary at the reactor outlet. The G–L interface and the positioning of the reaction area are controlled using surface modification (hydrophobization) techniques, as opposed to controlling trans–membrane pressure.
The heterogeneously palladium(Pd)–catalyzed hydrogenation of nitrite ions in aqueous phase was chosen as G–L–S model reaction system for this study. The removal of nitrite (NO_2^-) and nitrate (NO_3^-) ions from groundwater is a relevant reaction from an environmental point of view. It can be carried out via biologic and catalytic hydrogenation processes. Due to the low reaction rates of the biologic processes, the catalytic hydrogenation process is mentioned to be more promising for the nitrite

removal. Via the catalytic route the nitrite ions are converted to nitrogen (N_2) or the undesired product ammonia (NH_4^+)[17–21].

2.2 Experimental

2.2.1 Materials

Commercial α–Al_2O_3 hollow fibers InoCep M800 (Hyflux CEPAration Technologies (Europe)) with average pore diameter of 800 nm were used as membrane support in this study. The membrane fibers had an inner diameter of 2.8 mm, an outer diameter of 3.8 mm and they were prepared with a length of 13.5 cm. γ–Al_2O_3 (Alfa Aesar, 3 micron APS Powder), MilliQ-water, polyvinyl alcohol (PVA; Sigma-Aldrich, 99+% hydrolyzed) and acetic acid (Merck, pro analysi) were used for catalyst support preparation. Palladium(II) 2,4–pentanedione ($Pd(acac)_2$; Alfa Aesar, 34.7%) in toluene (Merck, ACS) was used as catalyst precursor solution. For the surface modification steps a perfluorinated octyltrichlorosilane (FOTS; Aldrich, 97%) and n–hexane as solvent (Merck, ACS) were used as received. An aqueous solution of Phenol Red sodium salt (Merck, ACS) was used as wetting indicator solution. Sodium nitrite ($NaNO_2$, Merck, ACS) was used as source for nitrite ions (NO_2^-).

2.2.2 Reactor preparation

The preparation of the porous ceramic mesoreactor consists of 3 main stages which are summarized in Figure 2.2.

The inner surface of the commercial α–Al_2O_3 membrane (BET surface area: $\sim$0.1 m^2/g) was coated with a γ–Al_2O_3 layer as catalyst support to increase the active surface area. For the coating procedure a standard recipe for the aqueous 20 wt% γ–Al_2O_3 suspension was used[22]. With the help of a syringe pump the suspension was fed into the fibers; the excess suspension was removed by flowing air (1 ml/min) through the fiber for 2 min. The coated samples were then dried in the oven at 50°C for 1h and then calcined at 600°C for 2 h.

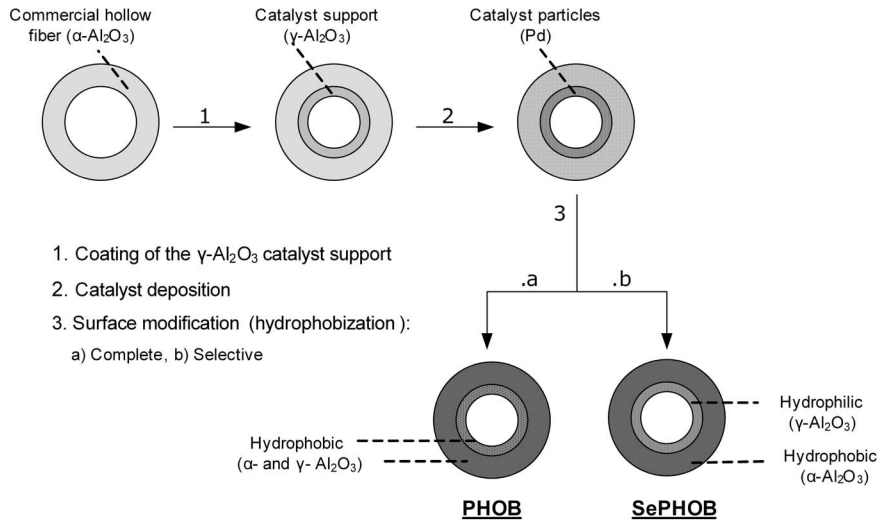

Figure 2.2: Summary of the porous ceramic mesoreactor preparation steps: drawings represent the cross–sections of the membranes after each step.

For the catalyst (Pd) deposition the samples were immersed into a precursor solution prepared of 300 mg of $Pd(acac)_2$ in 50 ml toluene for 24 h. The samples were removed from the solution and dried at 50°C in air overnight. Finally the samples were calcined for 1h at 250°C in oxygen (O_2), followed by a 1 h reduction treatment with hydrogen (H_2) at the same temperature. For a second group of samples, the above mentioned treatments (immersion, drying, calcination and reduction) were repeated 3 times on the same sample to increase the palladium (Pd) content in the reactor walls.

Al_2O_3 hollow fiber membranes were hydrophobized by coating their surface with a fluorinated alkyl trichlorosilane (FOTS). The surface modification process of Al_2O_3 is illustrated in Figure 2.3[23].

Two different routes were performed for the surface modification: *Complete* or *selective hydrophobization*.

Complete Hydrophobization (Liquid Phase):

Adapted from Geerken et al.[24] the samples were immersed in a solution containing a few drops of FOTS in 40 ml n–hexane. They were kept in the solution for 1 h, taken out and placed in an oven at 100°C for 1 h in order to realize the surface

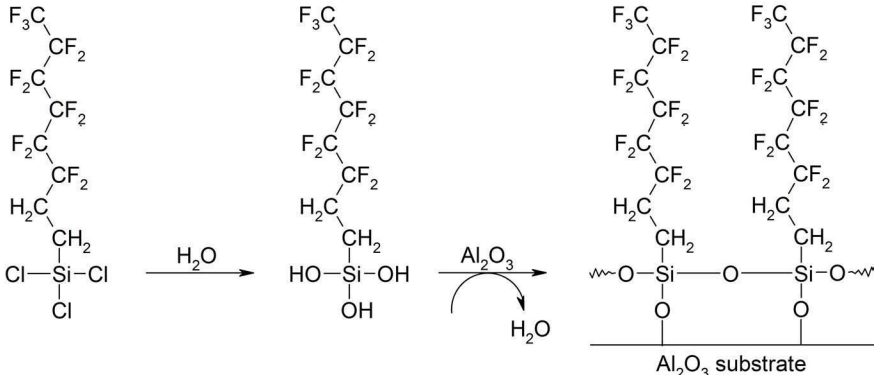

Figure 2.3: Schematic representation for the surface modification of Al_2O_3 using FOTS, adapted from Geerken et al.[23]

reaction between FOTS and Al_2O_3. After this reaction step the samples were rinsed with isopropanol to remove the excess FOTS on the membrane surface. The samples which were prepared using this method were labeled as *PHOB*.

Selective Hydrophobization (Gas Phase):

To prevent FOTS from reaching the γ–Al_2O_3 catalyst support on the inner part of the hollow fiber membrane, its ends were sealed (Figure 2.4). The principle of FOTS gas phase deposition was adapted from previous work[25,26] and modified to the requirements in this study. The sealed membranes were placed in a desiccator and vacuum was applied to $6{\cdot}10^{-2}$ mbar. After closing the vacuum pump FOTS was purged into the chamber for a short time (in the order of minutes). Then the FOTS compartment was closed and water vapor was introduced into the chamber for 10 s. The reaction of the FOTS with the surface took place at room temperature. These samples were labeled as *SePHOB* after this selective surface modification step.

2.2.3 Reactor characterization

The coating thickness and morphology were investigated by using Scanning Electron Microscopy (SEM; JEOL TSM 5600). The samples were sputtered with a thin gold layer (Baltzers Union SCD 40) before imaging. To determine the active surface area of the γ–Al_2O_3 layer, BET surface area was measured using the N_2–adsorption isotherm

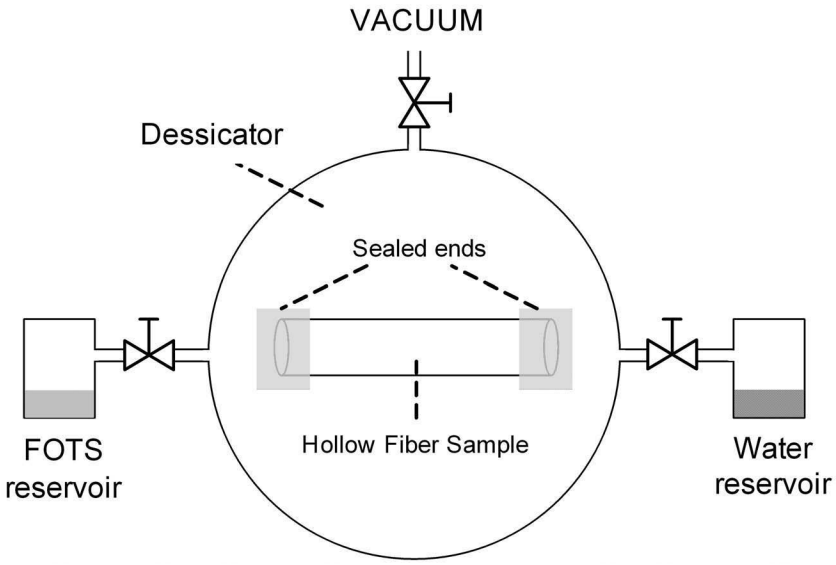

Figure 2.4: Illustration of the selective hydrophobization setup and method.

obtained at 77 K (Micromeritics Tristar). The weight of the sample before and after the coating of the γ–Al_2O_3 layer was measured with an analytical balance.

The average Pd content on the samples with and without γ–Al_2O_3 catalyst supports was determined using X–ray fluorescence spectroscopy (XRF). The qualitative distribution of Pd at the cross-sections of the γ–Al_2O_3 layer was obtained by Scanning Electron Microscopy (LEO 1550 FEG–SEM) with energy dispersive X–ray analysis (EDX; Thermo Noran Vantage system). The dispersion and active particle size of Pd was determined by CO–Chemisorption (Micromeritics, ChemiSorb 2750: Pulse Chemisorption system) at room temperature.

Contact angle measurements (OCA 15 Dataphysics) were carried out for each hydrophobization procedure. Due to the curved surface of the hollow fibers these measurements were performed on flat polished dense alumina wafers. Laplace pressures (for *PHOB* and *SePHOB* samples) at which the liquid (H_2O) wets the hydrophobic membrane from the tube to the shell side were measured. One end of the surface modified hollow fiber samples was sealed and water was pressurized from

inside until water droplets appeared on the outer surface. This pressure difference at which the wetting occurred (Δp) can be correlated to the Laplace equation:

$$\Delta p = -\frac{2 \cdot \gamma_{\mathrm{L}} \cdot \cos(\theta)}{r_{\max}} \tag{2.1}$$

where γ_{L} is the surface tension of the liquid, θ contact angle of the liquid on the membrane material and $r_{\max}$ the maximum pore radius of the membrane.
An aqueous Phenol Red sodium salt solution (∼300 mg/L) was prepared and pumped through the surface modified reactors (*PHOB* and *SePHOB*) for a minimum time of 15 min, in order to visualize the wetting behavior throughout the sample. Then the samples were cut and the cross-sections were examined by optical microscopy (Zeiss Axiovert 40).

2.2.4 Reactor operation

The performance of the reactor was tested for heterogeneously catalyzed hydrogenation of nitrite ions ($NO_2{}^-$) over palladium (Pd) catalyst in aqueous phase.

$$2NO_2^- + 3H_2 \overset{\mathrm{Pd}}{\rightarrow} N_2 + 2OH^- + 2H_2O \tag{2.2}$$

$$2NO_2^- + 6H_2 \overset{\mathrm{Pd}}{\rightarrow} 2NH_4^+ + 4OH^- \tag{2.3}$$

The conversion and the reaction rate of the nitrite ions ($NO_2{}^-$) were the main performance criteria. The production of the undesired product ammonia ($NH_4{}^+$) was also measured and used to calculate selectivity of the reaction. Selectivity to nitrogen (N_2) follows directly based on the well known fact that no other products are formed. The porous ceramic mesoreactors were placed into a stainless steel module with separate in- and outlets for liquid and gas (Figure 2.5). The module was placed in a vertical position (liquid inlet at the bottom) inside an oven at 298 K. The liquid reactant ($NO_2{}^-$) was pumped into the tube and the gaseous reactant (hydrogen: H_2, atmospheric pressure) was delivered to the shell side of the porous reactor.

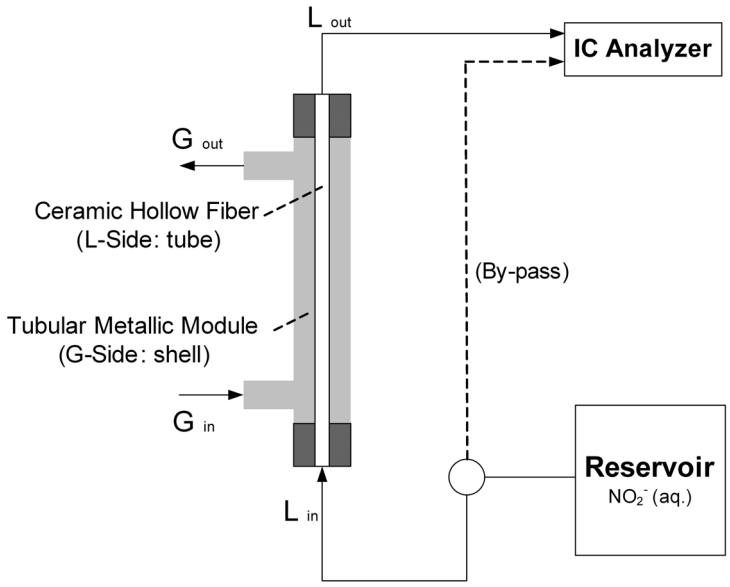

Figure 2.5: Schematic representation of the experimental setup.

Solutions of sodium nitrite with two different initial NO_2^- concentrations of ∼11 and ∼110 mg/l were prepared. The liquid reactants flow rates were chosen as 0.1 and 0.3 ml/min. The back pressure of the liquid before the entrance of the reactor was measured. The liquid outlet was connected to an ion chromatograph (IC; Dionex ICS 1000) and the NO_2^- and NH_4^+ concentrations were measured. The volumetric concentration of H_2 in the gas phase was varied between 1 and 100% using a mixture of H_2 and Argon (Ar) at different concentrations. The gas flow rate at the shell side was kept constant as 100 ml/min. The experimental parameters are summarized in Table 2.1.

In addition to the above mentioned 3-Phase (G-L-S: H_2(g)-NO_2^-(aq)-Pd(s)) experiments, a 2-Phase (L-S: H_2(aq) and NO_2^-(aq)-Pd(s)) operation mode was tested where the liquid was presaturated with H_2 (in a mixture with Ar) in a reservoir and fed to the reactor. During the 2-Phase operation mode pure Ar gas was flown at the shell side of the reactor.

Table 2.1: Experimental parameters: Reactor types and operation conditions.

Reactor types	PHOB - SePHOB
Catalyst (Pd) deposition on reactor, *times*	1 & 3
Reaction temperature, *K*	298
Reactor volume, *ml*	0.83
Initial nitrite concentration, *mg/l*	11 & 110
Liquid flow rates, *ml/min*	0.1 & 0.3
Liquid flow back pressures, *bar*	0.3 & 0.6
Gas flow rate, *ml/min*	100
Volumetric H_2 concentration in gas phase, *%*	1 - 100

2.3 Results and Discussion

2.3.1 Reactor characterization

The structures of the γ-Al_2O_3 coated ceramic hollow fiber used in this study are displayed in the SEM images in Figure 2.6. The micrographs show that there is a clear difference in the morphology between the α- and γ-Al_2O_3 layers. The BET active surface area of the γ-Al_2O_3 support was found to be around 73 m^2/g, which is significantly higher compared to the commercial α-Al_2O_3 support ($\sim$0.1 m^2/g). The weight increase of the sample due to the coated support was $\sim$5.6 wt%. Thickness of the support was on average 80 μm.

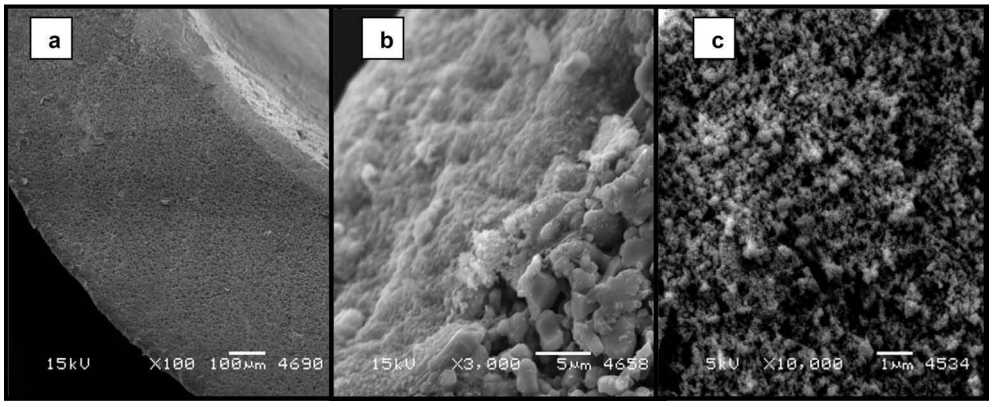

Figure 2.6: SEM images of the ceramic membrane cross-section after γ-Al_2O_3 catalyst support coating: *(a)*, *(b)* α-Al_2O_3 / γ-Al_2O_3 intersection *(c)* Porous structure of the γ-Al_2O_3.

Catalyst deposition was performed on samples with- and without γ-Al_2O_3 support coating. The overall weight percentage of Pd (measured by XRF) for the sample consisting of only α-Al_2O_3 was found to be $\sim$0.026 wt% and for the sample with additional γ-Al_2O_3 coating this value has increased to $\sim$0.073 wt%. This indicates that the amount of deposited catalyst could be significantly increased with the γ-Al_2O_3 coating due to the high surface area of this layer. For the samples with 3 times catalyst deposition the corresponding values increased to $\sim$0.12 and $\sim$0.26 wt%. It was observed that the Pd is mainly located in the γ-Al_2O_3 layer. The EDX results qualitatively showed a homogeneous distribution of Pd along the cross-section of the γ-Al_2O_3 coating. Both samples (containing additional γ-Al_2O_3 coating) with 1 and 3 times catalyst deposition were used in this work as reactors in order to study the effect of catalyst loading on the reactor performance. These samples were referred as Pd loading= 0.073 wt% (1 time deposition) and Pd loading= 0.26 wt% (3 time deposition).

The Pd dispersion of a sample (measured by CO-Chemisorption) with α- and γ-Al_2O_3 was $\sim$7.9% (average particle size$\approx$14 nm) after a single exposure for Pd deposition, and $\sim$6.5% (average particle size$\approx$17 nm) after 3 times repetitive Pd deposition. However, it must be noted that these XRF and CO-Chemisorption results were obtained for the entire sample (α- and γ-Al_2O_3) and not specifically for the γ-Al_2O_3 layer which is relevant for catalytic activity.

Contact angles were measured on dense flat Al_2O_3 samples after the hydrophobization step (for both liquid and gas phase hydrophobization methods). For both samples, the contact angles were around 115°, which confirms that both methods were successful in hydrophobizing Al_2O_3.

The wetting behavior of the porous ceramic fibers modified by the complete (*PHOB*) and selective (*SePHOB*) hydrophobization methods were investigated using an aqueous Phenol Red solution as wetting indicator. Samples without any surface modification were completely wetted by the indicator solution within a few seconds. For the *PHOB* (completely hydrophobized) sample no considerable coloring in the cross sections along the length of the fiber was observed indicating that the entire

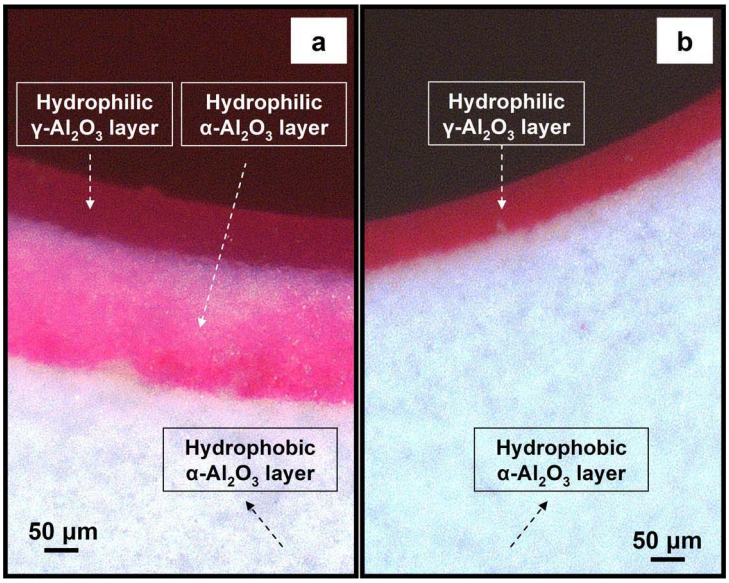

Figure 2.7: Visualization of the wetting behavior for the selectively hydrophobized (SePHOB) hollow fibers. Optical microscope cross-section images for tracking the liquid flow, indicating where the liquid reaches. *(a)* partially wetted α-Al_2O_3 layer, *(b)* Completely hydrophobic α-Al_2O_3 and hydrophilic γ-Al_2O_3 layers.

sample was hydrophobized. For the *SePHOB* (selectively hydrophobized) samples wetting was observed only in the γ-Al_2O_3 layer. This method apparently allows hydrophobizing only the α-Al_2O_3 selectively while γ-Al_2O_3 layer remains hydrophilic. Apparently, by sealing the ends of the fiber the direct transport of FOTS to the inner membrane surface and therefore hydrophobization of the γ-Al_2O_3 layer could be prevented.

To determine the parameters for the selective hydrophobization (*SePHOB*) procedure, the FOTS exposure time was varied and different degrees of wetting were observed (Figure 2.7). In samples with shorter exposure times wetting was seen also in the α-Al_2O_3 layer (Figure 2.7.a) which indicates that some regions also in this layer remained hydrophilic. But for longer FOTS exposure times it was observed that the α-Al_2O_3 layer became completely hydrophobic (Figure 2.7.b). Also the wetting behavior was identical along the length of the fiber. Further increase of the exposure time on the

order of minutes resulted in the same wetting behavior as in Figure 2.7.b; the γ-Al_2O_3 layer remained still hydrophilic. These results indicate that gas phase modification of the γ-Al_2O_3 layer is a slower process compared to modifying the α-Al_2O_3 layer. Most likely, this results from the adsorption of FOTS at the γ-Al_2O_3 layer, combined with the smaller pore sizes and high surface area of the γ-Al_2O_3 layer (Figure 2.6). Probably, the diffusion of FOTS is slower due to the smaller pores and larger amount of FOTS is needed to cover the high surface area in this layer.

Laplace pressures of the *PHOB* and *SePHOB* samples were measured. These pressures were 1.7 bar for the *PHOB* samples and 1.1 bar for the *SePHOB* samples. For the *PHOB* sample the liquid has to wet the hydrophobic γ-Al_2O_3 layer first, whereas for the *SePHOB* sample the hydrophilic γ-Al_2O_3 layer is already wetted, explaining the higher Laplace pressure for the *PHOB* sample. The measured Laplace pressure for the *SePHOB* sample is comparable to the value predicted from the Laplace equation for the α-Al_2O_3, $\sim$1.5 bar for a maximum pore radius of 800 nm. However, a higher wetting pressure than 1.7 bar should be expected for the *PHOB* sample due to the significantly smaller pore sizes in the γ-Al_2O_3 layer (Figure 2.6). This low value indicates the presence of defects in the γ-Al_2O_3 layer, such as macrovoids (large pores), cracks or incomplete hydrophobization.

It must be noted that both of the measured Laplace pressures are higher than the back pressures (Table 2.1) for each flow rate, which ensures a stable gas-liquid interface without the liquid reactant leaking to the gas side.

2.3.2 Reactor performance

The catalytic performance of the obtained reactors was investigated using heterogeneously Pd catalyzed hydrogenation of nitrite in aqueous phase as a model reaction. The main performance criteria were the nitrite conversion and the reaction rates which were determined by measuring the initial and final concentrations of the nitrite ions before and after the reactor.

In order to determine the influence of the surface properties on the reactor performance two reactors (Pd loading= 0.073 wt%) with different surface properties

were tested:

- *PHOB* (hydrophobic α- and γ-Al_2O_3 layers),
- *SePHOB* (hydrophobic α-Al_2O_3 and hydrophilic γ-Al_2O_3 layers).

Table 2.2 shows the overall conversions of nitrite ions, selectivities to ammonia and reaction rates as a function of the liquid flow rate for both reactors. It can be seen that the performance increased drastically by using the *SePHOB* reactor. These results clearly show the improvement achieved by altering wall wetting conditions. This significant increase in the nitrite conversions can be explained by the increased contact interface between the liquid reactant and the Pd catalyst. While in the *PHOB* reactor the liquid reactant was in contact with a hydrophobic γ-Al_2O_3 catalyst support preventing efficient contact between the nitrite solution and the active Pd, in the *SePHOB* reactor the liquid reactant was able to contact the complete hydrophilic γ-Al_2O_3 layer resulting in significantly higher conversion values. The measured selectivity values to ammonia were found to be approximately 53% for the *PHOB* and 40% for the *SePHOB* reactor.

Table 2.2: Effect of the surface properties on the reactor performance: NO_2^- conversions and reaction rates for *PHOB* and SePHOB reactors (Initial nitrite concentration≈11 mg/l, H_2 concentration=100%, Pd loading=0.073 wt%).

L-Flow rate, *ml/min*	Reactor type	NO_2^- conversion	Reaction rate $\cdot 10^5$, *mmol/min*
0.1	PHOB	25%	0.6
	SePHOB	71%	1.8
0.3	PHOB	11%	0.8
	SePHOB	39%	2.8

The effect of the H_2 concentration in the gas phase of the reactor was investigated for the *PHOB* and *SePHOB* reactors (Pd loading= 0.073 wt%). The flow rate of the gas phase was kept constant, but the volumetric concentration of gaseous reactant H_2 in the gas flow was varied between 1% and 100% (H_2 partial pressures) by using Ar as diluting agent.

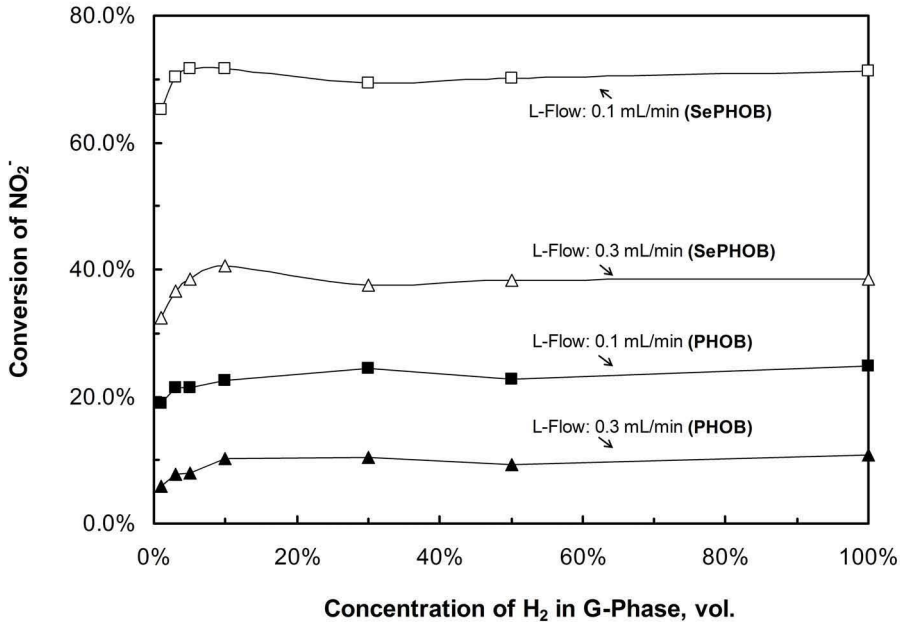

Figure 2.8: The effect of the hydrogen concentration on the reactor performance. Nitrite conversion values for *PHOB* and *SePHOB* reactors (Initial nitrite concentration≈11 mg/l, Pd loading=0.073 wt%).

As can be seen in Figure 2.8, the performance of the reactor remained constant with decreasing hydrogen concentration. A slight decrease in conversions was observed when the H_2 concentration dropped below 5%. The selectivity to the undesired product NH_4^+ decreased very slightly with decreasing H_2 concentration. Results show that even at low values of H_2 concentration, the gaseous reactant could easily reach the reaction area (γ-Al_2O_3 layer) through the non-wetted pores of the hydrophobic α-Al_2O_3. This concept ensures negligible mass transport limitations for the gas reactant. Even at low H_2 concentrations in the gas phase, enough hydrogen is provided to maintain the reaction with dissolved nitrite (∼0.24 mmol/l).

The initial nitrite concentration in the liquid phase was increased from 11 to 110 mg/l. The experiments were carried out with the *SePHOB* reactor for different H_2 concentrations (5 to 100%) and at two different liquid flow rates (0.1 and 0.3 ml/min).

For increased nitrite concentrations, even though the nitrite conversion values have decreased compared to the experiments with lower nitrite concentration (Table 2.3), the reaction rates have significantly increased. The selectivity of the reaction towards ammonia was approximately 24%. In addition, with the variation of the H_2 concentration (down to 5%) it was observed that the nitrite conversion performances again remained constant over the full concentration range. These high nitrite reaction rates at high initial nitrite concentration (∼2.40 mmol/l) show that the continuous supply of the gas phase provides enough H_2 to the reaction area even though H_2 has a low solubility in water (∼0.78 mmol/l at 25°C[27]). The apparent order in H_2 for this configuration is zero, suggesting that the Pd surface is almost completely covered with H-atoms. Apparently, this way of introducing H_2 is extremely efficient. The turn-over-frequency (TOF), representing the amount of NO_2^- ions converted per surface-Pd-atom, was calculated for the *SePHOB* reactor (Pd loading= 0.073 wt%, initial NO_2^- concentration≈11 mg/L) to be $\sim 0.5 \cdot 10^{-3} s^{-1}$. This value is relatively small compared to the TOF obtained in previous work ($\sim 3.4 \cdot 10^{-3} s^{-1}$) for γ-Al_2O_3 supported Pd catalyst[20]. However, this is not a surprise when considering the high level of conversion as reported in Table 2.3, as compared to differential experiments[20]. Therefore, the TOF obtained here is an averaged value due to variations in both nitrite concentration as well as pH along the axis of the reactor.

Table 2.3: Effect initial nitrite concentration on the performance of the SePHOB reactor: NO_2^- conversions and reaction rates for PHOB and SePHOB reactors (Initial nitrite concentration≈11 mg/l, H_2 concentration=100%, Pd loading= 0.073 wt%).

Initial NO_2^- Concentration	L-Flow Rate, *ml/min*	NO_2^- Conversion	Reaction Rate $\cdot 10^5$, *mmol/min*
∼ 11 mg/l	0.1	71%	1.8
	0.3	39%	2.8
∼ 110 mg/l	0.1	40%	9.9
	0.3	18%	13.7

In order to investigate the effect of the amount of catalytically active sites on the membrane wall, two reactors with two different catalyst loadings were tested. *SePHOB* reactors with 0.073 wt% Pd loading and with 0.260 wt% Pd loading were

used and the tests were carried out for initial nitrite concentrations of ∼11 and ∼110 mg/l.

Figure 2.9 illustrates the obtained nitrite conversions for each reactor under the different process conditions. Higher conversion values were obtained for the reactor with higher catalyst loading. The increments in conversions and reaction rates for each flow rate were more evident for higher initial nitrite concentrations (from 9.9 and $13.7 \cdot 10^{-5}$ mmol/min to 15.0 and $22.7 \cdot 10^{-5}$ mmol/min) because of the lower conversion levels (closer to differential conditions), where the concentration gradients along the axis are less significant. These results show that the performance can be improved by increasing the amount of Pd catalyst in the selectively hydrophobized reactor. However, the extent of the increase is far smaller than the increase in Pd loading, which is due to the high conversion levels (integral conditions) and hence a significantly lower concentration in the downstream of the reactor, as well as to the

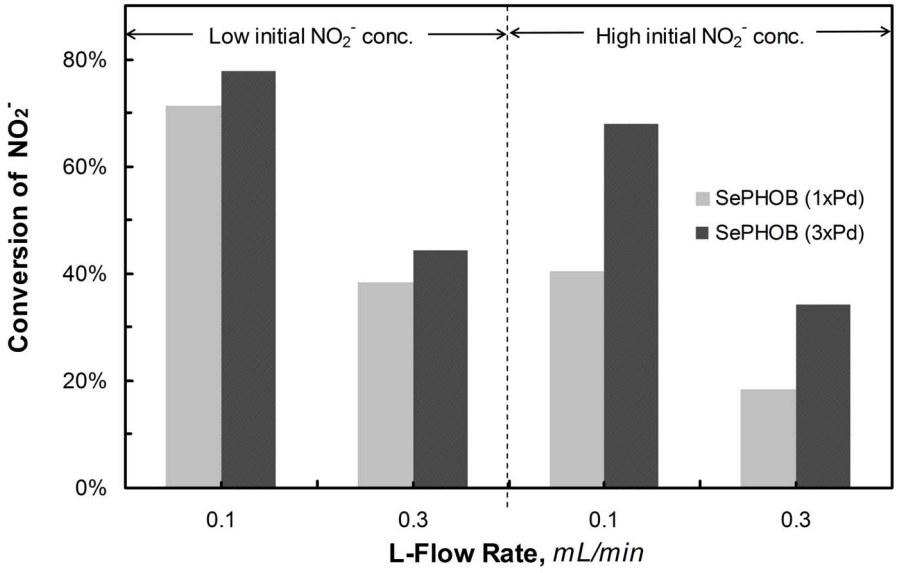

Figure 2.9: Effect of catalyst loading on the reactor performance. Nitrite conversion values for *SePHOB* reactors with 0.073 wt% and 0.260 wt% Pd loading (Initial nitrite concentration= ∼11 (low) and ∼110 (high) mg/l, H_2 concentration=100%)).

Table 2.4: Comparison of 2-Phase and 3-Phase Systems for a *SePHOB* reactor (Initial nitrite concentration≈11 mg/l, Pd loading = 0.260 wt%).

Operation Mode	L-Flow Rate, *ml/min*	Nitrite conversion $x(H_2)$,*vol*		H_2 conversion $x(H_2)$, *vol*		Selectivity to NH_4^+ $x(H_2)$, *vol*	
		10%	100%	10%	100%	10%	100%
2-Phase	0.1	11%	72%	51%	47%	5%	36%
	0.3	14%	53%	72%	40%	4%	60%
3-Phase	0.1	80%	80%	-	-	37%	40%
	0.3	46%	46%	-	-	42%	38%

decreased dispersion of Pd.

The nitrite conversions of the proposed 3-Phase concept were compared with the performance of a 2-Phase system for the same reaction using the same reactor. In the 2-Phase system the initial nitrite (NO_2^-) feed solution was saturated with the gaseous reactant of H_2 or its mixtures with Ar. For this mode, both reactants (NO_2^- and H_2) are dissolved in water (L) reacting on the catalyst (S) surface and no reactant (H_2) is fed from the gas phase. The solution was fed into the same porous ceramic mesoreactor. For this comparison, two different liquid flow rates (0.1 and 0.3 ml/min) and two different H_2 concentrations ($x(H_2)$) were used. Tests were carried out in the *SePHOB* reactor with 0.260 wt% Pd loading. The conversion values of the presaturated H_2 in the liquid phase were calculated for the 2-Phase experiments from the reaction stochiometry (2, 3) considering the selectivity of the reaction.

The experiments clearly show (Table 2.4) that the performance of the 2-Phase system is more sensitive to the H_2 concentration. For 10% H_2 concentration, the conversion values dropped drastically in the 2-Phase system while for 100% H_2 concentration these values were in the same range for both operation modes. The decrease of the conversions for low H_2 concentrations at 2-Phase operation mode is caused by depletion (exhaustion) of dissolved hydrogen in the liquid phase along the reactor axis. Presaturation with 10% H_2 (partial pressure= 0.1 bar) results in ∼0.078 mmol/l dissolved H_2 at 25°C, which is not sufficient to convert the dissolved nitrite (∼0.24 mmol/l) completely. These results demonstrate the key advantage of the proposed 3-Phase contacting system, where a continuous supply of the gaseous reactant along

the full length of the reactor via the membrane prevents depletion of the gaseous reactant, without dispersing the gas in the liquid phase.

2.4 Conclusions

In this study, a contacting concept for gas-liquid-solid (G-L-S) microreaction technology was studied. Porous ceramic mesoreactors in tubular geometry with controllable wetting properties and catalytic activity was developed. The reactors were characterized and the proposed reactor concept was applied for catalytic hydrogenation of nitrite. The developed reactors showed promising performance for this environmentally relevant catalytic reaction system.
Main conclusions of this study are as follows:

- The wetting behavior for the liquid reactant on the catalyst surface and the position of the G-L interface can easily be tuned and a stable G-L-S interface for heterogeneously catalyzed reaction processes can be obtained applying surface modification (hydrophobization) techniques.

- Reactors prepared with selective hydrophobization techniques (*SePHOB*), in which the membrane support is hydrophobized while the catalyst support remains hydrophilic, proved to be the most effective configuration for this reactor approach.

- The performance of the reactor remained constant even when the gaseous reactant (H_2) concentration was decreased. This concept provides very efficient transfer of H_2 by continuous addition through the membrane, allowing operating at low partial pressures of H_2.

Membrane technology shows to have a promising potential to be implemented for microreactors in G-L-S reaction systems. Despite the above mentioned conclusions some issues remain to be investigated. Next chapter is focused on different configurations inside the reactor such as the influence of different thicknesses of the

catalyst support layer, effect of the decreased internal diameters (microscale) and mixing strategies to increase the performance.

2.5 Acknowledgements

We are grateful to B. Geerdink, K. Altena -Schildkamp and J.A.M. Vrielink for analysis and technical support. The authors also greatly acknowledge J. Bennink (Tingle.nl) for the imaging and D. Salamon and J.M. Jani for the fruitful discussions.

Bibliography

[1] A. Gavriilidis, P. Angeli, E. Cao, K. K. Yeong, and Y. S. S. Wan. Technology and applications of microengineered reactors. *Chemical Engineering Research and Design*, 80(1):3 – 30, 2002. 25

[2] K. F. Jensen. Microreaction engineering – is small better? *Chemical Engineering Science*, 56(2):293 – 303, 2001.

[3] M. N. Kashid and L. Kiwi-Minsker. Microstructured reactors for multiphase reactions: State of the art. *Industrial & Engineering Chemistry Research*, 48(14):6465–6485, 2009. 25

[4] G. N. Doku, W. Verboom, D. N. Reinhoudt, and A. van den Berg. On-microchip multiphase chemistry–a review of microreactor design principles and reagent contacting modes. *Tetrahedron*, 61(11):2733 – 2742, 2005. 25

[5] P. L. Mills, D. J. Quiram, and J. F. Ryley. Microreactor technology and process miniaturization for catalytic reactions–a perspective on recent developments and emerging technologies. *Chemical Engineering Science*, 62(24):6992 – 7010, 2007. 25

[6] V. Hessel, P. Angeli, A. Gavriilidis, and H. Lowe. Gas-liquid and gas-liquid-solid microstructured reactors: Contacting principles and applications. *Industrial & Engineering Chemistry Research*, 44(25):9750–9769, 2005. 25

[7] J. Coronas and J. Santamaria. Catalytic reactors based on porous ceramic membranes. *Catalysis Today*, 51(3-4):377 – 389, 1999. 25

[8] R. Dittmeyer, K. Svajda, and M. Reif. A review of catalytic membrane layers for gas/liquid reactions. *Topics in Catalysis*, 29:3–27, 2004.

[9] A. G. Dixon. Recent research in catalytic inorganic membrane reactors. *International Journal of Chemical Reactor Engineering*, 1(R6), 2003.

[10] A. Julbe, D. Farrusseng, and C. Guizard. Porous ceramic membranes for catalytic reactors – overview and new ideas. *Journal of Membrane Science*, 181(1):3 – 20, 2001.

[11] J. Peureux, M. Torres, H. Mozzanega, A. Giroir-Fendler, and J-A. Dalmon. Nitrobenzene liquid-phase hydrogenation in a membrane reactor. *Catalysis Today*, 25(3-4):409 – 415, 1995.

[12] M. Vospernik, A. Pintar, G. Bercic, J. Batista, and J. Levec. Potentials of ceramic membranes as catalytic three-phase reactors. *Chemical Engineering Research and Design*, 82(5):659 – 666, 2004.

[13] M. Vospernik, A. Pintar, G. Bercic, and J. Levec. Experimental verification of ceramic membrane potentials for supporting three-phase catalytic reactions. *Journal of Membrane Science*, 223(1-2):157 – 169, 2003.

[14] R. Dittmeyer, V. Hollein, and K. Daub. Membrane reactors for hydrogenation and dehydrogenation processes based on supported palladium. *Journal of Molecular Catalysis A: Chemical*, 173(1-2):135 – 184, 2001. 25

[15] G. Chen, J. Yue, and Q. Yuan. Gas-liquid microreaction technology: Recent developments and future challenges. *Chinese Journal of Chemical Engineering*, 16(5):663 – 669, 2008. 25

[16] V. Hessel, S. Hardt, and H. Lowe. *Chemical Micro Process Engineering: Fundamentals, Modelling and Reactions, Sections 5.1-5.3*, pages 577–619. Wiley-VCH Verlag GmbH & Co. KGaA, 2005. 25

[17] A. Pintar, G. Bercic, and J. Levec. Catalytic liquid-phase nitrite reduction: Kinetics and catalyst deactivation. *AIChE Journal*, 44(10):2280–2292, 1998. 27

[18] K.D. Vorlop and T. Tacke. Erste schritte auf dem weg zur edelmetallkatalysierten nitrat– und nitrit–entfernung aus trinkwasser. *Chemie Ingenieur Technik*, 61, 1989.

[19] S. D. Ebbesen, B. L. Mojet, and L. Lefferts. In situ ATR–IR study of nitrite hydrogenation over Pd/Al_2O_3. *Journal of Catalysis*, 256(1):15 – 23, 2008.

[20] J.K. Chinthaginjala and L. Lefferts. Support effect on selectivity of nitrite reduction in water. *Applied Catalysis B: Environmental*, 101(1-2):144 – 149, 2010. 39

[21] J. K. Chinthaginjala, J. H. Bitter, and L. Lefferts. Thin layer of carbon-nano-fibers (CNFs) as catalyst support for fast mass transfer in hydrogenation of nitrite. *Applied Catalysis A: General*, 383(1-2):24 – 32, 2010. 27

[22] R. Zapf, C. Becker-Willinger, K. Berresheim, H. Bolz, H. Gnaser, V. Hessel, G. Kolb, P. Lob, A.-K. Pannwitt, and A. Ziogas. Detailed characterization of various porous alumina–based catalyst coatings within microchannels and their testing for methanol steam reforming. *Chemical Engineering Research and Design*, 81(7):721 – 729, 2003. 27

[23] M.J. Geerken, T.S. van Zanten, R.G.H. Lammertink, Z. Borneman, W. Nijdam, C.J.M. van Rijn, and M. Wessling. Chemical and thermal stability of alkylsilane based coatings for membrane emulsification. *Advanced Engineering Materials*, 6(9):749–754, 2004. 28, 29

[24] M.J. Geerken, R.G.H. Lammertink, and M. Wessling. Tailoring surface properties for controlling droplet formation at microsieve membranes. *Colloids and Surfaces A: Physicochemical and Engineering Aspects*, 292(2-3):224–235, 2007. 28

[25] H. Rathgen. *Superhydrophobic surfaces : from fluid mechanics to optics*. PhD thesis, Enschede, University of Twente, December 2008. 29

[26] N. D. Shinn P. J. Clews T. M. Mayer, M. P. de Boer and T. A. Michalske. Chemical vapor deposition of fluoroalkylsilane monolayer films for adhesion control in microelectromechanical systems. *Journal of Vacuum Science & Technology B*, 18, 2000. 29

[27] D.R. Lide and W.M. Haynes (Eds.). *CRC Handbook of Chemistry and Physics, 90th ed.* CRC Press/ Taylor and Francis, 2010. 39

Chapter 3

Influence of geometrical and operational parameters on the performance of porous ceramic meso- and microreactors

PARTS OF THIS CHAPTER ARE IN PREPARATION FOR PUBLICATIONS:
H.C. Aran, J.M. Jani, H. Klooster, M. Wessling, L. Lefferts, R.G.H. Lammertink.

ABSTRACT

In this study, porous membrane reactors with various characteristic length (inner diameter), controllable catalyst support thickness, active catalyst surface area and tunable wetting properties are described for heterogeneously catalyzed gas-liquid-solid (G-L-S) reactions. We developed porous ceramic membrane meso- and microreactors (porous Al_2O_3) with various geometrical parameters and applied these to a model G-L-S reaction. Integration of a catalyst support layer (γ–Al_2O_3), catalyst deposition (palladium) and surface modification (hydrophobization) steps were carried out to tailor these tubular porous ceramic reactors. These reactors were tested for catalytic hydrogenation of nitrite ions (NO_2^-) in water for different initial concentrations and flow rates. To improve the external mass transfer in the liquid phase, we integrated inert slug flow in our porous reactors, merging the advantages of both dispersed phase and membrane reactor operation. Results showed that the NO_2^- reaction rate per catalyst surface area decreased with increasing thickness of the catalyst support layer, indicating internal mass transfer limitations. Reducing the inner diameter of the reactor and also the integration of slug flow significantly enhanced the performance by improving the external mass transfer.

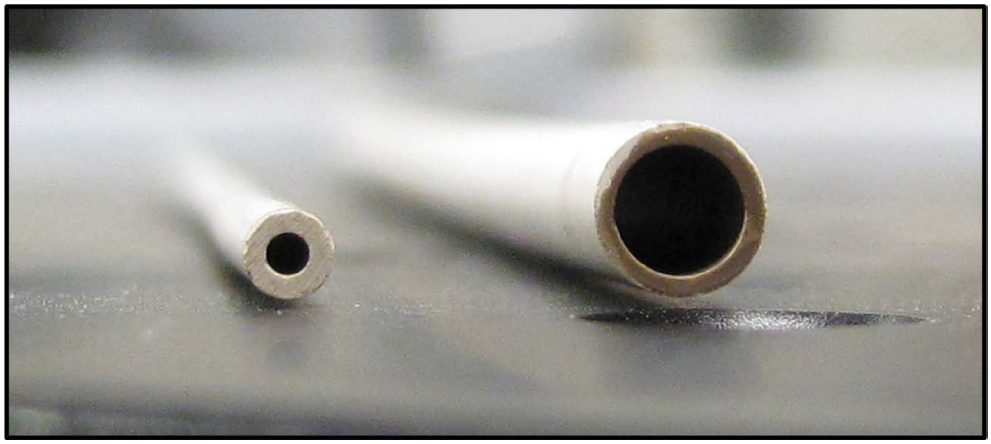

3.1 Introduction

Heterogeneously catalyzed gas-liquid-solid (G-L-S) reactions are of great importance for the chemical industry, including petrochemical, bulk and fine chemical processes. A variety of reactor types are used for these multiphase reactions; conventional ones are slurry phase and trickle/fixed bed reactors[1–3]. An alternative reactor design for these reactions is a membrane reactor. This alternative demonstrates a promising potential for future application due to its many advantages. They offer a stable and controlled G-L interface with a simple reactor design, in which the gas and liquid phases can be controlled independently. The phases are added to the reaction zone from the opposite sides of the membrane and meet precisely where the solid (S) catalyst is located. The gaseous reactant is distributed homogeneously along the full reactor length, which makes these reactors advantageous for processes with low gaseous reactant solubility or high gas consumption, preventing a possible depletion of this reactant in the reactor[4–14]. In past years, due to their favorable properties, these reactors were intensively investigated. A major drawback of these systems is mass transfer limitations in the liquid phase (reactant diffusion from bulk to the catalytic wall) due to the laminar flow in the reactor channel. Remarkable efforts were performed to overcome these limitations. Vospernik et al.[9] used a static mixer and Pashkova et al.[13] used glass beads (restructuring the flow) in the a reactor channel, in order to improve the mass transfer in the liquid phase.

A practical way to overcome mass transfer limitations in a chemical reaction process is the use of microreactor technology, by miniaturizing the characteristic dimension of the reactor channels. Microreactors are chemical reactors with reduced characteristic length and therefore high surface to volume ratio. They offer numerous advantages for chemical technology with their miniaturized dimensions, such as improved heat and mass transfer, operational safety, higher degree of control, sustainability, mobility[15,16]. Hence, microreactor technology is an attractive platform for G-L-S reactions.

Falling film microreactors[17], mesh microreactors[18], catalyst trap microreactors[19], dispersed phase microreactors[20] are commonly used reactor designs in this field. Excellent reviews on G-L-S processes in microreactors are already available[21–24]. According to our best knowledge there are only very few examples of membrane reactors available for G-L-S microreactor technology.[14,25].

In Chapter 2, we demonstrated a new method of preparation and application of porous ceramic mesoreactors for G-L-S reactions. We developed a selective surface modification (hydrophobization) strategy ensuring a stable gas-liquid-solid interface. By tuning the surface properties, we were able to define the reaction area and enhance the performance of the reactor[14].

The aim of the present work is to study the influence of geometrical and operational parameters on the reactor performance for this concept. This chapter consists of two sections. The effect of catalyst support thickness and the miniaturized channel dimensions (geometrical parameters) are described in Section 3.2. The integration of inert slug flow (operational parameter) is given in Section 3.3.

In both sections, Pd-catalyzed hydrogenation of nitrite ions (NO_2^-) in water is used as a model reaction to test the reactor performance. In this reaction, NO_2^- ions in aqueous solution (L-reactant) react with hydrogen (H_2; G-reactant) on the palladium

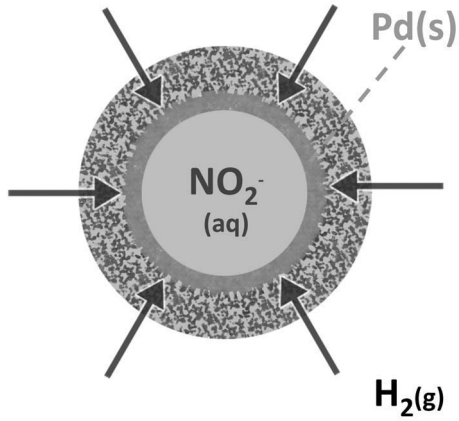

Figure 3.1: Contacting of gas, liquid and solid phases for the Pd-catalyzed hydrogenation of nitrite in a porous ceramic reactor.

(Pd; S-catalyst) surface and form the desired product nitrogen (N_2) and the undesired by-product ammonia (NH_4^+)[1,26,27]. In the present study, the conversion NO_2^- is the main performance criterion. No selectivity studies (N_2 or NH_4^+) were carried out.

$$2NO_2^- + 3H_2 \overset{Pd}{\rightarrow} N_2 + 2OH^- + 2H_2O \tag{3.1}$$

$$2NO_2^- + 6H_2 \overset{Pd}{\rightarrow} 2NH_4^+ + 4OH^- \tag{3.2}$$

3.2 Influence of geometrical parameters on reactor performance

In this section, the performance of the porous ceramic (membrane) reactors for different reactor configurations (catalyst support thickness, characteristic length) is investigated. Reactors with various properties were prepared and tested for catalytic hydrogenation of nitrite.

3.2.1 Experimental

3.2.1.1 Materials

As membrane support, commercial porous ceramic (α–Al_2O_3) hollow fibers (InoCep M800 -800 nm average pore size-; Hyflux CEPAration Technologies, Europe) with two different diameters of were used. The used fibers had inner diameters of 0.8 and 2.8 mm. The fibers were cut to a length of 13.5 cm. For catalyst support preparation, γ–Al_2O_3 (Alfa Aesar, 3 micron APS Powder), MilliQ-water, polyvinyl alcohol (PVA; Sigma-Aldrich, 87-89% hydrolyzed) and acetic acid (Merck) were used as received. For catalyst precursor solution, Palladium(II) 2,4-pentanedione ($(Pd(acac)_2$; Alfa Aesar, 34.7%)) and toluene (Merck) were used. Perfluorinated octyltrichlorosilane (FOTS; Aldrich, 97%) was used for the surface modification step. For the catalytic model reaction, sodium nitrite ($NaNO_2$, Merck) was used as reactant.

3.2.1.2 Reactor preparation

The reactor preparation consists of catalyst support coating, catalyst (palladium) deposition and surface modification steps, which were modified from our Chapter 2 for this study. These preparation steps were carried out identically for the hollow fibers with 0.8 and 2.8 mm inner diameters.

For the coating of the catalyst support layer, three different aqueous γ–Al_2O_3 suspensions were prepared. The recipes of the suspensions were adapted from a standard recipe of Zapf et al.[28] and Yeong et al.[17]. Each suspension consisted of 75 g water, 5 g PVA and 1 g acetic acid and γ–Al_2O_3 (20 g (Susp. 1), 10 g (Susp. 2), 5 g (Susp. 3)).

The coating procedure is illustrated in Figure 3.2. A glass vessel was filled with the corresponding γ–Al_2O_3 suspension and connected to the ceramic (α–Al_2O_3) hollow fibers by plastic tubing. With this communicating vessel system (adapted from Luiten

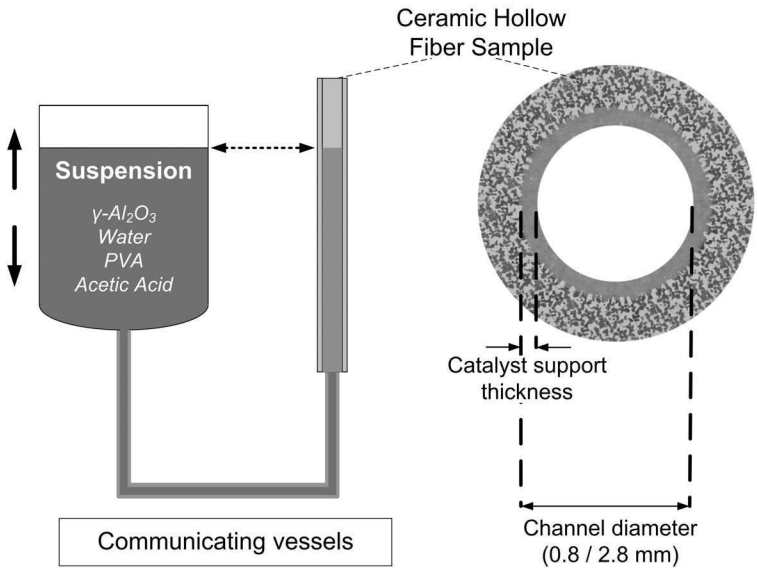

Figure 3.2: Schematic representation of the coating procedure of the γ–Al_2O_3 layer (catalyst support): Various suspension compositions were used to vary the catalyst support thickness inside porous α–Al_2O_3 hollow fibers with inner diameters of 0.8 and 2.8 mm.

et al.[29]) the position and the vertical velocity of the glass vessel were controlled by a motor driven stage. The filling/emptying speed of the hollow fiber with the suspension was 0.3 cm/s. After this step, the samples were dried at 50°C in a vertical position for ∼1.5 h and calcined at 600°C for 2 h.

Hollow fibers with an inner diameter (ID) of 2.8 mm were coated with Suspensions 1, 2 and 3 and they were labeled as *Sample 1, Sample 2* and *Sample 3*, respectively. The hollow fiber with ID of 0.8 mm was coated with Suspension 1 and labeled as *Sample 4* (Table 3.1).

For the catalyst (palladium) deposition (as described in Chapter 2), the γ–Al_2O_3 coated samples were immersed into a palladium (Pd) precursor solution consisting of $Pd(acac)_2$ in toluene for 24 h and dried at 50°C overnight. Following, calcination in O_2 and reduction in H_2 atmosphere were carried out at 250°C.

For the surface modification (hydrophobization) step, we deposited FOTS selectively on the Pd loaded samples, in order to ensure that only the α–Al_2O_3 became hydrophobic and the catalyst support γ–Al_2O_3 remained hydrophilic. The ends of the samples were sealed and a gas phase deposition of FOTS was performed, as described in Chapter 2.

3.2.1.3 Reactor characterization

The thickness of the resulting γ–Al_2O_3 layer was determined by Scanning Electron Microscopy (SEM; JEOL TSM 5600). The weight increase of the samples after the coating with the γ–Al_2O_3 layer was measured with an analytical balance. The active Pd surface area in the sample was measured by CO-chemisorption (Micromeritics, ChemiSorb 2750: Pulse Chemisorption system) at room temperature. For the visualization of the wetting properties, an aqueous dye solution (Phenol Red or Methylene Blue) was pumped through the modified hollow fiber and then the cross-sections of the hollow fibers were examined by optical microscopy (Zeiss Axiovert 40).

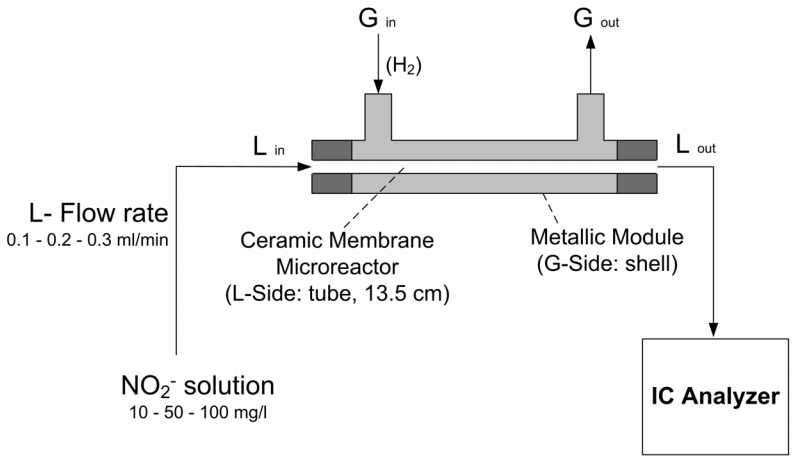

Figure 3.3: Schematic representation of the experimental setup and operational parameters.

3.2.1.4 Reactor operation

The prepared catalytic reactors were tested for the Pd-catalyzed hydrogenation of nitrite (NO_2^-). The conversion and reaction rate of NO_2^- were the main performance criteria. The average NO_2^- reaction rate per active catalytic (Pd) surface area was calculated for each sample and used as performance criterion.

Three different solutions of NO_2^- with initial concentrations of 10, 50 and 100 mg/l were prepared as liquid reactants. The flow rates of liquid reactants were 0.1, 0.2 and 0.3 ml/min. Gaseous hydrogen (H_2) was flown in the shell side of the reactor module with a flow rate of 100 ml/min. The NO_2^- concentrations at the reactor in- and outlet were measured by ion chromatography (Dionex ICS 1000).

3.2.2 Results and Discussion

3.2.2.1 Reactor characterization

By applying the above described preparation steps, we obtained reactors with controllable γ–Al_2O_3 catalyst support thickness, Pd catalyst surface area and wetting properties (Figure 3.4). Four samples were prepared for the purpose of this study. *Samples 1, 2* and *3* had an inner diameter (ID) of 2.8 mm and *Sample 4* of 0.8 mm.

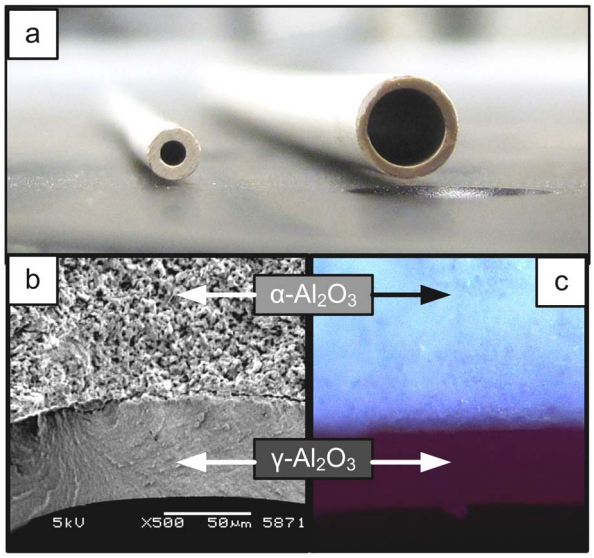

Figure 3.4: *(a)* Porous ceramic reactors with 0.8 and 2.8 mm inner diameters, *(b)* Cross-sectional SEM image of a reactor after γ–Al_2O_3 layer coating, *(c)* Wetting properties after the selective surface modification step: Aqueous dye wetted the hydrophilic γ–Al_2O_3 layer and not the hydrophobized α–Al_2O_3 layer.

The results for the γ–Al_2O_3 layer thickness (δ) and catalyst (Pd) deposition for the hollow fibers are summarized in Table 3.1.

Table 3.1: Thicknesses and porosity of the resulting catalyst support layer (γ–Al_2O_3) and active Pd surface area on each sample: Sample 1, 2 and 3 (ID=2.8 mm) were prepared by the use of different suspensions (1, 2, 3) with varying γ–Al_2O_3 content. Sample 4 (ID=0.8 mm) was coated with Suspension 1.

	Suspension	γ-Al_2O_3 layer		Catalyst
Sample	*γ–Al_2O_3 content (g/100 g)*	*thickness (μm)*	*Porosity*	*active Pd-surface (m^2/g total sample)*
1	20	~40	~66%	~13E-03
2	10	~20	~67%	~8.4E-03
3	5	~8	~64%	~3.8E-03
4	20	~60	~60%	~4.5E-03

The thickness of the γ-Al_2O_3 layer (δ) can be controlled by varying the γ-Al_2O_3 content in the coating suspension. With increasing γ-Al_2O_3 thickness (volume) the deposited amount and active surface area of Pd also increase to a similar extend, as

characterized by the CO-Chemisorption results. The porosity of the γ-Al_2O_3 layer was estimated with the weight increase of the sample and layer thickness and it is very similar for all of the samples. The BET surface area of the γ-Al_2O_3 layer was found to be around 73 m^2/g.

It was observed, that the Pd is mainly located in the γ-Al_2O_3 layer of the reactor. In Chapter 2, we used the same Pd deposition method and found by energy dispersive X-Ray (EDX) analysis, that Pd was homogeneously distributed in the γ-Al_2O_3 layer. The selective surface modification step was carried out after the Pd deposition and characterized by using an aqueous dye solution (Figure 3.4.b). The optical microscope images showed that the solution wetted only the γ-Al_2O_3 layer, where most of the catalyst was deposited. On the other hand, the α-Al_2O_3 layer remained not wetted, as we also observed in Chapter 2. This hydrophobization step creates a stable G-L interface by keeping the liquid flow inside the porous reactor channel. In addition, the selective nature of this surface modification ensures that the reaction takes place on the entire γ-Al_2O_3 layer, where most of the Pd catalyst is deposited.

3.2.2.2 Reactor operation

The reactors were tested for different operational parameters: Liquid flow rates (0.1, 0.2, 0.3 ml/min) and initial NO_2^- concentrations (10, 50, 100 mg/l). All samples showed significant activity for the catalytic hydrogenation of NO_2^- ions. Results for the reactors with 2.8 mm inner diameter (*Samples 1, 2* and *3*) are displayed in Figure 3.5.

For all the samples, the NO_2^- conversion decreases with increasing flow rate, due to decreasing residence time. For higher initial concentrations of NO_2^-, the conversion values (in %) decrease compared for the experiments with lower initial concentrations; however, the absolute amount of converted NO_2^- is significantly higher.

The comparison of *Samples 1, 2* and *3* shows that with increasing δ (thickness of the γ-Al_2O_3 layer) the NO_2^- conversion increases; caused by the increased amount of the deposited Pd (Table 3.1). Nevertheless, the increment in the conversion is not as significant as in the amount of the Pd loading. *Sample 1* has almost 4 times more Pd

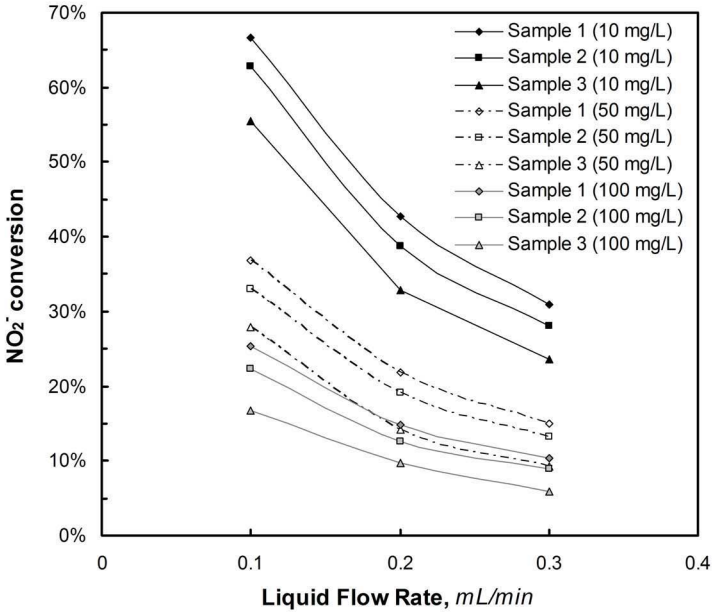

Figure 3.5: Nitrite conversion values for reactors Sample 1 ($\delta \approx 40$ μm, ID=2.8 mm), Sample 2 ($\delta \approx 20$ μm, ID=2.8 mm) and Sample 3 ($\delta \approx 8$ μm, ID=2.8 mm) as a function of the liquid flow rate for different initial nitrite concentrations (10, 50 and 100 mg/l). The lines between data points are only for guiding purposes.

area than *Sample 3* (Table 3.1), but the enhancement in the conversion is only 1.2 to 1.7 times for all concentrations and flow rates. The enhancement is more pronounced for high initial concentrations and liquid flow rates, which is due to a lower conversion range and therefore differential conditions for these operational parameters.

In order evaluate the efficiency of the deposited catalyst, the samples were compared for r'', the averaged reaction rate of the $NO_2{}^-$ ions (mmol/min) per active Pd surface area (m^2) for each initial concentration.

Another important aspect for a fair comparison between the samples is the level of $NO_2{}^-$ conversion, which influences the concentration profile in the liquid bulk (differential or integral conditions). We must make sure that each reactor is evaluated for the same level of $NO_2{}^-$ conversion. For that purpose, we manually interpolated (from Figure 3.5) the conversion values of Sample 1 for the L-Flow rate of 0.3 ml/min

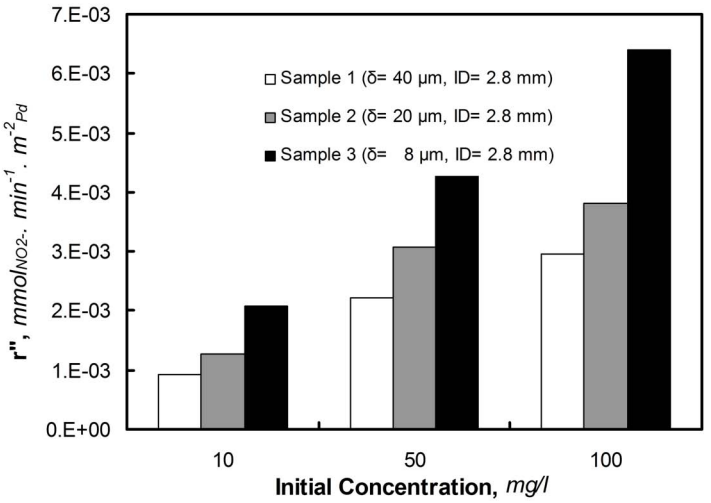

Figure 3.6: Influence of the γ-Al_2O_3 layer thickness (δ) on the reactor performance: r'' is NO_2^- averaged reaction rate per active Pd surface in the reactors for each initial concentration (10, 50 and 100 mg/l) for identical NO_2^- conversions (31%, 15% and 10%, respectively), interpolated from Figure 3.5.

for each initial concentration (31% for 10 mg/l, 15% for 50 mg/l and 10% for 100 mg/l). With the interpolation, we obtained the corresponding liquid flow rates for each sample for these conversion values and calculated average reaction rate per active Pd surface area (r'') for the corresponding condition (Figure 3.6).

The r'' values are displayed in Figure 3.6. As can be seen, *Sample 3* with the thinnest γ-Al_2O_3 coating has the highest palladium (Pd) turn-over-frequencies for each concentration.

The catalyst efficiency for each of these reactors can be estimated by calculating the Thiele moduli and internal effectiveness factors for each γ-Al_2O_3 layer thickness (δ_x). Thiele modulus (ϕ_x) is a measure of the ratio of the surface reaction rate to the reactant diffusion rate through a catalyst pellet [30].

$$\phi_x = \delta_x \cdot \sqrt{\frac{k \cdot S'''_{c,x}}{D_{eff}}} \tag{3.3}$$

In Equation 3.3, δ_x represents the thickness of the diffusion path (catalyst support), k the intrinsic rate constant, $S^{'''}_{\mathrm{c,x}}$ surface area of catalyst per support volume and D_{eff} the effective diffusivity of the reactant in the porous catalyst support [1,30].
The internal effectiveness factor (η_{x}) indicates the importance of diffusion and reaction limitations for a support thickness. It is the ratio of observed overall reaction rate to the reaction rate that can be achieved by exposing the entire interior catalyst surface to the external pellet surface conditions [30]. For a flat geometry (catalyst slab), this ratio can be estimated from the Thiele modulus (ϕ_{x}) as follows [31,32]:

$$\eta_{\mathrm{x}} = \frac{\tanh(\phi_{\mathrm{x}})}{\phi_{\mathrm{x}}} \tag{3.4}$$

As shown in Table 3.1, the γ-Al_2O_3 layers for *Samples 1, 2* and *3* exhibit similar internal characteristics (porosity- see Table 3.1.), therefore we assume that D_{eff} (Equation 3.3) is the same for each reactor. Since k value is constant (intrinsic) for nitrite hydrogenation reaction, we can assume that the Thiele modulus for our samples scales with the layer thickness and the catalytic surface area: $\phi_1/(\delta_1 \cdot \sqrt{S^{'''}_{\mathrm{c,1}}}) = \phi_2/(\delta_2 \cdot \sqrt{S^{'''}_{\mathrm{c,2}}}) = \phi_3/(\delta_3 \cdot \sqrt{S^{'''}_{\mathrm{c,3}}})$. Furthermore, the ratio of the effectiveness factors can be estimated with observed reaction rates per surface area of catalyst ($r^{''}$) for each sample: $\eta_1/r^{''}_1 = \eta_2/r^{''}_2 = \eta_3/r^{''}_3$ [30]. By using these ratios of the Thiele moduli and effectiveness factors together with Equations 3.3 and 3.4, we can calculate the Thiele modulus for each sample (Equation 3.5- as an example). In these calculations, $r^{''}$ values for the initial nitrite concentration of 100 mg/l and 10% conversion (interpolated) were used.

$$\frac{\eta_1}{\eta_2} = \frac{r^{''}_2}{r^{''}_1} = \frac{\tanh(\phi_1)/\phi_1}{\tanh(\phi_2)/\phi_2} = \frac{\tanh(\phi_1)/\phi_1}{\tanh(\frac{\phi_1 \cdot (\delta_2 \cdot \sqrt{S^{'''}_{c,2}})}{\delta_1 \cdot \sqrt{S^{'''}_{c,1}}}) / (\frac{\phi_1 \cdot (\delta_2 \cdot \sqrt{S^{'''}_{c,2}})}{\delta_1 \cdot \sqrt{S^{'''}_{c,1}}})} \tag{3.5}$$

Solving Equation 3.5 for *Samples 1, 2* and *3*, we find ϕ_1(40 μm)≈2.5±1.0, ϕ_2(20 μm)≈1.4±0.6, ϕ_3(8 μm)≈0.6±0.2. The obtained value for ϕ_2(20 μm) is in good

agreement with values reported by Chinthaginjala et al.[26] (1.12 for a 20 μm particle size γ-Al_2O_3 pellet). The effectiveness factors, η_1, η_2 and η_3 are 0.4±0.2, 0.6±0.2 and 0.9±0.07, respectively.

From the obtained Thiele moduli (ϕ), we can have a closer look at the corresponding concentration profiles (Figure 3.7). These profiles can be obtained by solving the mass balance for diffusion and reaction in a flat plate catalyst pellet:

$$\frac{\partial^2 c}{\partial x^2} - \frac{\phi^2}{\delta^2} \cdot c = 0 \tag{3.6}$$

where c is the reactant concentration, x is the distance into the catalyst layer and δ the total catalyst layer thickness. Solving this differential equation provides the concentration profiles inside the catalyst layer for a given value of ϕ. In Figure 3.7, the normalized concentration profiles along the catalyst support are presented for the obtained Thiele moduli of *Samples 1, 2* and *3*. For the thinnest catalyst

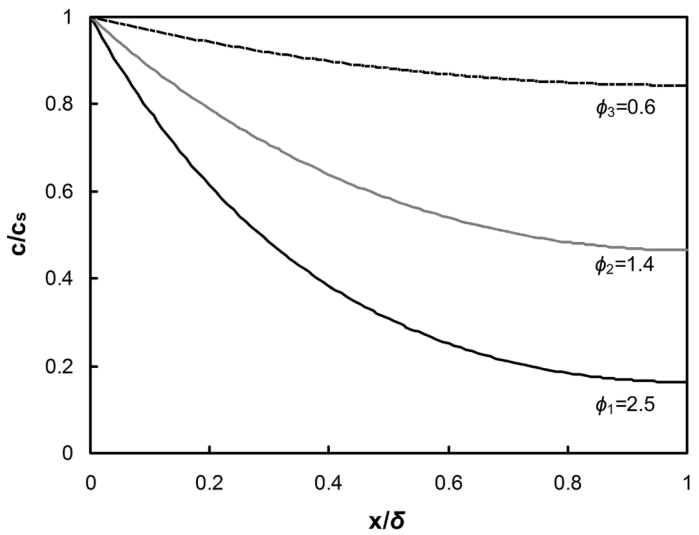

Figure 3.7: Normalized reactant concentration profiles (c normalized to surface concentration c_s) along the catalyst support (x normalized to support thickness δ) for various Thiele moduli(ϕ).

layer, the modulus of 0.6 (ϕ_3) results in the highest concentration values throughout the catalyst support layer and hence the highest efficiency. A higher modulus, such as 2.5 (ϕ_1) for the thickest catalyst support layer, results in relatively low reactant concentrations throughout a large portion of that layer. These results show that the catalytic activity is significantly affected by the γ-Al_2O_3 support thickness (δ) and internal mass transfer limitations. This influence is pronounced especially for a γ-Al_2O_3 catalyst support because of its small pore size ($\sim$20 nm[17]) and high tortuosity ($\sim$4[33]).

In order to study the influence of the inner diameter to the reactor productivity, the performances of *Sample 1* (ID = 2.8 mm, $\delta\approx$40 μm) and *Sample 4* (ID = 0.8 mm, $\delta\approx$60 μm) are compared. These two samples are chosen for this comparison because of the comparable catalyst support thickness (δ).

Figure 3.8.a shows that with *Sample 4* (ID = 0.8 mm) lower conversion values were obtained than with *Sample 1* (ID = 2.8 mm) for the same liquid flow rates. However, *Sample 1* has a reactor volume of 0.83 ml, while *Sample 4* only has 0.07 ml, which means that for the same flow rates the liquid reactant has 12.3 times higher residence time in *Sample 1*.

In order carry out a comparison between the two reactors, the nitrite reaction rate per active Pd surface area, r'', was calculated (Figure 3.8.b). We compared the reactors for the liquid flow rates, for which they show similar conversion levels (*Sample 1*: 0.3 ml/min, *Sample 4*: 0.1 ml/min) at each initial concentration (indicated by dotted lines in Figure 3.8.a). In this way, the reactor can be evaluated at similar concentration conditions (under differential or integral conditions).

Figure 3.8.b shows that higher reaction rates per catalytic surface area were achieved with the miniaturized dimensions. *Sample 4* (ID = 0.8 mm) showed to have higher efficiency per active Pd surface area than *Sample 1* (ID = 2.8 mm) at each initial concentration.

The kinetics of Pd-catalyzed hydrogenation of nitrite as a surface reaction can be described by a Langmuir-Hinshelwood mechanism (Equation 3.7). Matatov-Meytal et al.[34] and Pintar et al.[35] also suggested similar mechanism for this reaction.

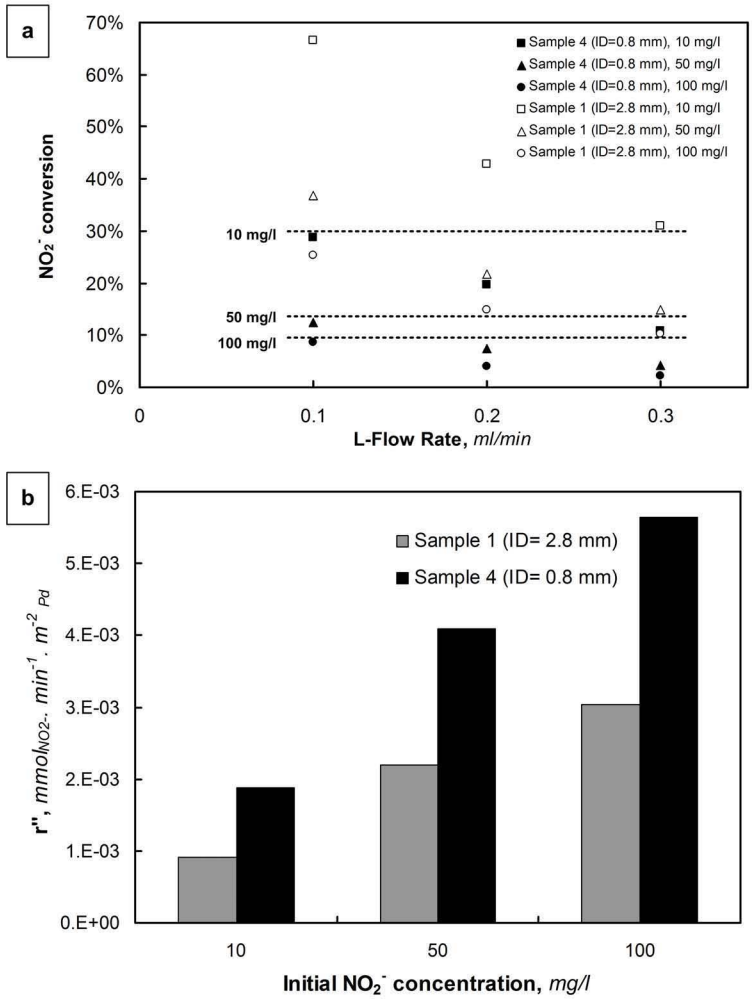

Figure 3.8: Effect of the reactor inner diameter (characteristic length) on the performance of the ceramic membrane microreactor: *(a)* NO_2^- conversion values for Sample 1 and 4 at various initial concentration and liquid flow rates (dotted lines indicate similar conversion values of the reactors at different flow rates for each concentration), *(b)* Average NO_2^- reaction rate per active Pd surface in the reactors (for the indicated operating conditions in Figure 3.8.a.)

$$r_{\mathrm{x}}^{'''} = \frac{\mathrm{d}(\mathrm{c}_{\mathrm{NO_2^-}})}{\mathrm{d}(t)} = \frac{k_{\mathrm{app}} \cdot K \cdot \mathrm{c}_{\mathrm{NO_2^-}}}{1 + K \cdot \mathrm{c}_{\mathrm{NO_2^-}}} \tag{3.7}$$

where $r_{\mathrm{x}}^{'''}$ is the average rate of $NO_2{}^-$ reaction per reactor volume, $\mathrm{c}_{\mathrm{NO_2^-}}$ concentration of $NO_2{}^-$ ions in the water, k_{app} the apparent reaction rate constant, K the adsorption coefficient of $NO_2{}^-$. In our case, we did not include the gaseous reactant hydrogen (H_2) term in the reaction mechanism because of its efficient (non-limiting) transport to the reaction zone. For the identical reactor design, in Chapter 2 we did not observe any significant influence of the H_2 concentration to the reactor performance.
As demonstrated by Gorges et al.[36], k_{app} and K values can be determined with the linearization of Equation 3.7.

$$\frac{1}{r_{\mathrm{x}}^{'''}} = \frac{1}{k_{\mathrm{app}}} + \frac{1}{k_{\mathrm{app}} \cdot K \cdot \mathrm{c}_{\mathrm{NO_2^-}}} \tag{3.8}$$

The observed $NO_2{}^-$ reaction rates are shown as a function of nitrite concentrations in the double-reciprocal plot (Figure 3.9). We used the average value of the initial and final $NO_2{}^-$ concentrations for $\mathrm{c}_{\mathrm{NO_2^-}}$. From this linear relationship, k_{app} values of 0.1 (ID=2.8 mm) and 0.3 mmol/l.min (ID=0.8 mm) and K values of 1.9±0.4 and 2.3±0.5 l/mmol were obtained. The k_{app} (apparent rate constant) values depend strongly on the experimental conditions[36] and in our case, they considerably differ for each reactor, since the mass transfer properties do vary due to the different internal diameters. On the other hand, the K (adsorption coefficient of $NO_2{}^-$ on Pd/Al_2O_3) values were in good agreement for both reactors. According to our best knowledge, a Langmuir-Hinshelwood mechanism was previously not applied on a similar system ($NO_2{}^-$ on Pd/Al_2O_3), therefore these values cannot be directly compared to literature values.
The higher productivity values and higher reaction rate constants of the miniaturized reactor (*Sample 4*) can be explained by its higher surface to volume ratio, which leads to enhanced mass transfer characteristics compared to in *Sample 1*. Due to

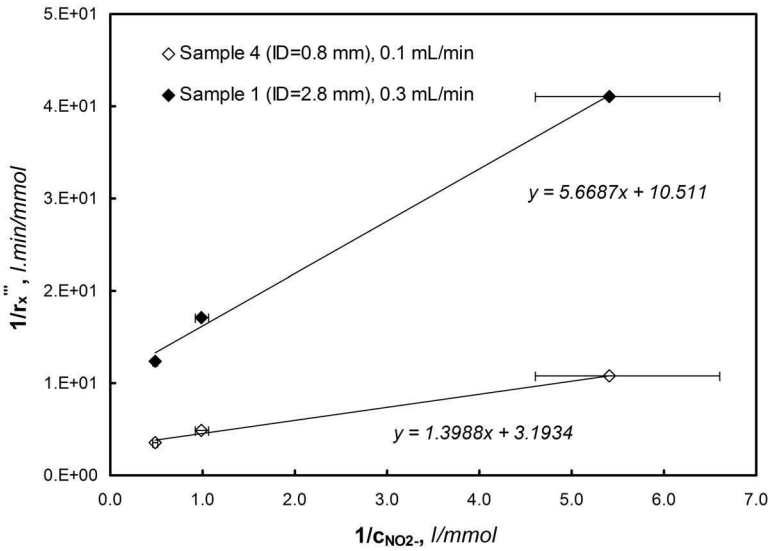

Figure 3.9: Reaction rate (per volume) as a function of the nitrite concentration: Double-reciprocal plot to determine k_{app} (apparent rate constant) and K (adsorption coefficient) from Equations 3.7 and 3.8. $c_{NO_2^-}$ is the average value of the initial and final $NO_2{}^-$ concentrations. Error bars indicate the initial and final concentrations for each experiment.

the laminar flow profile (low flow rates) in our reactor channels, diffusion is the dominant mechanism for mass transport in the radial direction. The slow nature of the diffusion process in the liquid phase usually leads to mass transfer limitations in membrane reactors[8]. By decreasing the characteristic dimension, the diffusion path of the reactant in the liquid bulk to the reactor wall is reduced, which results in improved mass transfer characteristics for *Sample 4*.

The results in this study indicate some limitations and possible improvement strategies in our membrane reactor concept. The availability of the solid catalyst at G-L interface, needs to be improved e.g. (a) by decreasing the catalyst support thickness (as proven in this work), (b) by integrating catalyst supports with higher pore volumes and lower tortuosity (e.g. carbon nanofibers[26]), (c) by applying other catalyst deposition strategies for higher dispersion of the catalyst. Furthermore,

external mass transfer limitations cannot be neglected due to the laminar flow profile. As this study showed, it can be reduced by simply decreasing the characteristic dimension (hydraulic diameter) of the reactor channel, evidently paying a pressure drop penalty. Other potential strategies would be the use of active (external energy input[8]) or passive mixing (restructuring the flow[13,37]) techniques in order to improve the external mass transfer. Next section describes another possible technique to transport enhancement inside these microchannels; integration of slug flow (passive mixing).

3.3 Slug flow in porous membrane reactors: An experimental study

As already mentioned in the previous sections, membrane reactors with large characteristic length (inner diameter), typically suffer from mass transfer limitations in G-L-S reactions. This is due to the laminar flow; radial diffusion is the dominant mechanism for the transport of the reactant from liquid bulk to the reactor wall. To suppress these limitations, in the previous section (3.2), the miniaturization of the channel diameter was applied, which improved the external mass transfer characteristics in the reactor. In this section, we propose integrated slug-flow (inert) in the membrane reactor channel, in order to enhance mixing and mass transfer (Figure 3.10).

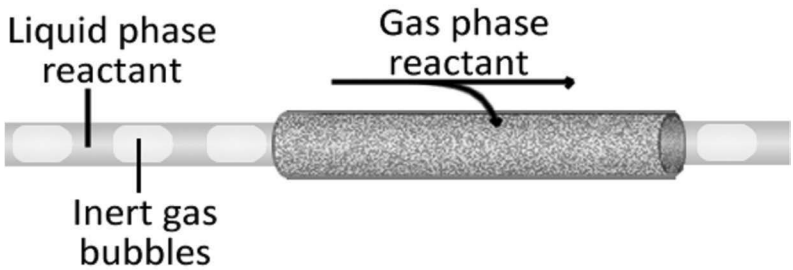

Figure 3.10: Slug flow in a membrane reactor for G-L-S reactions.

Slug flow (Taylor-flow) is a favorable pattern for microreactors. With this flow pattern, torroidal vortices are formed in the liquid slugs between the bubbles (see Figure 1.4), which improves mixing in the microchannel. In microfluidics, slug flow patterns are used for enhancement of transport, i.e. for biosensors[38], but more commonly in G-L(-S) chemistry it is used as a source for the gaseous reactant (disperse phase microreactors)[20,21,24].

With the present study, we aim to merge the advantages of the dispersed phase microreactors (slug flow pattern) with the advantages of the membrane reactors. Taylor-flow is obtained in the reactor channel using inert gas bubbles (air), while the gaseous reactant is supplied through the porous membrane wall directly to the reaction zone.

3.3.1 Experimental

3.3.1.1 Reactor preparation

The prepared tubular reactor had an inner diameter of 2.8 mm and a length 13.5 cm. For the reactor preparation, same materials were used and same preparation methods (γ-Al_2O_3 catalyst support coating, palladium catalyst deposition and selective hydrophobization) were carried out as in Section 3.2.

3.3.1.2 Reactor operation

In this experimental study two operation modes were carried out (Figure 3.11): *Continuous Flow* and *Inert Slug Flow*.

In both operation modes, the liquid phase consisted of an aqueous nitrite (NO_2^-) solution (50 mg/l). Liquid flow rates were 0.1, 0.2 and 0.3 ml/min. The gaseous reactant hydrogen (H_2) was fed to the shell side of the porous membrane reactor, as demonstrated in Figure 3.11. In the *Continuous Flow* operation mode (standard membrane reactor operation as in Section 3.2), only liquid reactant was flown in the tube side of the reactor. In the *Inert Slug Flow* operation mode, an inert gas phase was dispersed in the liquid phase and the created slug flow was fed to the tube side

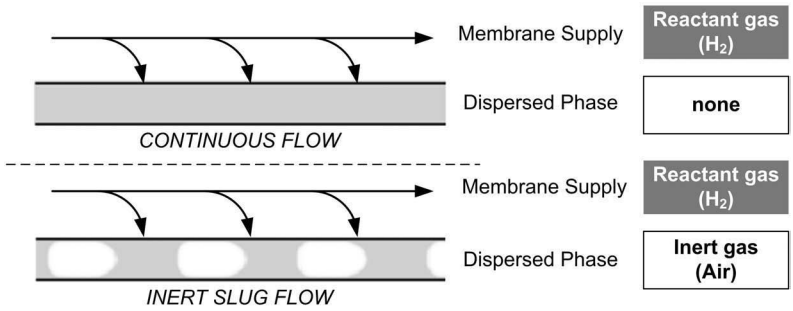

Figure 3.11: Reactor operation modes: *(top)* Continuous Flow, *(bottom)* Inert Slug Flow.

of the reactor. The same reactor (prepared as decribed in Section 3.2) was used for both operation modes.

In order to create the slug flow, the liquid phase and the inert gas phase were fed to a y-mixer by using two separate syringes. The inert gas phase consisted of air at a gas/liquid flow ratio of 1/1 for all the experiments.

The product at the reactor outlet was collected in a reservoir and injected manually to an ion chromatograph (Dionex ICS 1000) for analysis.

3.3.1.3 Results and Discussion

Figure 3.12 shows the nitrite (NO_2^-) conversion values for *Continuous* and *Inert Slug Flow* modes for three different liquid flow rates. We must remark that in the *Inert Slug Flow* mode the inert gas/liquid flow rate was 1/1. This means that the residence time of the NO_2^- reactant in this operation mode was half the residence time of it in *Continuous* mode.

As can be seen from Figure 3.12, the NO_2^- conversion values are significantly higher in the *Inert Slug Flow* mode for each flow rate. The comparable conversion values for 0.1 ml/min *Continuous Flow* and 0.2 ml/min *Inert Slug Flow* show that for these operation conditions the slug flow induced mixing enhances the reactor performance by $\sim$2 times. In addition, since the residence time of the *Inert Slug Flow* was half of the *Continuous Flow*, the conversion enhancement can be considered as $\sim$4 times higher for the *Inert Slug Flow*.

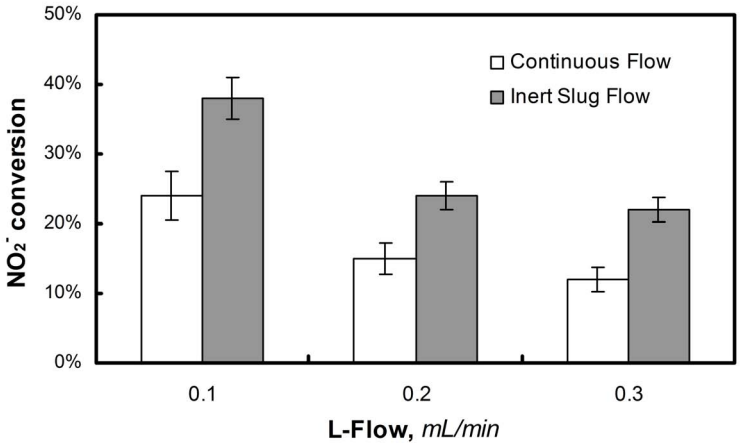

Figure 3.12: Reactor performances for Continuous Flow and Inert Slug Flow operation modes: NO_2^- conversion as a function of liquid flow rate (Initial NO_2^- concentration=50 mg/l).

These results clearly demonstrate the benefits of introducing slug flow (even inert) in a membrane reactor. The slug flow improves external mass transfer properties in the liquid phase, which is a major drawback for membrane reactors.

3.4 Conclusions

In this work, we studied the influence of geometrical and operational parameters on the performance of ceramic (Al_2O_3) membrane microreactors in gas-liquid-solid (G-L-S) reactions. These reactors are beneficial for multiphase reactions because of their well-controlled and stabilized G-L-S interface.

We prepared porous tubular membrane reactors by integrating a γ–Al_2O_3 layer as catalyst support, depositing palladium (Pd) catalyst and performing a selective hydrophobization technique. We obtained reactors with various inner diameters, controllable catalyst support thickness and active Pd surface area, and tunable wetting properties. The prepared catalytic reactors were tested with the Pd-catalyzed hydrogenation of nitrite as a model reaction for different operational parameters

(liquid flow rate and initial concentration).

Section 3.2 shows that the NO_2^- conversion rates per active catalyst surface area were significantly higher for thinner catalyst support coatings. The results indicated that with the increasing thickness of the γ–Al_2O_3 catalyst support the reactors suffer from internal mass transfer limitations, which is due to the small pore sizes and high tortuosity of γ–Al_2O_3. Furthermore, reactors with smaller inner diameter (0.8 mm) showed higher NO_2^- conversion rates per active Pd surface than the ones with bigger inner diameter (2.8 mm). This shows that the miniaturization of the characteristic length and therefore the diffusion path in the liquid phase enhances the performance in these reactors thanks to the improved external mass transfer properties.

Section 3.3 describes the integration of slug flow in a membrane reactor for a G-L-S reaction. This design merges the advantages of dispersed phase concept and a membrane reactor. The results in this study clearly showed that the performance of a membrane reactor can be significantly improved by integrating slug flow (Taylor-flow) in the reactor channel. With the combination of these concepts, the slug flow improves the mixing in the liquid phase, while the gaseous reactant is very efficiently supplied to the reaction zone thanks to the porous membrane, thereby avoiding possible depletion. The combination of membrane and microreactor technology has an interesting potential for G-L-S reactions. The miniaturization of the membrane reactors is an easy approach to reduce the mass transfer limitations in these types of reactors, while microreactors benefit from well-defined G-L-S interface with membrane technology.

3.5 Acknowledgements

We are grateful to K. Altena -Schildkamp, J.A.M. Vrielink, M. Luiten-Olieman, B. Geerdink and C. Reed for analysis, technical support and fruitful discussions.

Bibliography

[1] J. K. Chinthaginjala. *Hairy foam : thin layers of carbon nanofibers as catalyst support for liquid phase reactions.* PhD thesis, Enschede, University of Twente, June 2010. 49, 51, 59

[2] P.A.Ramachandran and R.V. Chaudhari. *Three-phase catalytic reactors.* Gordon and Breach Science, 1983.

[3] F. Larachi M.P. Dudukovic and P.L. Mills. Multiphase catalytic reactors: a perspective on current knowledge and future trends. *Catalysis Reviews*, 44(1):123–246, 2002. 49

[4] R. Dittmeyer, V. Hollein, and K. Daub. Membrane reactors for hydrogenation and dehydrogenation processes based on supported palladium. *Journal of Molecular Catalysis A: Chemical*, 173(1-2):135 – 184, 2001. 49

[5] R. Dittmeyer, K. Svajda, and M. Reif. A review of catalytic membrane layers for gas/liquid reactions. *Topics in Catalysis*, 29:3–27, 2004.

[6] A. G. Dixon. Recent research in catalytic inorganic membrane reactors. *International Journal of Chemical Reactor Engineering*, 1(R6), 2003.

[7] J. Coronas and J. Santamaria. Catalytic reactors based on porous ceramic membranes. *Catalysis Today*, 51(3-4):377 – 389, 1999.

[8] M. Vospernik, A. Pintar, G. Bercic, and J. Levec. Experimental verification of ceramic membrane potentials for supporting three-phase catalytic reactions. *Journal of Membrane Science*, 223(1-2):157 – 169, 2003. 64, 65

[9] M. Vospernik, A. Pintar, G. Bercic, J. Batista, and J. Levec. Potentials of ceramic membranes as catalytic three-phase reactors. *Chemical Engineering Research and Design*, 82(5):659 – 666, 2004. 49

[10] J. Peureux, M. Torres, H. Mozzanega, A. Giroir-Fendler, and J-A. Dalmon. Nitrobenzene liquid-phase hydrogenation in a membrane reactor. *Catalysis Today*, 25(3-4):409 – 415, 1995.

[11] W.N. Lau, K.L. Yeung, X.F. Zhang, and R. Martin-Aranda. Zeolite membrane microreactors and their performance. In J. Chen R. Xu, Z. Gao and W. Yan, editors, *From Zeolites to Porous MOF Materials - The 40th Anniversary of International Zeolite Conference, Proceedings of the 15th International Zeolite Conference*, volume 170 of *Studies in Surface Science and Catalysis*, pages 1460 – 1465. Elsevier, 2007.

[12] A. Julbe, D. Farrusseng, and C. Guizard. Porous ceramic membranes for catalytic reactors – overview and new ideas. *Journal of Membrane Science*, 181(1):3 – 20, 2001.

[13] A. Pashkova, R. Dittmeyer, N. Kaltenborn, and H. Richter. Experimental study of porous tubular catalytic membranes for direct synthesis of hydrogen peroxide. *Chemical Engineering Journal*, 165(3):924 – 933, 2010. 49, 65

[14] H. C. Aran, J. K. Chinthaginjala, R. Groote, T. Roelofs, L. Lefferts, M. Wessling, and R. G. H. Lammertink. Porous ceramic mesoreactors: A new approach for gas-liquid contacting in multiphase microreaction technology. *Chemical Engineering Journal*, 169(1-3):239 – 246, 2011. 49, 50

[15] K. Jahnisch, V. Hessel, H. Lowe, and M. Baerns. Chemistry in microstructured reactors. *Angewandte Chemie International Edition*, 43(4):406–446, 2004. 49

[16] A. Gavriilidis, P. Angeli, E. Cao, K. K. Yeong, and Y. S. S. Wan. Technology and applications of microengineered reactors. *Chemical Engineering Research and Design*, 80(1):3 – 30, 2002. 49

[17] K.K. Yeong, A. Gavriilidis, R. Zapf, and V. Hessel. Catalyst preparation and deactivation issues for nitrobenzene hydrogenation in a microstructured falling film reactor. *Catalysis Today*, 81(4):641 – 651, 2003. 50, 52, 61

[18] C. Amador, D. Wenn, J. Shaw, A. Gavriilidis, and P. Angeli. Design of a mesh microreactor for even flow distribution and narrow residence time distribution. *Chemical Engineering Journal*, 135(Supplement 1):S259 – S269, 2008. 50

[19] S. McGovern, G. Harish, C.S. Pai, W. Mansfield, J.A. Taylor, S. Pau, and R.S. Besser. Multiphase flow regimes for hydrogenation in a catalyst-trap microreactor. *Chemical Engineering Journal*, 135:S229 – S236, 2008. 50

[20] M. T. Kreutzer, F. Kapteijn, J. A. Moulijn, and J. J. Heiszwolf. Multiphase monolith reactors: Chemical reaction engineering of segmented flow in microchannels. *Chemical Engineering Science*, 60(22):5895 – 5916, 2005. 50, 66

[21] V. Hessel, P. Angeli, A. Gavriilidis, and H. Lowe. Gas-liquid and gas-liquid-solid microstructured reactors: Contacting principles and applications. *Industrial & Engineering Chemistry Research*, 44(25):9750–9769, 2005. 50, 66

[22] M. N. Kashid and L. Kiwi-Minsker. Microstructured reactors for multiphase reactions: State of the art. *Industrial & Engineering Chemistry Research*, 48(14):6465–6485, 2009.

[23] G. Chen, J. Yue, and Q. Yuan. Gas-liquid microreaction technology: Recent developments and future challenges. *Chinese Journal of Chemical Engineering*, 16(5):663 – 669, 2008.

[24] V. Hessel, S. Hardt, and H. Lowe. *Chemical Micro Process Engineering: Fundamentals, Modelling and Reactions, Sections 5.1-5.3*, pages 577–619. Wiley-VCH Verlag GmbH & Co. KGaA, 2005. 50, 66

[25] C. P. Park and D.-P. Kim. Dual-channel microreactor for gas-liquid syntheses. *Journal of the American Chemical Society*, 132(29):10102–10106, 2010. 50

[26] J. K. Chinthaginjala, J. H. Bitter, and L. Lefferts. Thin layer of carbon-nano-fibers (CNFs) as catalyst support for fast mass transfer in hydrogenation of nitrite. *Applied Catalysis A: General*, 383(1-2):24 – 32, 2010. 51, 60, 64

[27] J.K. Chinthaginjala and L. Lefferts. Support effect on selectivity of nitrite reduction in water. *Applied Catalysis B: Environmental*, 101(1-2):144 – 149, 2010. 51

[28] R. Zapf, C. Becker-Willinger, K. Berresheim, H. Bolz, H. Gnaser, V. Hessel, G. Kolb, P. Lob, A.-K. Pannwitt, and A. Ziogas. Detailed characterization of various porous alumina–based catalyst coatings within microchannels and their testing for methanol steam reforming. *Chemical Engineering Research and Design*, 81(7):721 – 729, 2003. 52

[29] M.W.J. Luiten, N.E. Benes, C. Huiskes, H. Kruidhof, and A. Nijmeijer. Robust method for micro-porous silica membrane fabrication. *Journal of Membrane Science*, 348(1-2):1–5, 2010. 53

[30] H.S. Fogler. *Elements of Chemical Reaction Engineering*. Prentice Hall, 1999. 58, 59

[31] R. E. Hayes, B. Liu, R. Moxom, and M. Votsmeier. The effect of washcoat geometry on mass transfer in monolith reactors. *Chemical Engineering Science*, 59(15):3169 – 3181, 2004. 59

[32] G.F. Froment and K.B. Bischoff. *Chemical Reactor Analysis and Design*. Wiley, 1990. 59

[33] K.C. Metaxas and N.G. Papayannakos. Studying the internal mass transfer phenomena inside a Ni/Al_2O_3 catalyst for benzene hydrogenation. *Chemical Engineering Journal*, 140(1-3):352 – 357, 2008. 61

[34] Y. Matatov-Meytal, V. Barelko, I. Yuranov, and M. Sheintuch. Cloth catalysts in water denitrification: I. Pd on glass fibers. *Applied Catalysis B: Environmental*, 27(2):127 – 135, 2000. 61

[35] A. Pintar, G. Bercic, and J. Levec. Catalytic liquid-phase nitrite reduction: Kinetics and catalyst deactivation. *AIChE Journal*, 44(10):2280–2292, 1998. 61

[36] R. Gorges, S. Meyer, and G. Kreisel. Photocatalysis in microreactors. *Journal of Photochemistry and Photobiology A: Chemistry*, 167(2-3):95–99, 2004. 63

[37] J.M. Jani, M. Wessling, and R.G.H. Lammertink. Geometrical influence on mixing in helical porous membrane microcontactors. *Journal of Membrane Science*, In Press, Corrected Proof:–, 2011. 65

[38] M. Fumagalli, V. van Steijn, C.R. Kleijn, L.C.P.M. de Smet, E.J.R. Sudholter, and M.T. Kreutzer. Enhancement of transport in biosensing using flow segmentation. *Proceedings of the 1st European conference on Microfluidics, Italy*, 2008. 66

Chapter 4

Porous metallic microreactors with carbon nanofibers

A REVISED VERSION OF THIS CHAPTER HAS BEEN PUBLISHED:

H.C. Aran, S. Pacheco Benito, M.W.J. Luiten-Olieman, S. Er, M. Wessling, L. Lefferts, N.E. Benes, and R.G.H. Lammertink, Carbon nanofibers in catalytic membrane microreactors, *Journal of Membrane Science*, 381(1-2), 244–250, 2011.

ABSTRACT

In this study, we report on the fabrication and operation of new hybrid membrane microreactors for gas-liquid-solid (G-L-S) reactions. The presented reactors consist of porous stainless steel tubes onto which carbon nanofibers (CNFs) are grown as catalyst support, all encapsulated by a gas permeable coating. Such reactors benefit from a controlled G-L-S interface of a membrane reactor and high surface area of carbon nanofibers as catalyst support. Preparation steps such as porous stainless steel hollow fiber fabrication, CNF growth on the stainless steel surface, palladium catalyst immobilization and an outer gas permeable polymeric coating steps are presented. The fabricated microreactors have high surface area, mechanical strength and catalytic activity for nitrite reduction in water. Results proved high nitrite reduction performance of these reactors, even without the presence of palladium (Pd) or additional hydrogen (H_2) supply. Our results suggest intrinsic reductant properties and catalytic activity of the reactors, which make them very suitable for hydrogenation reactions.

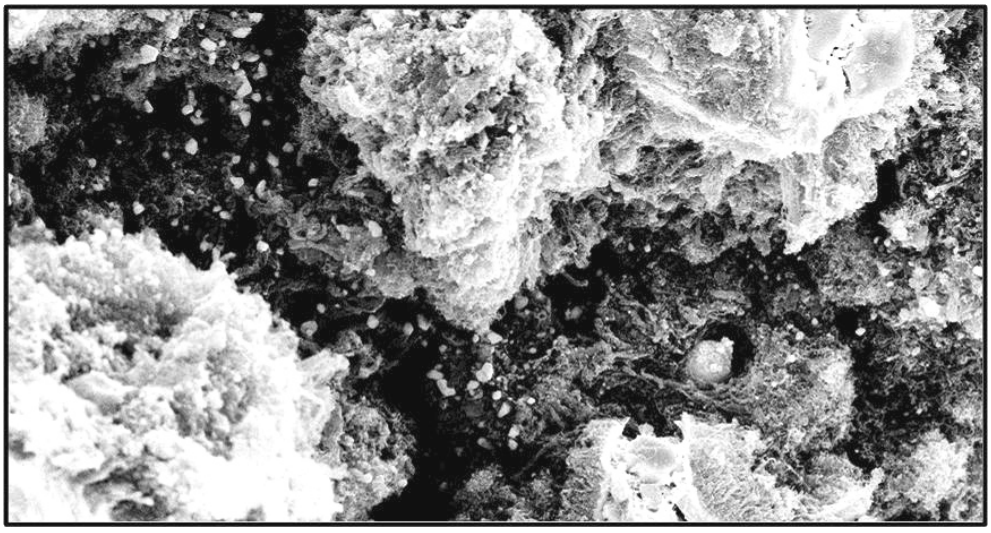

4.1 Introduction

Microreactors are miniaturized devices for carrying out chemical reactions, which in recent years have become favorable for chemical technology due to their small dimensions (characteristic length). The high surface to volume ratio in these devices provide them improved heat and mass transfer compared to macro-scale reactors[1–5]. In this study, we particularly focus on heterogeneously catalyzed gas-liquid-solid (G-L-S) reactions in microreactors. Typical reactor designs applied for these reaction systems are the falling film microreactors[4,5], dispersed phase microreactors[6], catalyst trap microreactors[7] and mesh microreactors[8,9].

Recently, we demonstrated an alternative membrane reactor design for these reactions in microsystems[1]. In contrast to most of the other designs, in membrane reactors the gas and liquid phases are contacted precisely where the solid catalyst is located. These phases can be independently controlled during the process and the gas-liquid interface is well-defined and stabilized by the membrane[10–12]. In Chapters 2 and 3, we performed the contacting of the gas and liquid reactants using a porous ceramic (Alumina-Al_2O_3) membrane, which also acts as support for the solid (S) catalyst. The stabilization of the G-L-S interface in the porous Al_2O_3 membrane was obtained by a selective surface modification technique.

The aim of the present work is to utilize porous metallic materials with carbon nanofibers (CNFs) as catalyst support for a G-L-S reaction process using a membrane reactor concept: Porous metallic microreactors (Figure 4.1). Carbon nanofibers (CNFs) are very promising materials as catalyst support, which is due to their favorable physical and chemical characteristics. CNFs have a high surface area (>100 m^2/g) and large pore volumes (>0.5 cm^3/g) leading to low tortuosity and efficient internal mass transfer. Moreover, CNFs are mechanically strong and chemically inert[13–19].

In our concept (Figure 4.1), the liquid flows in the tube side of the hollow fiber and the contact between the liquid and gas phases takes place on the porous hollow fiber (in microscale) where the CNF catalyst support is located. The outer surface of the

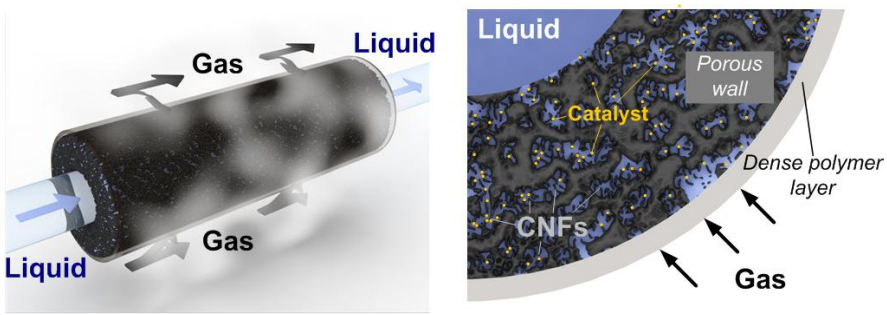

Figure 4.1: Gas-liquid contacting in porous metallic microreactors for multiphase reactions: Porous stainless steel membrane decorated with carbon nanofibers (CNFs) as catalyst support. Reactor encapsulated with a selective, gas permeable PDMS layer.

porous hollow fiber is covered with a dense gas permeable polymeric coating in order to stabilize the G-L-S interface. In this concept, the gas is continuously supplied to the reaction zone through the membrane along the whole length of the reactor. The developed reactor is tested for a model multiphase reaction, the catalytic reduction of nitrite ions in water.

4.2 Experimental

4.2.1 Materials

Stainless steel powder (316L, Epson Atmix Corporation, D50, particle size = 4.17 μm), polyethersulfone (PES; Ultrason, 6020P) and N-methylpyrrolidone (NMP; 99,5wt%, Aldrich) were used for the stainless steel suspension preparation. PES and the stainless steel powder were dried prior to use. The other chemicals were used without further treatment. Hydrogen, nitrogen (99.999%, Praxair), and ethylene (99.95%, Praxair) were used for CNFs formation without further purification. Palladium(II) 2,4-pentanedione ($Pd(acac)_2$; Alfa Aesar, 34.7%) and toluene (Merck) were used for the catalyst precursor solution. For the PDMS coating a General Electric PDMS RTV 615 kit was used (purchased from Permacol B.V.), which consisted of two components; a vinyl terminated pre-polymer (RTV-A) and a Pt-catalyzed cross-linker (RTV-B).

Toluene (Merck) was used as solvent for PDMS.

4.2.2 Reactor preparation

Four different types of samples were prepared: *SS* (Porous stainless steel hollow fibers), *SS+CNF* (Porous SS hollow fibers with carbon nanofibers (CNF)), *SS+CNF+Pd* (Porous SS hollow fibers with CNF and palladium (Pd)), *SSH2* (Porous SS hollow fibers with H_2 treatment (725°C)).

The preparation steps of the all samples are shown in Figure 4.2. All the samples were coated with PDMS (gas permeable) on the outer surface before operation in nitrite hydrogenation.

Fabrication of porous metallic hollow fibers: Modified from previous work[20], a stainless steel suspension consisting of 80 wt% stainless steel powder, 5 wt% PES (binder) and 15 wt% NMP (solvent) was prepared. The prepared suspension was

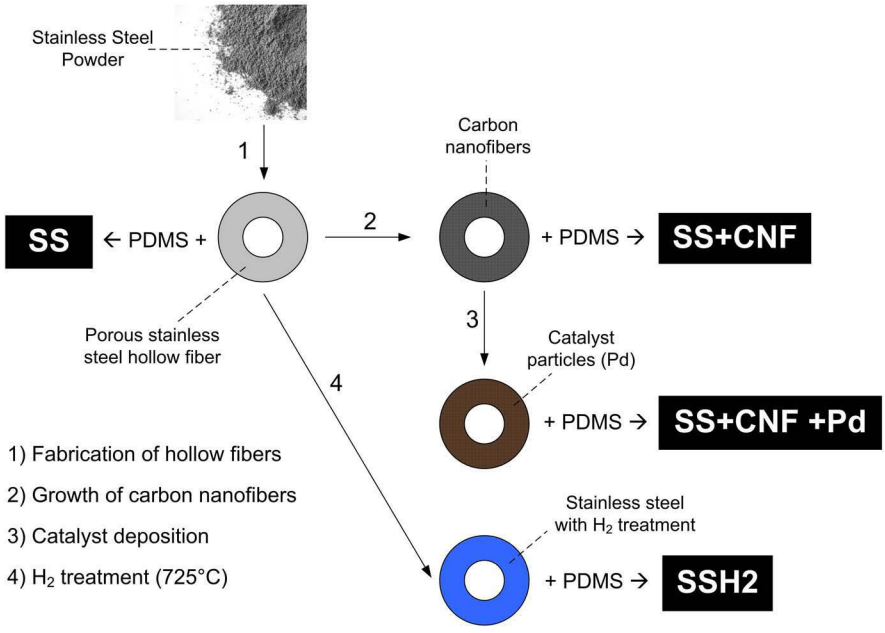

Figure 4.2: Preparation steps of porous metallic microreactors: Four samples with various properties (SS, SS+CNF, SS+CNF+Pd and SSH2) represented in cross-sectional view.

pressurized in a stainless steel vessel using nitrogen (2 bars) and pressed through a spinneret with an inner diameter of 0.8 mm and an outer diameter of 2.0 mm, followed by immersion in a coagulating bath. The air gap was 3 cm and de-ionized water was pressed through the bore of the spinneret (7 ml/min). The fibers were kept in a water bath for 1 day for removal of the NMP and consequently dried for 1 day. Finally, the samples were sintered at 1100°C for 30 min in N_2 atmosphere.

Growth of carbon nanofibers: Catalytic chemical vapor deposition method was used to grow carbon nanofibers (CNFs) on the surfaces of the porous stainless steel hollow fibers. The hollow fibers were placed in an in-house built 12 mm inner diameter quartz reactor. Based on previous work[17], the samples were heated up to 725°C (heating rate = 7.5°C/min) in diluted air (9% air and balance N_2). The total flow was always kept at 100 ml/min, unless otherwise mentioned. Next, they were treated with hydrogen (100%) for 2 h and then in diluted air (9% air and balance N_2) for 1 h at the same temperature. Then the temperature in the reactor was decreased to 700°C with N_2. For the growth of the CNFs a gas mixture of hydrogen and ethylene (C_2H_4) in N_2 was fed to the reactor (25% C_2H_4, 5% H_2 and balance N_2) for 2 h with a total flow of 200 ml/min. After the growth step, the samples were cooled down to room temperature under N_2 flow.

Lastly, an aqueous ultrasound treatment was applied to the samples in order to remove the loose carbon nanofibers from the metal surface, followed by a drying step under vacuum at 100°C overnight.

Catalyst deposition: The porous metallic hollow fiber with carbon nanofibers were immersed in a precursor solution consisting of 300 mg $Pd(acac)_2$ in 50 ml toluene for 24 h. Consequently, the samples were dried overnight at 50°C, calcined for 1 h and reduced for 1 h at 250°C.

SSH2 sample preparation (H_2 treatment): Same procedure was followed as for the growth of carbon nanofibers, where only the final growth step with the carbon source ethylene (C_2H_4) was skipped.

PDMS coating: Adapted from Dutczak et al.[21], a PDMS/toluene solution was pre-crosslinked before the coating procedure. RTV-A and RTV-B components (3.75

wt% in total) of the PDMS kit were dissolved in toluene and kept at 80°C for 2 h. Following that, the cross-linking reaction was continued at 60°C until the viscosity of the solution reached approximately 100 mPa·s. The viscosity measurements were carried out at 25°C with a Brookfield DV-II+ Pro viscometer using a spindle nr-61. The pre-crosslinked PDMS/toluene solution was coated at the outer surface of the hollow fiber using an automated set-up with an immersion/pull up velocity of 0.9 cm/s. The hollow fiber samples were dip-coated in the solution with a contact time of approximately 30 s, as described in detail elsewhere[21]. One end of the hollow fiber was sealed by glue prior to the coating step. Finally, the coated hollow fibers were placed in an oven at 60°C for 8 h to finalize the crosslinking reaction.

4.2.3 Reactor operation

The prepared reactors were tested for the catalytic reduction of nitrite (NO_2^-) ions in water (Figure 4.3). The conversion of NO_2^- ions in water and the formation of the reaction product ammonia (NH_4^+) were measured. An aqueous NO_2^- solution

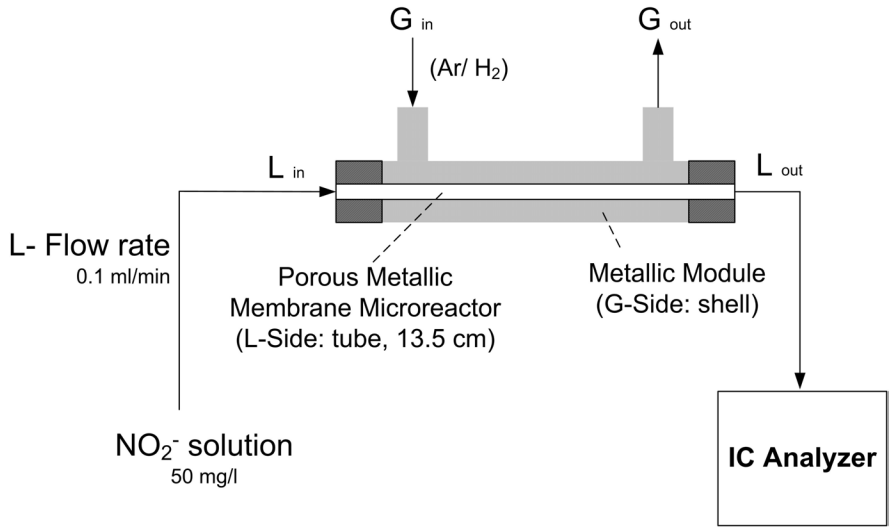

Figure 4.3: Schematic representation of the experimental setup and operational parameters.

with initial concentration 50 mg/l was prepared as the liquid reactant and fed to the microreactor (tube side) with a flow rate of 0.1 ml/min. Hydrogen (H_2) or Argon (Ar) was fed to the shell side of the reactor module (100 ml/min). The NO_2^- and NH_4^+ concentrations at the reactor in- and outlet were measured by an ion chromatograph (Dionex ICS 1000).

4.3 Results and Discussion

4.3.1 Reactor characterization

Figure 4.4 shows the cross-section of a sintered porous stainless steel hollow fiber. The hollow fiber has high mechanical strength together with high porosity. The wall of the hollow fiber (a) contains thin and long macrovoids. This structure is favorable for the diffusive transport of the NO_2^- reactant (liquid phase) in the porous structure during the operation, so that the immobilized catalyst is easily accessible for the liquid reactant. Furthermore, the outer skin of the hollow fiber (b) does not contain macro voids and presents a smoother and denser structure. This is beneficial for applying a thin and defect free PDMS layer in the later stage of reactor preparation. The BET surface area of the porous stainless steel hollow fibers was $\sim$0.4 m^2/g.

As can be seen in Figure 4.5, carbon nanofibers (CNFs) are successfully grown along the full cross-section of the porous stainless steel hollow fiber. The CNF deposition on the hollow fibers can be identified both visually and by SEM analysis (Figure 4.5). A clear difference in morphology can be seen between samples with and without CNFs. We also observe metal-nano-particles (iron, nickel) on the tip of the grown nanofibers (tip-growth[17,22]), as can be seen in Figure 4.6.a.

The weight increase due to the CNF growth was $\sim$16%. The BET surface area of the whole sample after the CNF growth was $\sim$21.3 m^2/g, significantly higher than before the growth. The surface area of only the carbon on the surface was calculated as $\sim$151 m^2/g, which is in the same range with values reported in the literature[14,18,19]. The EDX results (not shown here) qualitatively showed carbon content was highest near the outer skin of the sample, which is most likely because the packing density

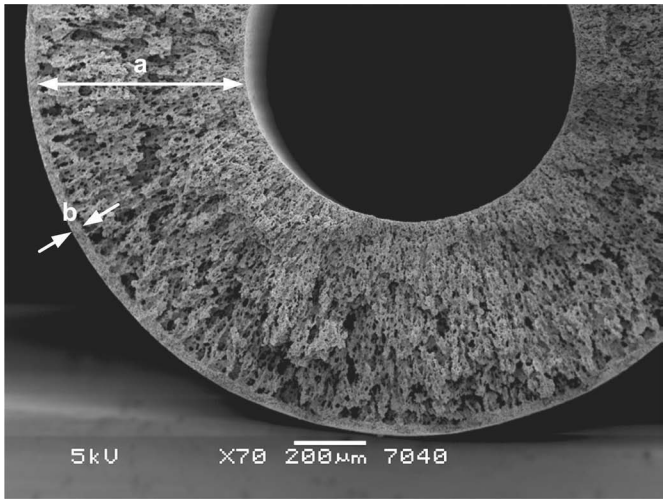

Figure 4.4: Cross-section of the porous stainless steel hollow fiber after the sintering step: *(a)* Wall of the hollow fiber with thin macrovoids, *(b)* Outer skin of the hollow fiber with a denser structure.

Figure 4.5: Porous stainless steel hollow fibers before *(left)* and after *(right)* the growth of the carbon nanofibers.

of porous stainless steel was higher at the outer skin compared to the inner wall of the hollow fiber (see Figure 4.4). This may also be caused by the better access of the hydrocarbon source (ethylene gas) to the outer surface of the porous hollow fiber during the CNF growth. The adhesion strength of the carbon nanofibers has been

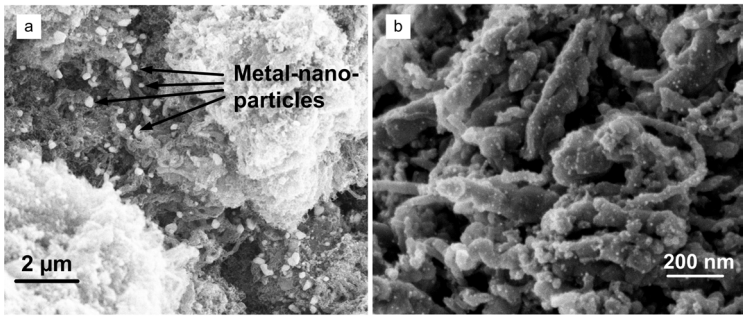

Figure 4.6: Carbon nanofibers grown on the porous stainless steel surface: *(a)* Metal- nano-particles (iron, nickel) on the tip of the grown CNFs, *(b)* Pd particles immobilized on the surface of CNFs.

investigated by an aqueous ultrasonic treatment and only a little amount of loose CNFs was released. No considerable weight loss was measured.

After the catalyst immobilization, the average Pd weight percentage on the sample was ∼0.1 wt% (measured by XRF). The immobilized Pd particles on the CNFs are displayed in Figure 4.6.b. Unfortunately, the Pd distribution along the cross-section of the hollow fiber could not be characterized by the EDX measurements due to the excessive amount of carbon on the stainless steel surface.

Each sample was coated with a selective PDMS layer before the operation. The thickness of the PDMS coating was ∼20 μm and was able to keep the liquid inside the microchannel at our operation conditions.

4.3.2 Reactor operation

Catalytic reduction (hydrogenation) of nitrite (NO_2^-) is chosen as a model reaction to test the developed microreactors. Hydrogenation of NO_2^- is known to be a fast reaction that induces mass transfer limitations. In addition, NO_2^- is a harmful compound for human health and removal of NO_2^- ions from water is environmentally relevant due to its increased amount in ground waters. During the catalytic reduction, NO_2^- is converted to nitrogen (N_2) and the undesired product ammonia (NH_4^+). The Pd-catalyzed hydrogenation of nitrite in the presence of hydrogen gas (H_2) typically takes place as follows[1,15,16,23,24].

$$2NO_2^- + 3H_2 \overset{Pd}{\rightarrow} N_2 + 2OH^- + 2H_2O \quad (4.1)$$

$$2NO_2^- + 6H_2 \overset{Pd}{\rightarrow} 2NH_4^+ + 4OH^- \quad (4.2)$$

In the present study, the conversion of $NO_2{}^-$ and the formation of $NH_4{}^+$ are measured to characterize the performance of our reactors. Our main performance criterion in this model reaction is the $NO_2{}^-$ conversion. The concentration of $NH_4{}^+$ is only measured to confirm the $NO_2{}^-$ reduction process.

Figure 4.7 shows an overview of the $NO_2{}^-$ conversion results for the prepared reactors *SS* (stainless steel), *SS+CNF* (stainless steel + carbon nanofibers) and *SS+CNF+Pd* (stainless steel + carbon nanofibers + palladium) with the supply of H_2 as gaseous reactant or argon (Ar) as inert gas to the shell side of the membrane reactor.

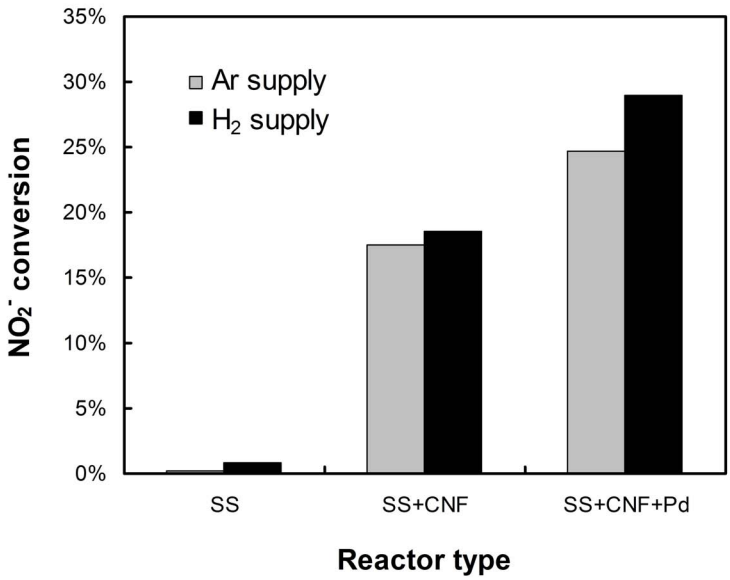

Figure 4.7: Nitrite reduction performances (liquid flow rate= 0.1 ml/min, initial nitrite concentration= 50 mg/l) of the prepared microreactors: SS (stainless steel), SS+CNF (stainless steel with carbon nanofibers), SS+CNF+Pd (stainless steel with carbon nanofibers and palladium catalyst).

Results demonstrate that the reactor *SS+CNF+Pd* shows the highest nitrite reduction performance. The *SS* reactor shows no considerable activity for the conversion of NO_2^-. On the other hand, with the *SS+CNF* reactor almost 20% of the NO_2^- ions in the initial reaction solution is reduced, even though no Pd catalyst is present in the reactor, which will be discussed later. For the *SS+CNF* and *SS+CNF+Pd* reactors formation of the reaction product ammonia (NH_4^+) was observed. The selectivity values to NH_4^+ under H_2 supply were ∼49% (*SS+CNF*) and ∼67% (*SS+CNF+Pd*). The NH_4^+ production with the *SS* reactor was negligible.

An extraordinary result is that the reaction was also taking place even without the supply of the reactant gas H_2 to the reactor (Figure 4.7- Ar supply). Both *SS+CNF* and *SS+CNF+Pd* reactors converted significant amounts of NO_2^- and formed NH_4^+.

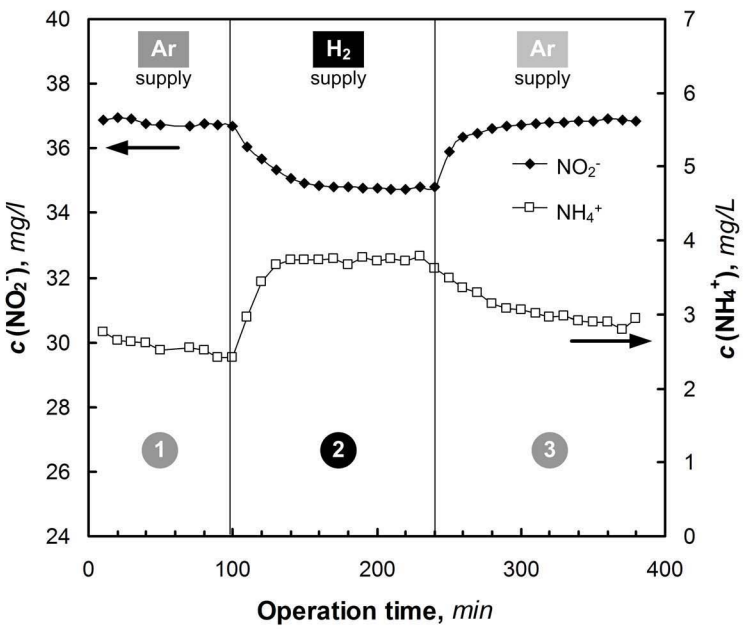

Figure 4.8: Effect of the gas phase composition on the performance of SS+CNF+Pd reactor (stainless steel with carbon nanofibers and palladium catalyst): $c(NO_2^-)$, $c(NH_4^+)$= Concentrations of nitrite (reactant) and ammonia (reaction product) at the reactor outlet. (Liquid flow rate= 0.1 ml/min, initial nitrite concentration= 50 mg/l).

Experiments show that for the *SS+CNF* reactor the conversion of NO_2^- and the formation of NH_4^+ are comparable for the experiments with and without H_2 supply. The only considerable contribution of the H_2 supply on the reactor performance is observed for the reactor *SS+CNF+Pd*, which is due to the presence of Pd as hydrogenation catalyst (Figure 4.8).

Figure 4.8 displays the changes in concentration of NO_2^- and NH_4^+ at the reactor outlet with and without H_2 supply during the operation. At the initial stage of the experiment (1), the reaction proceeds under inert argon (Ar) flow in the gas side, resulting in a NO_2^- conversion of ∼25%. When the gas phase composition is switched to pure H_2 (2), the final NO_2^- concentration decreases indicating a higher NO_2^- conversion of ∼30%. Moreover, the concentration of NH_4^+ increases. At the final stage of the experiment (3), when the H_2 gas is substituted again with Ar, the outlet concentrations of NO_2^- and NH_4^+ reach the same values as the initial stage of the experiment.

In all of our reactors, *SS*, *SS+CNF* and *SS+CNF+Pd*, a decrease in the NO_2^- concentration and a simultaneous increase in the NH_4^+ concentration is observed. However, the reactors show significantly different NO_2^- conversion rates (ξ), as $\xi(SS) << \xi\ (SS{+}CNF) < \xi(SS{+}CNF{+}Pd)$. Interestingly, the reaction also proceeds in the absence of external hydrogen supply, as shown in Figure 4.7. Additionally, in reactor *SS+CNF* no Pd catalyst is present, but the NO_2^- conversion still proceeds drastically, even at lower rates compared to the *SS+CNF+Pd* reactor. The remarkable performance of our reactors in the absence of hydrogen gas or Pd catalyst is discussed in the next paragraphs.

Firstly, during the growth of CNFs the porous stainless steel fibers were exposed to H_2 gas for more than 1 h at elevated temperatures (T≥700°C). This method of CNF growth may be responsible for the storage of hydrogen inside the metal bulk of our microreactors. It is well known that some metals and metal alloys, when exposed to hydrogen gas, form metal hydrides and store significant amounts of hydrogen. The formation of the hydrides takes place by adsorption of hydrogen on the metal surface and formation of a solid hydrogen solution phase in the metal, followed by

the growth of the metal hydride phase[25–27]. In our case, the stainless steel contains large amounts of Fe, Ni and Cr. The hydrides of these metal mixtures may form as a result of the exposure to hydrogen gas at high temperatures. Later, during the NO_2^- conversion reaction, these metal hydrides may act as an additional source of hydrogen and release their stored hydrogen into the reaction medium. Previous studies show that the metal hydrides act both as a catalyst and as a hydrogen source. Snijder et al.[28], in their cyclohexene hydrogenation reaction, observed that the complex metal hydride ($LaNi_{5-x}Al_xH_n$) acted as an additional source of hydrogen.

To understand whether the metal components of our microreactors can act as a source of hydrogen, we prepared the *SSH2* reactor. The *SSH2* reactor, similar to the *SS* reactor, does not contain any CNFs but involves a pretreatment step under hydrogen atmosphere at 725°C. Using the *SSH2* reactor, we performed the NO_2^- conversion experiments with and without an external hydrogen gas source. The observed NO_2^- conversion values were small: 3 and 2%, respectively for the cases with and without external hydrogen supply. Additionally, at the outlet of the *SSH2* reactor a considerable amount of NH_4^+ concentration (up to 0.2 mg/l) was observed, which was notably higher than the *SS* reactor that was prepared with no hydrogen pretreatment step. These results support the idea that the storage of atomic hydrogen inside the metal compartments of our microreactors is possible, however the reactor performance was significantly lower than that of *SS+CNF* reactors. Obviously, the presence of CNFs is crucial for the efficiency of our microreactors.

Secondly, carbon nanofibers (CNFs) and carbon nanotubes (CNTs) are known to store hydrogen via physisorption. Accordingly, the binding energy of hydrogen to these materials is low and hydrogen storage takes place only under specific conditions, such as low temperatures and high hydrogen pressures[29–32]. Since our experiments were performed at room temperature and under low or no hydrogen gas pressure, we assume that the amount of physisorbed hydrogen on the CNFs inside our microreactors is very limited.

Thirdly, the reductive properties of metal particles on the CNFs with high surface area may be responsible for the NO_2^- reduction process. CNFs are known to grow

catalytically on metal surfaces, particularly on iron (Fe), nickel (Ni) and cobalt (Co)[13–15,22]. In this study, the preparation of the porous stainless steel hollow fibers was carried out with 316L powder, consisting of ∼67% Fe and ∼13% Ni (Epson Atmix Corporation). These metals promote the CNF growth on the porous stainless steel surface with the help of a carbon source, in our case ethylene. Typically, the growth of CNFs occurs by deposition of carbon under these metal growth-catalysts (Fe, Ni). Therefore, the metal particles are squeezed out of the surface and stay at the tip of the fibers (tip growth)[17,22]. Accordingly, in our case, the CNFs do not only support the Pd catalyst, but also contain other metal-nano-particles (Fe, Ni) in an open and available form on their surfaces (Figure 4.6.a), although part of the particles may be encapsulated by carbon.

Among these particles, literature studies show that metallic iron (Fe^0) particles act as a reductant of nitrite ($NO_2{}^-$) and nitrate ($NO_3{}^-$) ions in water, where an additional supply of hydrogen gas is not present[33–37]. Similarly, iron particles in their oxidized state (Fe^{2+}) were reported to act as a reducing agent[35,36]. According to Hu et al.[34], the $NO_2{}^-$ reduction process can occur by the direct reduction on Fe^0, or by the indirect reduction with the hydrogen that is generated from the proton reduction reaction of Fe^0. They showed that the reaction takes place much faster in acidic conditions, rather than in neutral or alkaline conditions[34]. In our study, no pH adjustment was carried out. Similarly, Liang et al.[33] used nanoscale Fe^0 for the $NO_2{}^-$ reduction, however they did not observe a dependence on pH of the initial $NO_2{}^-$ solutions. They suggested the following reduction mechanism for the nitrite ions in water:

$$3Fe^0 + NO_2^- + 8H^+ \rightarrow 3Fe^{2+} + NH_4^+ + 2H_2O \tag{4.3}$$

$$3Fe^0 + 2NO_2^- + 8H^+ \rightarrow 3Fe^{2+} + N_2 + 4H_2O \tag{4.4}$$

$$Fe^0 + NO_2^- + 6H_2O \rightarrow 3Fe(OH)_2 + NH_4^+ + 2OH^- \tag{4.5}$$

We observe that the conversion values of our *SS+CNF* microreactor is significantly

higher than that of our SS microreactor, revealing that the presence of the CNFs is very important in the conversion process. The CNFs do not only increase the surface area, but also increase the availability of metal particles, particularly Fe. The total amount of Fe within the reactors is approximately 12 mmol (reactor weight without CNFs = 1 g), while the calculated reduction rate of nitrite using the *SS+CNF* reactor is only $2{\cdot}10^{-5}$ mmol/min. Evidently, not all of iron inside our reactors is available for reaction. Still, even if 1% of the Fe in the reactor is available for the nitrite reduction, the reactor can be operated for 100 h until this effect will end.

Accordingly, these metal nanoparticles on the tips of the CNFs shall be responsible for the reduction of $NO_2{}^-$ in our microreactors with H_2 supply, noticeably more than the other factors discussed in here.

4.4 Conclusions

In this study, porous metallic microreactors with carbon nanofibers (CNFs) catalyst support were developed and applied for catalytic nitrite ($NO_2{}^-$) reduction in water. Porous stainless steel (SS) hollow fibers with high porosity and mechanical strength were fabricated and CNFs with high surface area were successfully grown on the porous SS surface. For particular samples, also palladium (Pd) catalyst was immobilized on the CNFs as a hydrogenation catalyst. Finally, all the reactors were encapsulated with a gas permeable polymeric coating. The fabricated microreactors showed to have a high surface area, mechanical strength and catalytic activity, which was tested for the catalytic reduction of nitrite ($NO_2{}^-$) reaction.

The presence of the CNF on the SS surface had a significant effect on the reactor performance. Even without the presence of H_2 and Pd, the $NO_2{}^-$ ions were successfully reduced, which was confirmed by the disappearance of $NO_2{}^-$ reactant and formation of ammonia ($NH_4{}^+$). These results indicate the reductive properties of the reactor material. We proposed that the reductive properties of iron (Fe) particles, which are located on the tip of the grown CNFs, shall be responsible for the reduction of $NO_2{}^-$ without hydrogen supply.

We also demonstrated that in our Pd-immobilized reactors the NO_2^- reduction proceeds by both catalytic reduction (with Pd and H_2) and by the reactor material itself (i.e., by Fe on CNFs). Eventually, the latter effect will exhaust in time and the reaction will still proceed with the immobilized Pd-catalyst on the CNFs and the membrane-assisted supply of H_2.
In short, we show that the porous metallic microreactors decorated with carbon nanofibers are suitable materials for the reduction of nitrite and the reactor design is very promising for the multiphase microreactor technologies.

4.5 Acknowledgements

We are grateful to K. Altena -Schildkamp, J.A.M. Vrielink, M. A. Smithers, B. Geerdink, J. Bennink (Tingle.nl) and C. Reed for analysis, technical support, images and fruitful discussions.

Bibliography

[1] H. C. Aran, J. K. Chinthaginjala, R. Groote, T. Roelofs, L. Lefferts, M. Wessling, and R. G. H. Lammertink. Porous ceramic mesoreactors: A new approach for gas-liquid contacting in multiphase microreaction technology. *Chemical Engineering Journal*, 169(1-3):239 – 246, 2011. 75, 82

[2] M. N. Kashid and L. Kiwi-Minsker. Microstructured reactors for multiphase reactions: State of the art. *Industrial & Engineering Chemistry Research*, 48(14):6465–6485, 2009.

[3] A. Gavriilidis, P. Angeli, E. Cao, K. K. Yeong, and Y. S. S. Wan. Technology and applications of microengineered reactors. *Chemical Engineering Research and Design*, 80(1):3 – 30, 2002.

[4] V. Hessel, P. Angeli, A. Gavriilidis, and H. Lowe. Gas-liquid and gas-liquid-solid microstructured reactors: Contacting principles and applications. *Industrial & Engineering Chemistry Research*, 44(25):9750–9769, 2005. 75

[5] V. Hessel, S. Hardt, and H. Lowe. *Chemical Micro Process Engineering: Fundamentals, Modelling and Reactions, Sections 5.1-5.3*, pages 577–619. Wiley-VCH Verlag GmbH & Co. KGaA, 2005. 75

[6] M. T. Kreutzer, F. Kapteijn, J. A. Moulijn, and J. J. Heiszwolf. Multiphase monolith reactors: Chemical reaction engineering of segmented flow in microchannels. *Chemical Engineering Science*, 60(22):5895 – 5916, 2005. 75

[7] S. McGovern, G. Harish, C.S. Pai, W. Mansfield, J.A. Taylor, S. Pau, and R.S. Besser. Multiphase flow regimes for hydrogenation in a catalyst-trap microreactor. *Chemical Engineering Journal*, 135:S229 – S236, 2008. 75

[8] R. Abdallah, V. Meille, J. Shaw, D. Wenn, and C. de Bellefon. Gas-liquid and gas-liquid-solid catalysis in a mesh microreactor. *Chem. Commun.*, pages 372–373, 2004. 75

[9] David A. Wenn, John E. A. Shaw, and Bina Mackenzie. A mesh microcontactor for 2-phase reactions. *Lab Chip*, 3:180–186, 2003. 75

[10] R. Dittmeyer, K. Svajda, and M. Reif. A review of catalytic membrane layers for gas/liquid reactions. *Topics in Catalysis*, 29:3–27, 2004. 75

[11] J. Coronas and J. Santamaria. Catalytic reactors based on porous ceramic membranes. *Catalysis Today*, 51(3-4):377 – 389, 1999.

[12] M. Vospernik, A. Pintar, G. Bercic, and J. Levec. Experimental verification of ceramic membrane potentials for supporting three-phase catalytic reactions. *Journal of Membrane Science*, 223(1-2):157 – 169, 2003. 75

[13] J. K. Chinthaginjala, K. Seshan, and L. Lefferts. Preparation and application of carbon-nanofiber based microstructured materials as catalyst supports. *Industrial & Engineering Chemistry Research*, 46(12):3968–3978, 2007. 75, 87

[14] J.K. Chinthaginjala, D.B. Thakur, K. Seshan, and L. Lefferts. How carbon-nano-fibers attach to Ni foam. *Carbon*, 46(13):1638 – 1647, 2008. 80

[15] J. K. Chinthaginjala, J. H. Bitter, and L. Lefferts. Thin layer of carbon-nano-fibers (CNFs) as catalyst support for fast mass transfer in hydrogenation of nitrite. *Applied Catalysis A: General*, 383(1-2):24 – 32, 2010. 82, 87

[16] J.K. Chinthaginjala and L. Lefferts. Support effect on selectivity of nitrite reduction in water. *Applied Catalysis B: Environmental*, 101(1-2):144 – 149, 2010. 82

[17] S. Pacheco-Benito and L. Lefferts. The production of a homogeneous and well-attached layer of carbon nanofibers on metal foils. *Carbon*, 48(10):2862 – 2872, 2010. 78, 80, 87

[18] N.M. Rodriguez, M.-S. Kim, and R. Terry K. Baker. Carbon nanofibers: A unique catalyst support medium. *The Journal of Physical Chemistry*, 98(50):13108–13111, 1994. 80

[19] N.A. Jarrah, J.G. van Ommen, and L. Lefferts. Mechanistic aspects of the formation of carbon-nanofibers on the surface of ni foam: A new microstructured catalyst support. *Journal of Catalysis*, 239(2):460 – 469, 2006. 75, 80

[20] M.W.J. Luiten-Olieman, L. Winnubst, A. Nijmeijer, M. Wessling, and N.E. Benes. Porous stainless steel hollow fiber membranes via dry-wet spinning. *Journal of Membrane Science*, 370(1-2):124 – 130, 2011. 77

[21] S.M. Dutczak, M.W.J. Luiten-Olieman, H.J. Zwijnenberg, L.A.M. Bolhuis-Versteeg, L. Winnubst, M.A. Hempenius, N.E. Benes, M. Wessling, and D. Stamatialis. Composite capillary membrane for solvent resistant nanofiltration. *Journal of Membrane Science*, 372(1-2): 182–190, 2011. 78, 79

[22] R.T.K. Baker, M.A. Barber, P. S. Harris, F. S. Feates, and R. J. Waite. Nucleation and growth of carbon deposits from the nickel catalyzed decomposition of acetylene. *Journal of Catalysis*, 26(1):51 – 62, 1972. 80, 87

[23] A. Pintar, G. Bercic, and J. Levec. Catalytic liquid-phase nitrite reduction: Kinetics and catalyst deactivation. *AIChE Journal*, 44(10):2280–2292, 1998. 82

[24] S. D. Ebbesen, B. L. Mojet, and L. Lefferts. In situ ATR–IR study of nitrite hydrogenation over Pd/Al_2O_3. *Journal of Catalysis*, 256(1):15 – 23, 2008. 82

[25] L. Schlapbach and A. Zuttel. Hydrogen-storage materials for mobile applications. *Nature*, 414(6861):353–358, 2001. 86

[26] S. Er, D. Tiwari, G.A. de Wijs, and G. Brocks. Tunable hydrogen storage in magnesium–transition metal compounds: First-principles calculations. *Phys. Rev. B*, 79(2):024105, 2009.

[27] S. Er, D. Tiwari, G.A. de Wijs, and G. Brocks. Tuning the hydrogen storage in magnesium alloys. *The Journal of Physical Chemistry Letters*, 1(13):1982–1986, 2010. 86

[28] E.D. Snijder, G.F. Versteeg, and W.P.M. van Swaaij. Hydrogenation of cyclohexene with $LaNi_{5-x}Al_xH_n$ metal hydrides suspended in cyclohexane or ethanol. *Chemical Engineering Science*, 48(13):2429 – 2441, 1993. 86

[29] S.K. Bhatia and A.L. Myers. Optimum conditions for adsorptive storage. *Langmuir*, 22(4):1688–1700, 2006. 86

[30] S. Banerjee, S. Murad, and I.K. Puri. Hydrogen storage in carbon nanostructures: Possibilities and challenges for fundamental molecular simulations. *Proceedings of the IEEE*, 94(10):1806 –1814, 2006.

[31] S. Er, D. Tiwari, G.A. de Wijs, and G. Brocks. Hydrogen storage by polylithiated molecules and nanostructures. *The Journal of Physical Chemistry C*, 113(20):8997–9002, 2009.

[32] S. Er, G.A. de Wijs, and G. Brocks. Dft study of planar boron sheets: A new template for hydrogen storage. *The Journal of Physical Chemistry C*, 113(43):18962–18967, 2009. 86

[33] F. Liang, J. Fan, Y. Guo, M. Fan, J. Wang, and H. Yang. Reduction of nitrite by ultrasound-dispersed nanoscale zero–valent iron particles. *Industrial & Engineering Chemistry Research*, 47(22):8550–8554, 2008. 87

[34] H.-Y. Hu, N. Goto, and K. Fujie. Effect of ph on the reduction of nitrite in water by metallic iron. *Water Research*, 35(11):2789 – 2793, 2001. 87

[35] Y.H. Huang and T.C. Zhang. Nitrite reduction and formation of corrosion coatings in zerovalent iron systems. *Chemosphere*, 64(6):937 – 943, 2006. 87

[36] I.F. Cheng, R. Muftikian, Q. Fernando, and N. Korte. Reduction of nitrate to ammonia by zero-valent iron. *Chemosphere*, 35(11):2689 – 2695, 1997. 87

[37] A. Shukla, J. Pande, A. Bansiwal, P. Osiceanu, and R. Biniwale. Catalytic hydrogenation of aqueous phase nitrate over fe/c catalysts. *Catalysis Letters*, 131:451–457, 2009. 87

Chapter 5

Porous Photocatalytic Membrane Microreactors (P2M2): A new reactor concept for photochemistry

A REVISED VERSION OF THIS CHAPTER HAS BEEN ACCEPTED FOR PUBLICATION:

H.C. Aran, D. Salamon, T. Rijnaarts, G. Mul, M. Wessling, and R.G.H. Lammertink, Porous Photocatalytic Membrane Microreactors (P2M2): A New Reactor Concept for Photochemistry, *Journal of Photochemistry and Photobiology A: Chemistry*, **in press**.

ABSTRACT

In this study, a new membrane microreactor concept for multiphase photocatalytic reactions is demonstrated. Microfabrication, photocatalyst immobilization and surface modification steps were performed to develop a Porous Photocatalytic Membrane Microreactor (P2M2). This concept benefits from a stable gas-liquid-solid (G-L-S) interface allowing a continuous supply of gaseous reactants and a reduced light path. A surface modification technique was devised to alter the wetting conditions of the reactor wall. Through a complete hydrophobization and a selective hydrophilization step by use of UV-light, we obtained a hydrophobic porous membrane support with hydrophilic photocatalytic microchannels. The photocatalytic degradations of methylene blue and phenol were used as model reactions to test the device, demonstrating significant degradation performance. We further demonstrated the effect of additional oxygen supply to the performance of the reactor for both reaction systems.

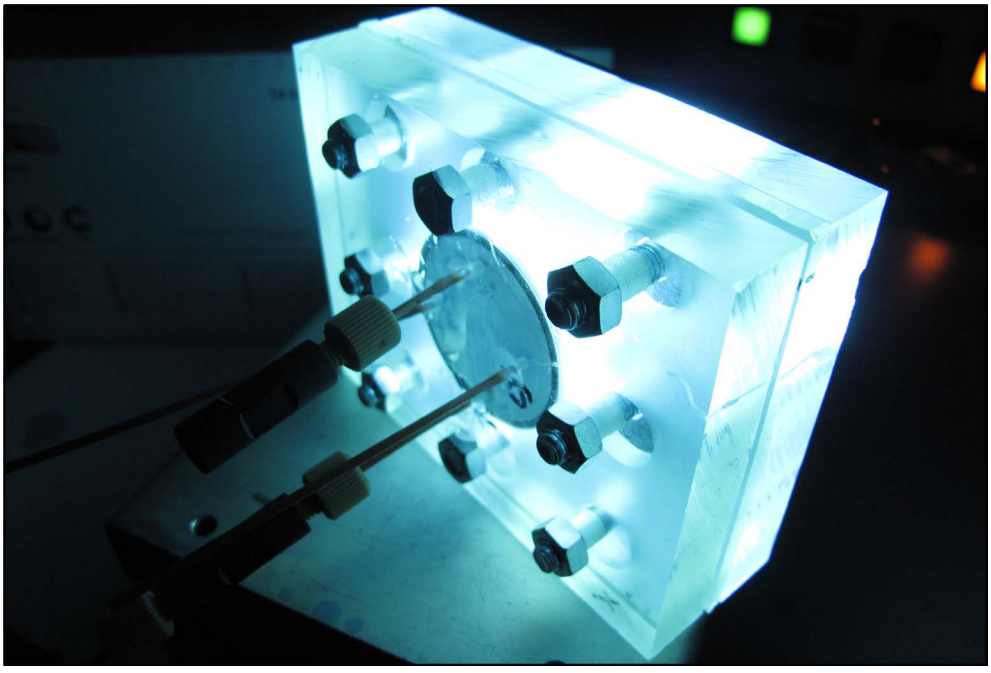

5.1 Introduction

Microreactors provide high surface to volume ratio, which leads to enhanced heat and mass transfer in these devices. Additionally, due to their miniaturized dimensions they facilitate safer operations, occupy small space and create less waste. These properties make them superior for many applications (e.g. in heterogeneous catalysis) and open new routes for chemical technology [1–5].

In recent years, microreactors also became attractive for photochemistry and photocatalytic processes [6–9]. Their high surface to volume ratio reduces mass transfer limitations, such that they overcome the setback of the low surface area of the immobilized macroscale wall reactors for photocatalysis [8,10]. Moreover, the miniaturized dimensions in the microreactors provide a reduced path for the light decreasing photon transfer limitations and lead to high illumination homogeneity along the reactor [6,8].

Many of the already existing concepts from microreaction technology have been adapted for photochemical and photocatalytic gas-liquid (G-L) and gas-liquid-solid (G-L-S) reactions. A remarkable reactor design for these purposes is the commercially available falling film microreactors utilized in G-L reactions [6]. In these reactors, a thin falling liquid film flows by gravitational force along a microstructured surface while it is illuminated by UV light and exposed to the co-flowing gas. Jähnisch et al. [11,12] applied falling film microreactors for photooxidation and photochlorination reactions, in which the liquid reactant was saturated with the gaseous reactant in this continuous manner. These reactors are well-suited for G-L photochemical reactions. However, for photocatalytic G-L-S reactions these reactors can suffer from mass transfer limitations, as the gas has to diffuse through the liquid film to reach an immobilized solid catalyst on the microstructured surface.

Another possible microreactor type for the application of photocatalysis is the dispersed phase microreactors. In these reactors the gaseous reactant is dispersed in the liquid phase (e.g. slug flow, annular flow) flowing in the microchannel. The dispersed phase microreactors benefit from enhanced mixing (mass transfer) in the

liquid slugs inside the microchannel[13,14]. Lindstrom et al.[14] integrated slug flow and Matsushita et al.[15,16] investigated annular flow in microreactors for photocatalytic model reactions and they showed significant improvement in the performance of their microreactors, compared to single phase operation. For applications in which long microchannels are required, dispersed phase operation can result in depletion of gaseous reactants due to its consumption by the reaction[17]. In addition, the presence of gas bubbles in microchannels decreases the residence time of the liquid reactant in the reactor.

The aim of this study is to demonstrate a new concept for multiphase (G-L-S) photocatalytic reactions inside microreactors: Porous Photocatalytic Membrane Microreactor (P2M2). In this concept, the contacting of the G-L-S phases is established using membrane technology. The liquid flows inside microchannels (fabricated in porous Aluminium oxide: α-Al_2O_3), where the photocatalyst (Titanium dioxide: TiO_2) is immobilized on the channel wall (Figure 5.1). The gas permeates through the porous wall of the membrane reaching the liquid that is flowing inside the microchannel. The microchannels are illuminated from the top by UV-light to stimulate the photocatalytic reaction.

This reactor design ensures that the liquid (L) - gas (G) interface is located at the solid (S) photocatalyst surface. We obtain this stable G-L-S interface by selective

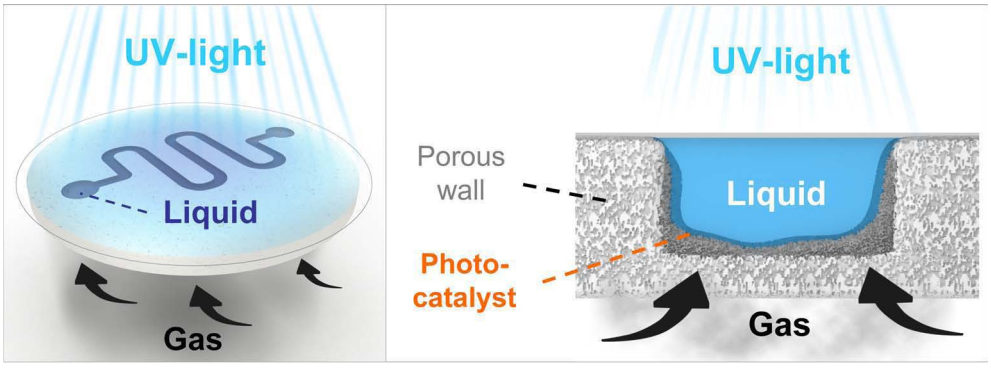

Figure 5.1: Contacting concept of Porous Photocatalytic Membrane Microreactor (P2M2).

surface modification steps (hydrophobization and selective hydrophilization) of the intrinsically hydrophilic porous reactor materials. Photocatalytic degradations of methylene blue and phenol on TiO_2 catalyst were selected as model reactions in this work, in order to study the performance of the microreactor and the influence of oxygen (O_2) in these processes. The presence of O_2 is known to improve photocatalytic degradation of organic compounds[14–16,18]. The reactor concept presented in this study offers continuous supply of O_2 to the entire photocatalytic microreactor, avoiding its depletion due to consumption.

5.2 Experimental

5.2.1 Materials

Polyvinyl alcohol (PVA; Aldrich, Mowiol 8-88), MilliQ water, aluminum oxide (α-Al_2O_3; AKP-30, Sumitomo Chemical), nitric acid (HNO_3, Sigma Aldrich, puriss, 65%) were used for the fabrication of the porous α-Al_2O_3 substrates. For the preparation of the photocatalyst coating, titanium dioxide (TiO_2; Evonik, Aeroxide P25, 99.5%), PVA (Aldrich, MW=13000-23000 g/mol, 87-89%), acetic acid (Merck), 2-Propanol (Merck) were used. Perfluorinated octyltrichlorosilane (FOTS; Aldrich, 97%) and n-hexane (Merck) were used as received for the surface modification step. Methylene blue hydrate (MB; Fluka, purum p.a.) and phenol (Sigma Aldrich) were used as model degradation compounds in this study.

5.2.2 Reactor preparation

The preparation of the Porous Photocatalytic Membrane Reactor (P2M2) consists of 5 main stages (Figure 5.2): 1) Porous α-Al_2O_3 substrate fabrication, 2) Micro-fabrication, 3) Photocatalyst immobilization, 4) Surface modification (a- Complete Hydrophobization, b- Selective Hydrophilization), 5) Module assembly.

1) Porous α-Al_2O_3 substrates: These were prepared using an α-Al_2O_3 (AKP-30) suspension and colloidal filtration technique, as described elsewhere[19], resulting in circular supports with an average pore diameter of 80 nm and a porosity of 35%.

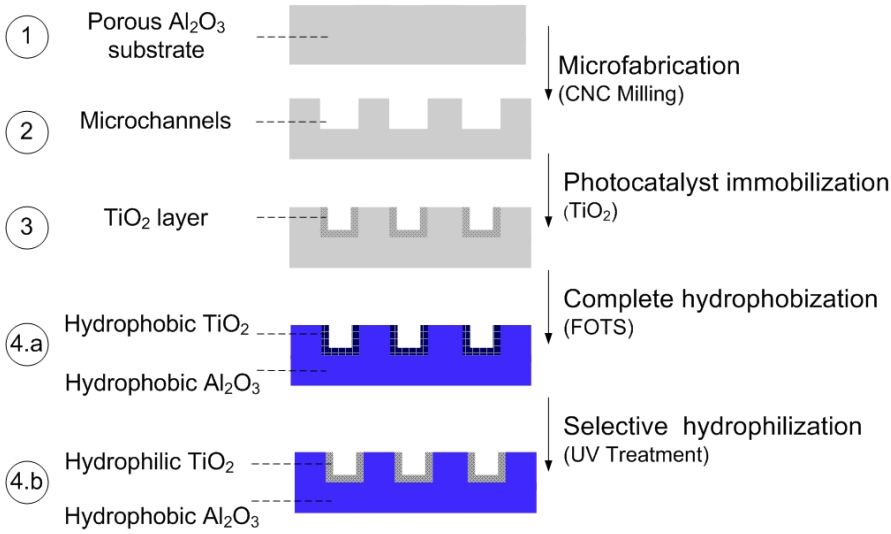

Figure 5.2: Summary of P2M2 preparation steps: The illustrations represent the cross-section after each preparation step.

After the sintering step (1100°C), the substrates were cut and polished to reach a diameter of 39 mm and a thickness of 2 mm.

2) Microfabrication: Substrates were fixed on a glass plate and 1 mm wide channels with a depth of 500 μm were milled in the flat α-Al_2O_3 substrates using a Sherline 5410 automated CNC-mill and a double cutter of 1 mm diameter. The channel length was 65 mm and the volume ~32.5 μl.

3) Photocatalyst immobilization: A TiO_2 suspension consisting of 1 g TiO_2, 1 g PVA, 50 ml 2-propanol and 50 ml H_2O was prepared. The pH was adjusted to ~2 by adding 5 g of acetic acid (CH_3COOH). The suspension was applied in the microchannels with a pipette. The excess suspension around the microchannels was wiped off with a tissue paper. The substrate was dried at 50°C and sintered at 500°C for 2 h. Subsequently, the substrate surface was polished to remove the excess TiO_2 outside the microchannels. The morphology of the immobilized TiO_2 catalyst was characterized by Scanning Electron Microscopy (SEM; JEOL TSM 5600). The BET surface area of the TiO_2 layer was measured using N_2-adsorption (Micromeritics Tristar).

4) Surface modification: For complete hydrophobization (α- Al_2O_3 and TiO_2), the samples were immersed in a solution containing 0.2 g of FOTS in 50 ml n-hexane. The substrate was kept in the solution for 1 h, taken out of the solution and then placed in the oven at 100°C (adapted from Chpater 2). For selective hydrophilization of the TiO_2 photocatalyst layer, the completely hydrophobized sample was exposed to UV-light. The exposure time was varied in the order of minutes to determine optimum modification parameters. The surface properties (hydrophobicity) of the porous α-Al_2O_3 and TiO_2 were characterized by water contact angle measurements (OCA 15 Dataphysics) on each layer. The measurements were performed after the complete hydrophobization step and also after each UV-exposure time interval. The samples were rinsed with 2-propanol and then dried after each surface modification stage.

5) Module assembly: The open microchannels on the substrate were covered with a UV-transparent foil (Hevel). The foil was softened on the top of the substrate with a heat treatment in the oven at 120°C for 30 min. After cooling down, the foil attached to the surface of the substrate. Following that, the reactor was placed in an in-house built gas-tight module (PMMA, prepared by CNC Milling), which was connected to the light-guides of the UV-light source (Figure 5.3).

5.2.3 Reactor operation

Aqueous solutions of methylene blue (∼70 μM) and phenol (∼1 mM) were prepared as liquid reactants. The liquid reactant solutions were pumped to the microreactor with flow rates of 10, 30 and 50 μl/min using a syringe pump (Harvard, Picoplus). Oxygen (O_2), air or nitrogen (N_2) was fed as gaseous reactant to the gas reservoir of the module (25 ml/min, atmospheric pressure).

The methylene blue (MB) concentration at the reactor inlet and outlet was determined by light absorbance measurements using an online UV-Vis Detector (Varian, Prostar 340) with a tungsten lamp (380-800 nm) at a fixed wavelength. The wavelength (λ) was set to 663 nm (maximum absorption of MB) and calibration was carried out for different concentrations of MB solution (from 10 to 100 μM).

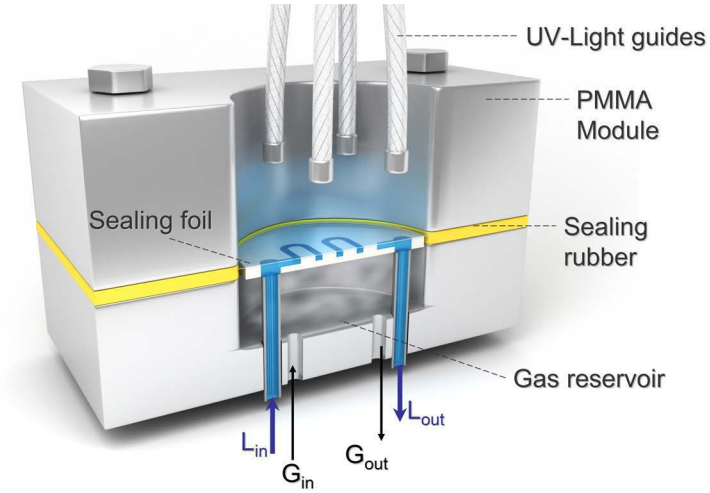

Figure 5.3: Schematic representation of the fabricated PMMA reactor module (Cross-sectional view).

The photocatalytic degradation of phenol and its products were characterized by analyzing the UV-VIS Spectrum of the reactor in- and outlet. The reactor outlet was connected to a micro HPLC flow-through cell (ZEUTEC). The flow-through cell was attached to a deuterium halogen light source (DT-Mini-2-GS, Mikropack GmbH) and a high-resolution fiber optic spectrometer (HR4000, Ocean optics Inc.) via two optical fibers (SR 600 nm, Ocean optics Inc.), as described by Costantini et al. [20].
As light source for the photocatalytical reactions, a 120 W UV-lamp (HP-120, Dr. Gröbel UV-elektronik GmbH) was used. The light was focused on the reactor using four light-guides. The average measured light intensity (at λ=365 nm) on the reactor surface was approximately 100 mW/cm^2.

5.3 Results and Discussion

5.3.1 Reactor characterization

Figure 5.4 shows a fabricated microchannel in porous α-Al_2O_3 substrate with the TiO_2 layer inside after the surface modification steps. It was observed that the inner

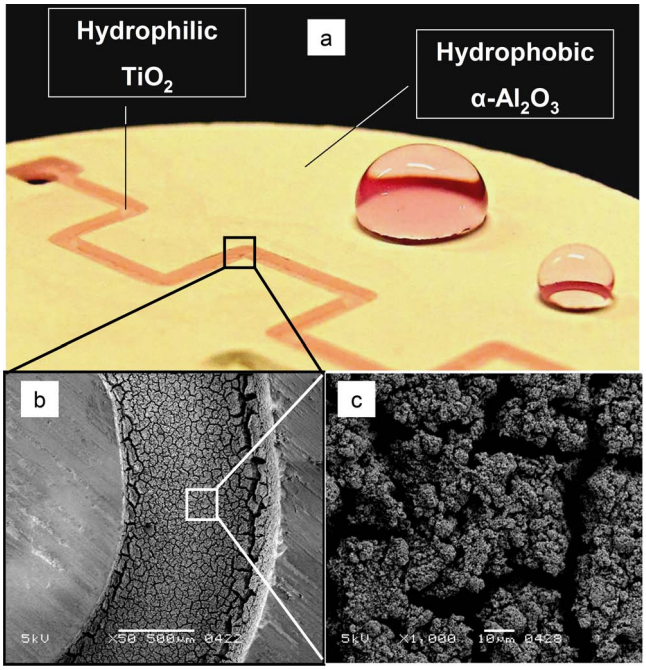

Figure 5.4: Home-fabricated porous α-Al_2O_3 microreactor with immobilized TiO_2 and modified surface properties. (a) Visualization of the surface properties after the selective hydrophilization step, (b) and (c) SEM images of the ceramic membrane after photocatalyst immobilization: immobilized TiO_2 in the porous Al_2O_3 microchannel.

walls of the microchannel were entirely covered with TiO_2 (Figure 5.4.b and 5.4.c). The BET surface area of the TiO_2 layer was found to be approximately 45 m^2/g. With the first surface modification step, the complete sample (α-Al_2O_3 and TiO_2) was successfully hydrophobized. The contact angles for both layers were around 150°, measured on porous α-Al_2O_3 and TiO_2 layers. In Chapter 2, we have shown that a dense α-Al_2O_3 layer with FOTS coating reaches a contact angle of approximately 115°. The surface roughness of the porous layers further enhances the hydrophobicity. This complete hydrophobization step ensures that the liquid does not wet the porous α-Al_2O_3 substrate. It also hydrophobizes the TiO_2 layer in the microchannel. The hydrophobicity of the TiO_2 layer prevents an intensive contact between this photocatalyst layer and the liquid reactant, which would limit the reactor performance. Therefore, a selective hydrophilization step was carried out by means of UV-

irradiation. After 1 h of UV-irradiation on the sample, the TiO_2 became hydrophilic. The contact angle of the α-Al_2O_3 layer remained constant. This method ensures a stable G-L-S interface in the microreactor on the porous α-Al_2O_3 hydrophobic membrane, while providing an intensive contact of the liquid reactant with the hydrophilic TiO_2 photocatalyst inside the microchannel (Figure 5.4.a).

The change in the surface properties of TiO_2 in the presence of UV-light was previously observed and investigated in literature[21–25]. This phenomenon attracted much attention; however the understanding of it is still under debate. One of the most widely accepted hypotheses explains it by the photocatalytic properties of the TiO_2 layer. With UV-illumination the hydrocarbons on the surface get photocatalytically decomposed by TiO_2[24,25]. Another hypothesis is the structural change of the TiO_2 by formation of surface hydroxyl groups under UV-irradiation, which cause the switch to the hydrophilic state[21,23]. This hypothesis would be valid for TiO_2 films without an additional hydrocarbon coating. Regardless of the reason for this phenomenon, the presented method allows us to selectively tune the surface properties in the microchannel for a porous membrane reactor application in heterogeneous catalysis.

5.3.2 Reactor operation

The photocatalytic properties of P2M2 were tested for the degradations of MB ($C_{16}H_{18}ClN_3S$) and phenol (C_6H_5OH) and showed promising degradation properties with additional O_2 supply through the porous membrane. The main performance criterion was degradation rate for both compounds. The presence of the UV-light, liquid reactant flow rate and the gas supply through the porous membrane were studied for these reactions.

Photocatalytic Degradation of Methylene Blue:

Figure 5.5 displays the MB concentration of the outlet flow in time. At the initial stage of the experiment (1) without the presence of UV-light, MB adsorbs on the surface of the TiO_2 in the microchannel, which leads to a lower MB concentration at the reactor outlet. After ∼60 min, equilibrium was reached and the UV-light was exposed to the reactor (2). With the illumination the MB concentration at the reactor outlet

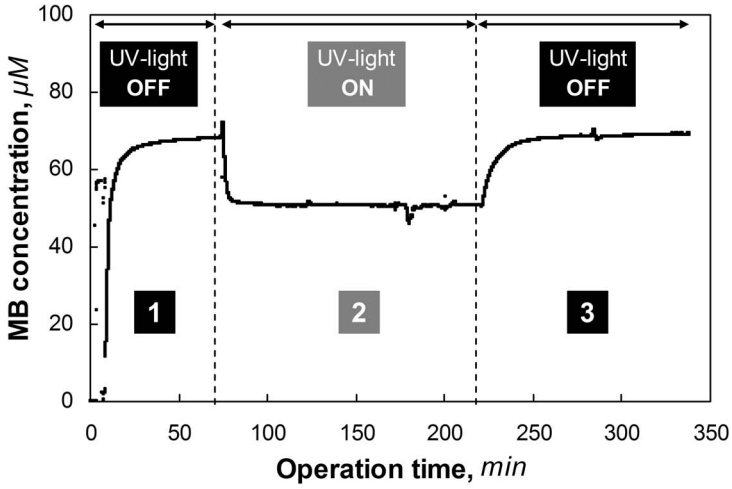

Figure 5.5: Effect of UV-light on the MB degradation (initial MB concentration=70 μM, liquid flow rate= 50 μl/min, without O_2 supply): MB concentrations are based on absorbance measurements of the reactor outlet at λ= 663 nm.

decreases significantly due to the photocatalytic degradation. The decrease in the concentration indicated a MB degradation of ∼27% (without additional O_2 supply). At the final stage (3), when the UV-light was turned off, the product concentration reached the initial MB concentration again.

The degradation of MB was studied for different liquid flow rates with O_2 supply. As expected, with increasing flow rate (10, 30 and 50 μl/min), the degradation of MB decreased (90%, 55% and 35%) due to the decreasing residence time.

In order to determine the influence of O_2 in the MB degradation, tests with and without additional O_2 supply were performed. The conversion with air and pure O_2 supply were comparable (Figure 5.6). The results showed that the conversion values with O_2 supply were slightly higher than without O_2 supply.

O_2 is known to act as an electron acceptor in the photocatalytic degradation, forming superoxide radicals (O_2^-) as an oxidant. Furthermore, the presence of O_2 decreases recombination of the electron (e^-) and hole (h^+) pairs, which are generated by the photocatalyst. This also increases the efficiency of the formation of powerful

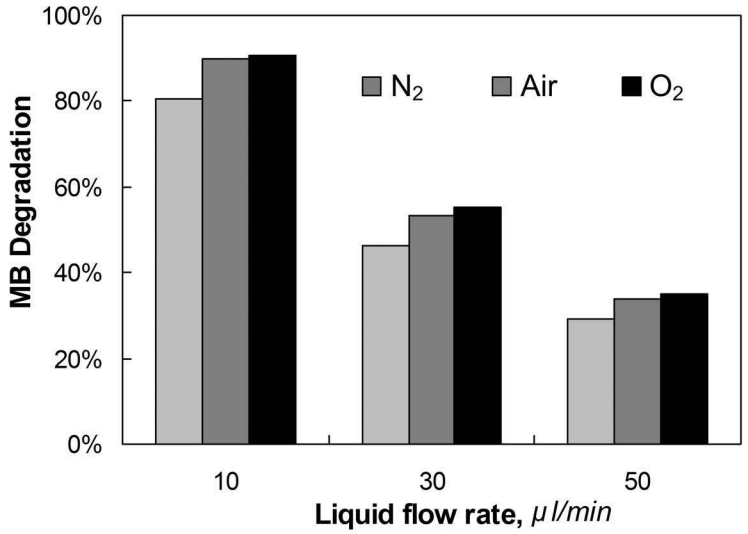

Figure 5.6: Effect of O_2 supply and liquid flow rate on the MB degradation (initial MB concentration=70 μM).

oxidants such as hydroxyl radicals[14,26,27]. Nevertheless, as can be seen in Figure 5.6, the additional supply of O_2 did not affect the degradation rate of methylene blue drastically. This can be explained by possible mass transfer limitations in the liquid phase or the low initial concentration (70 μM) of methylene blue, requiring only little amount of additional O_2. Apparently, for our configuration the hydroxyl radicals were formed fast enough by the UV-irradiation and the contribution of the superoxide free radicals was smaller.

Wu et al.[26] reported that the increase of dissolved O_2 concentration in the liquid reactant did not have an effect on the MB degradation rate in a batch slurry reactor. On the other hand, Lindstrom et al.[14] proved a significant positive effect of additional O_2 supply on the degradation of methylene blue in a microreactor. It must be noted that in the work of Lindstrom et al.[14] O_2 bubbles were dispersed in the liquid microchannel creating slug flow, which would also improve the mass transfer properties in this channel. In our reactor, the hydrodynamic properties in the microchannel were identical for the experiments with and without additional O_2

supply, so that merely the impact of O_2 in the reaction can be analyzed.

Photocatalytic Degradation of Phenol:

In order to analyze the phenol degradation, the UV-VIS absorbance of the in- and outlet product were monitored online. The analysis of the absorbance was performed at wavelengths of $250<\lambda<400$ nm (Figure 5.7).

The photocatalytic degradation of phenol was studied for different gas phase compositions. The additional O_2 supply increased the degradation of phenol drastically. As can be seen in Figure 5.7 (initial phenol concentration=1 mM, liquid flow rate= 10 μl/min), with O_2 supply (air or pure O_2), the absorbance peak of phenol at 270 nm decreased significantly compared to the values with N_2 supply.

The photocatalytic degradation of phenol was intensively studied as a model reaction in photocatalysis. It is a well-known fact that during phenol degradation, several aromatic intermediates are formed such as hydroquinone, benzoquinone and catechol. The formation of these intermediates was also observed in our reaction product, which

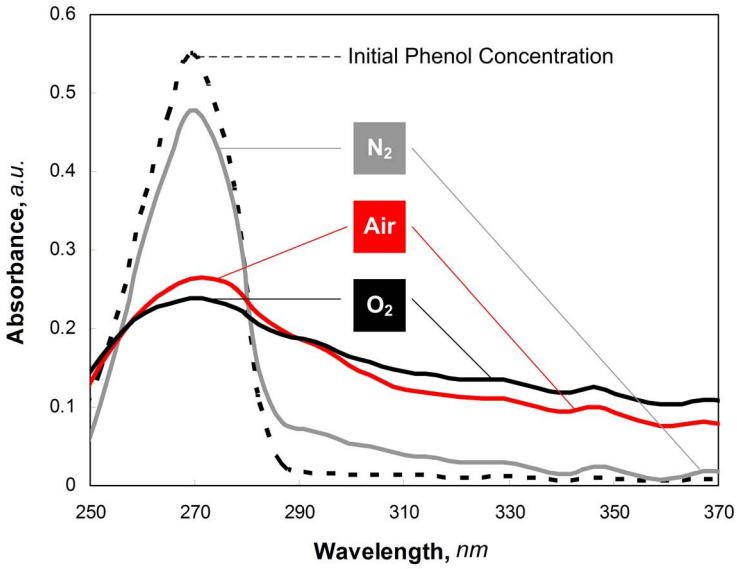

Figure 5.7: Effect of O_2 supply on the photocatalytic phenol degradation (initial phenol concentration=1 mM, liquid flow rate=10 μl/min). Absorbance spectrum of the reactor in- and outlet streams for different gas phase compositions.

is indicated by the increased absorbance at wavelengths higher than 290 nm (Figure 5.7). Moreover, the product had a very light yellow/brown color, which is most likely due to the formation of reaction intermediates [18,28–30].

With increasing flow rate (decreasing residence time) the degradation of phenol decreased. Unfortunately, the decreasing peak of phenol cannot be related directly to the conversion value of phenol. The formed intermediate products (e.g. 1, 4-Benzoquinone, Hydroquinone) also absorb around 270 nm.

Nevertheless, the measurements clearly show that the phenol degradation is improved with the membrane-assisted O_2 supply to the reaction zone. These results prove that the utilization of membrane technology in photocatalytic processes is an attractive and promising alternative for multiphase systems.

5.4 Conclusions

A new microreactor concept for photocatalytic gas-liquid-solid (G-L-S) systems was introduced in this work. In contrast to the existing concepts, Porous Photocatalytic Membrane Microreactor (P2M2) exploits tuned interfaces to ensure a well-defined and stable G-L-S interface for the reaction and allows supplying the gaseous reactant continuously along the length of the microreactor. Microreactors with controlled surface properties and photocatalytic activity were successfully prepared by microfabrication, photocatalyst immobilization and selective surface modification steps.

We showed that the selective surface modification step ensures that the photocatalyst becomes hydrophilic precisely in photocatalytically active areas. This method can be applied for membrane reactors especially in heterogeneously catalyzed processes.

We also proved that the availability of the gaseous reactant O_2 in photocatalytic processes can be significantly improved by its continuous distribution to the reaction zone through a porous membrane. The presented results showed that the membrane-assisted supply of O_2 enhanced the photocatalytic degradation of phenol and methylene blue.

5.5 Acknowledgements

We are grateful to J.G.F. Heeks, R. Kooijman and J.A.M. Vrielink for technical support and analysis. The authors also greatly acknowledge J.M. Jani for the fruitful discussions and J.Bennink (Tingle.nl) for the illustrations.

Bibliography

[1] M. N. Kashid and L. Kiwi-Minsker. Microstructured reactors for multiphase reactions: State of the art. *Industrial & Engineering Chemistry Research*, 48(14):6465–6485, 2009. 95

[2] V. Hessel, P. Angeli, A. Gavriilidis, and H. Lowe. Gas-liquid and gas-liquid-solid microstructured reactors: Contacting principles and applications. *Industrial & Engineering Chemistry Research*, 44(25):9750–9769, 2005.

[3] H. C. Aran, J. K. Chinthaginjala, R. Groote, T. Roelofs, L. Lefferts, M. Wessling, and R. G. H. Lammertink. Porous ceramic mesoreactors: A new approach for gas-liquid contacting in multiphase microreaction technology. *Chemical Engineering Journal*, 169(1-3):239 – 246, 2011.

[4] A. Gavriilidis, P. Angeli, E. Cao, K. K. Yeong, and Y. S. S. Wan. Technology and applications of microengineered reactors. *Chemical Engineering Research and Design*, 80(1):3 – 30, 2002.

[5] K. Jahnisch, V. Hessel, H. Lowe, and M. Baerns. Chemistry in microstructured reactors. *Angewandte Chemie International Edition*, 43(4):406–446, 2004. 95

[6] E. E. Coyle and M. Oelgemoller. Micro-photochemistry: photochemistry in microstructured reactors. the new photochemistry of the future? *Photochem. Photobiol. Sci.*, 7:1313–1322, 2008. 95

[7] R. Gorges, S. Meyer, and G. Kreisel. Photocatalysis in microreactors. *Journal of Photochemistry and Photobiology A: Chemistry*, 167(2-3):95–99, 2004.

[8] T. van Gerven, G. Mul, J. Moulijn, and A. Stankiewicz. A review of intensification of photocatalytic processes. *Chemical Engineering and Processing*, 46(9):781–789, 2007. 95

[9] Y. Matsushita, N. Ohba, S. Kumada, K. Sakeda, T. Suzuki, and T. Ichimura. Photocatalytic reactions in microreactors. *Chemical Engineering Journal*, 135(Supplement 1):S303–S308, 2008. 95

[10] R. van Grieken, J. Marugán, C. Sordo, and C. Pablos. Comparison of the photocatalytic disinfection of e. coli suspensions in slurry, wall and fixed-bed reactors. *Catalysis Today*, 144(1-2):48–54, 2009. 95

[11] K. Jahnisch and U. Dingerdissen. Photochemical generation and [4+2]-cycloaddition of singlet oxygen in a falling-film micro reactor. *Chemical Engineering & Technology*, 28(4):426–427, 2005. 95

[12] H. Ehrich, D. Linke, K. Morgenschweis, M. Baerns, and K. Jahnisch. Application of microstructured reactor technology for the photochemical chlorination of alkylaromatics. *CHIMIA International Journal for Chemistry*, 56:647–653(7), 2002. 95

[13] M. T. Kreutzer, F. Kapteijn, J. A. Moulijn, and J. J. Heiszwolf. Multiphase monolith reactors: Chemical reaction engineering of segmented flow in microchannels. *Chemical Engineering Science*, 60(22):5895 – 5916, 2005. 96

[14] H. Lindstrom, R. Wootton, and A. Iles. High surface area titania photocatalytic microfluidic reactors. *AIChE Journal*, 53(3):695–702, 2007. 96, 97, 104

[15] Y. Matsushita, M. Iwasawa, T.Suzuki, and T. Ichimura. Multiphase photocatalytic oxidation in a microreactor. *Chemistry Letters*, 38(8):846–847, 2009. 96

[16] Y. Matsushita, M. Iwasawa, N. Ohba, S. Kumada, T. Suzuki, and T. Ichimura. Photocatalytic oxidation and alkylation processes in microreactors. In *Nano/Micro Engineered and Molecular Systems, 2007. NEMS '07. 2nd IEEE International Conference on*, pages 851 –854, 2007. 96, 97

[17] A. Leclerc, M. Alame, D. Schweich, P. Pouteau, C. Delattre, and C. de Bellefon. Gas-liquid selective oxidations with oxygen under explosive conditions in a micro-structured reactor. *Lab on a Chip*, 8:814–817, 2008. 96

[18] M. Subramanian and A. Kannan. Effect of dissolved oxygen concentration and light intensity on photocatalytic degradation of phenol. *Korean Journal of Chemical Engineering*, 25:1300–1308, 2008. 97, 106

[19] A. Nijmeijer, H. Kruidhof, R. Bredesen, and H. Verweij. Preparation and properties of hydrothermally stable α-alumina membranes. *Journal of the American Ceramic Society*, 84(1):136–140, 2001. 97

[20] F. Costantini, W. P. Bula, R. Salvio, J. Huskens, H. J. G. E. Gardeniers, D. N. Reinhoudt, and Willem Verboom. Nanostructure based on polymer brushes for efficient heterogeneous catalysis in microreactors. *Journal of the American Chemical Society*, 131(5):1650–1651, 2009. 100

[21] M. Miyauchi, N. Kieda, S. Hishita, T. Mitsuhashi, A. Nakajima, T. Watanabe, and K. Hashimoto. Reversible wettability control of TiO_2 surface by light irradiation. *Surface Science*, 511(1-3):401–407, 2002. 102

[22] Y.-H. Tseng, C.-S. Kuo, C.-H. Huang, T. Hirakawa, N. Negishi, and H.-L. Bai. Photoinduced hydrophilicity of TiO_2 film as the effect of H_2O_2 addition. *Micro Nano Letters, IET*, 5(2):81 –84, 2010.

[23] M. Fernandez-Rodriguez, V. J. Rico, A. R. Gonzalez-Elipe, and A. Alvarez-Herrero. Uv irradiation effects on TiO_2 thin films. *physica status solidi (c)*, 5(5):1164–1167, 2008. 102

[24] M. Takeuchi, K. Sakamoto, G. Martra, S. Coluccia, and M. Anpo. Mechanism of photoinduced superhydrophilicity on the TiO_2 photocatalyst surface. *The Journal of Physical Chemistry B*, 109(32):15422–15428, 2005. 102

[25] E. Balaur, J. M. Macak, L. Taveira, and P. Schmuki. Tailoring the wettability of TiO_2 nanotube layers. *Electrochemistry Communications*, 7(10):1066 – 1070, 2005. 102

[26] C.-H. Wu and J.-M. Chern. Kinetics of photocatalytic decomposition of methylene blue. *Industrial & Engineering Chemistry Research*, 45(19):6450–6457, 2006. 104

[27] A. Houas, H. Lachheb, M. Ksibi, E. Elaloui, C. Guillard, and J.-M. Herrmann. Photocatalytic degradation pathway of methylene blue in water. *Applied Catalysis B: Environmental*, 31(2):145 – 157, 2001. 104

[28] S. K. Pardeshi and A. B. Patil. A simple route for photocatalytic degradation of phenol in aqueous zinc oxide suspension using solar energy. *Solar Energy*, 82(8):700 – 705, 2008. 106

[29] Y.-T. Lin, C. Liang, and J.-H. Chen. Feasibility study of ultraviolet activated persulfate oxidation of phenol. *Chemosphere*, 82(8):1168 – 1172, 2011.

[30] B. Roig, C. Gonzalez, and O. Thomas. Monitoring of phenol photodegradation by ultraviolet spectroscopy. *Spectrochimica Acta Part A: Molecular and Biomolecular Spectroscopy*, 59:303–307(5), 2003. 106

Chapter 6

Summary and Outlook

The research described in this thesis aimed to explore new concepts for microreactors in multiphase gas-liquid-solid (G-L-S) reactions by utilizing membrane technology for contacting these phases. Porous micro- and mesoreactors were developed using various preparation steps and tested for gas-liquid-solid (G-L-S) model reaction systems. In this work, we fabricated, modified and characterized porous ceramic (Alumina: Al_2O_3) and metallic (stainless steel) reactors in planar and in tubular geometry. These reactors were applied for catalytic hydrogenation and photocatalytic degradation reactions of selected compounds in water and showed promising potential for future applications in microreactor technology.

6.1 Summary

Chapter 1 provides a general view about microreactors and existing concepts for multiphase reactions in these devices. Furthermore, an overview of conventional membrane reactors is given, followed by some background information on model reactions, which were performed in this study. Lastly, the scope and outline of the thesis are presented.

Chapter 2 demonstrates the preparation of porous ceramic mesoreactors and their application for catalytic hydrogenation of nitrite ions in water. Tubular reactors with tailored wetting properties and catalytic activity were developed by utilizing fabrication, catalyst immobilization and surface modification (hydrophobization) techniques. With surface modification, the wetting behavior of the liquid reactant on the catalyst surface and the position of the G-L interface could be easily tuned. A stable G-L-S interface for heterogeneously catalyzed reaction processes was realized by applying hydrophobization techniques. Reactors with tunable wetting properties were obtained, in which the porous support was hydrophobized while the catalyst support remained hydrophilic. The developed reactors showed high catalytic activities for this model reaction, reaching nitrite conversion values up to 80%. In addition, the reactor performance remained constant even at relatively low concentrations of hydrogen (H_2), proving very efficient transfer of the gas phase by continuous addition through the membrane.

In **Chapter 3**, we studied the influence of geometrical and operational parameters on the performance of ceramic (Al_2O_3) micro- and mesoreactors. We prepared reactors with various inner diameters, controllable catalyst support thickness (γ-Al_2O_3 layer) and active Pd surface area, and tunable wetting properties. In addition, we utilized inert slug flow in our porous membrane reactor, merging the advantages of both dispersed phase and continuous phase operation. The prepared reactors were tested for the catalytic hydrogenation of nitrite. Results showed that with the increasing catalyst support thickness the performance of the reactor increased, due to the higher amount of Pd catalyst at the interface. However, the enhancement is not as prominent

as the increase in Pd amount at the interface, suggesting further internal mass transfer limitations with increasing thickness of the γ-Al_2O_3 layer. Furthermore, reactors with smaller inner diameter showed higher reactor performance compared with the ones with larger inner diameter. This shows that lowering of the characteristic length enhances the performance in these reactors due to improved mass transfer. In addition, we showed that the integration of slug flow (inert) in a membrane reactor could further enhance the external mass transfer in the liquid phase.

Chapter 4 describes the utilization of porous stainless steel hollow fibers with carbon nanofibers (CNFs) as membrane microreactor material. Porous stainless steel (SS) hollow fibers with high porosity and mechanical strength were obtained and CNFs with high surface area were successfully grown on the porous SS surface. The fabricated microreactors displayed a high surface area, mechanical strength and promising nitrite reduction activity. Results indicated that the presence of CNFs on the SS surface had a significant effect on the reactor performance. On CNF deposited reactors, even without the presence of H_2 and Pd, the NO_2^- ions were successfully reduced. These results indicate the intrinsic reducing properties of the developed reactor material.

Chapter 5 demonstrates the application of porous microreactors for photocatalytic gas-liquid-solid (G-L-S) systems in planar chip geometry. Porous Photocatalytic Membrane Microreactors (P2M2) with controlled surface properties and photocatalytic activity were successfully prepared by micromilling (on porous Al_2O_3), photocatalyst (TiO_2) immobilization and selective surface modification steps. The reactor was employed in the (UV-light induced) photocatalytic degradation of methylene blue and phenol in water, where additional O_2 was supplied to the reaction zone. High photocatalytic activity with conversion values up to 90% were obtained. In addition, results showed that with the membrane-assisted supply of O_2 in these photocatalytic processes, the degradation rate in the reactor was significantly improved, illustrating the advantage of the developed concept.

6.2 Outlook

6.2.1 Fabrication of porous ceramic and metallic microchannels by replication/templating

As described in the previous chapters of this thesis, porous inorganic materials have a great potential to be applied in microfluidics. However, existing methods for preparation of these materials are limited by the high characteristic length (hydraulic diameter) or relatively high wall thickness [1,2]. Two alternative techniques are described, which can be applied for the fabrication of novel porous inorganic (e.g. ceramic, metallic) microfluidic devices.

Porous microchannels in planar geometry via replication:

Chapter 5 demonstrates milling as a simple and cheap approach for microstructuring of porous ceramic materials in planar geometry. Even with all its advantages, fabrication of channels with dimensions <100 μm becomes challenging and this direct microfabrication technique is not applicable on every type of porous substrate. Moreover, relatively thick substrates have to be used for mechanical strength, which results in a low *channel volume/total reactor volume*.

Microfabrication via replication (indirect fabrication) is a promising alternative for producing microstructured channels [3–6]. Within the scope of this thesis [7], preliminary studies on this method were carried out for the fabrication of thin porous ceramic microreactors. This method comprises of precipitation of polymers with dispersed particles while in contact with a microstructured mold (Figure 6.1). It can be applied for a wide variety of materials, allows fabrication of very thin microfluidic films (∼100 μm) and microstructures with very small characteristic length (<100 μm).

A polymer-particle suspension, consisting of polymer, solvent and dispersed particles (e.g. ceramic particles) is cast on a microstructured mold [7]. Subsequently, the solvent is removed from the cast suspension (e.g. by evaporation). The remaining polymer-particle composite (green tape) is released from the microstructured mold and several green tapes can be stacked together. This is then followed by a final sintering step, in which the polymer is selectively removed at high temperatures, leaving a porous

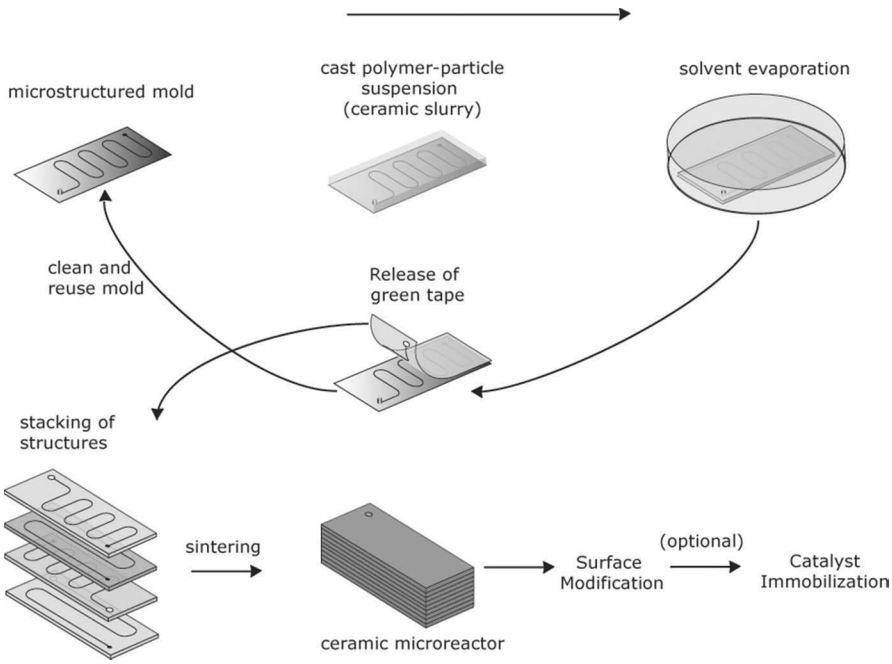

Figure 6.1: Microfabrication steps of porous ceramic microreactors by replication: Microstructuring of a polymer-particle composite by the use of a mold, followed by stacking and sintering step (adapted from[7]).

structure behind. According to the final application, surface modification and catalyst immobilization steps can be carried out before the operation (Figure 6.1).

In preliminary studies, we prepared homogenous ceramic (α-Al_2O_3) slurries (adapted from[4]) and performed accurate micropatterning. We carried out stacking of green tapes (lamination) and high temperature sintering. For the lamination of green tapes, we used a commercial adhesive (Pritt-Stick, Henkel) as temporary laminating agent, which was later eliminated during the sintering step (inspired from[8]). Figure 6.2 (a, b) shows the resulting porous ceramic microchannels fabricated via this replication method with characteristic channel dimensions of $\sim$25 μm.

With this technique, small and thin porous ceramic microstructured substrates could be easily fabricated. However, during the fabrication of bigger samples with an area of larger than $\sim$2 cm^2, we observed that the samples curled, resulting in "potato-chips"-like shapes during the sintering step (Figure 6.2.c). To prevent bending, we

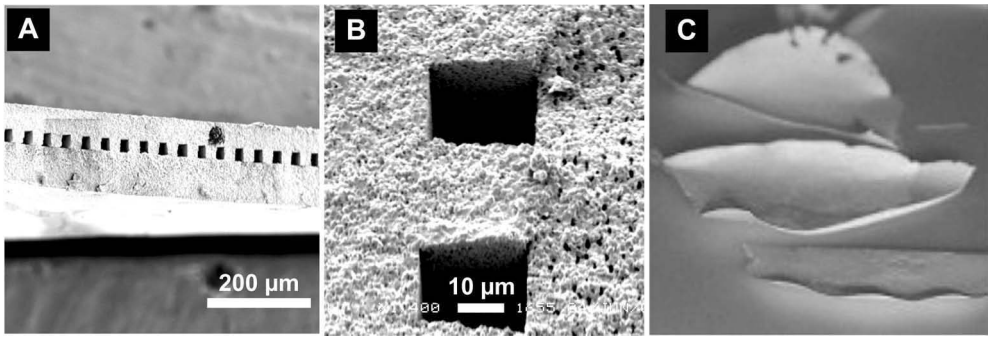

Figure 6.2: Porous ceramic microchannels in planar geometry: *(a)*, *(b)* Microchannels fabricated by replication, lamination and sintering steps. *(c)* Bending behavior of thin ceramic substrates after sintering.

"sandwiched" the green tapes between two ceramic blocks during the sintering step. In the case of only one green tape, the bending could be prevented. Nevertheless, if more than one green tape was stacked on each other, the final ceramic structure showed cracks on its surface.

This bending problem has to be overcome in order to make these microfluidic devices feasible for future applications. Possible reasons for bending are density gradients in the green tape before the sintering and/or temperature gradients in the sample during the sintering step. These gradients would cause shrinkage mismatches during the sintering, leading to a curled or cracked final structure. Density gradients can possibly be avoided by the use of gas permeable (porous or dense) microstructured molds, in order to make the evaporation of the solvent more homogeneous along the cross-section. Furthermore, the use of conductive plates at the bottom and/or the top of the sample could decrease the heat transfer gradients and the shrinkage mismatches during sintering.

Tubular porous microchannels fabricated by microtemplating:

In Chapters 2 and 3, porous commercial ceramic hollow fibers (from HyFlux CEPAration) were used as starting materials for tubular meso- or microreactors. Extrusion and spinning methods are commonly used for fabrication of porous ceramic and metallic hollow fibers. These methods provide hollow fibers with a well-

defined and smooth interface; however, costly equipment is needed for these types of fabrication.

Within the project, a simple technique was developed for the fabrication of tubular porous ceramic (or metallic) microchannels (hollow fibers). Salamon et al.[1] recently reported a technique, which comprises of microtemplating polymeric hollow fibers to fabricate porous ceramic microchannels (Figure 6.3).

In this method, a polymeric hollow fiber is dip-coated in a suspension consisting of dispersed inorganic particles (ceramic or metallic), a solvent and organic matter (binder, plasticizer, dispersant). Subsequently, the coated hollow fiber is left for drying to remove the solvent. After the drying, the composite material is sintered at a high temperature, so that the initial polymeric hollow fiber template and the organic matter of the suspension are both removed. Finally, a porous tubular microchannel is obtained (Figure 6.4).

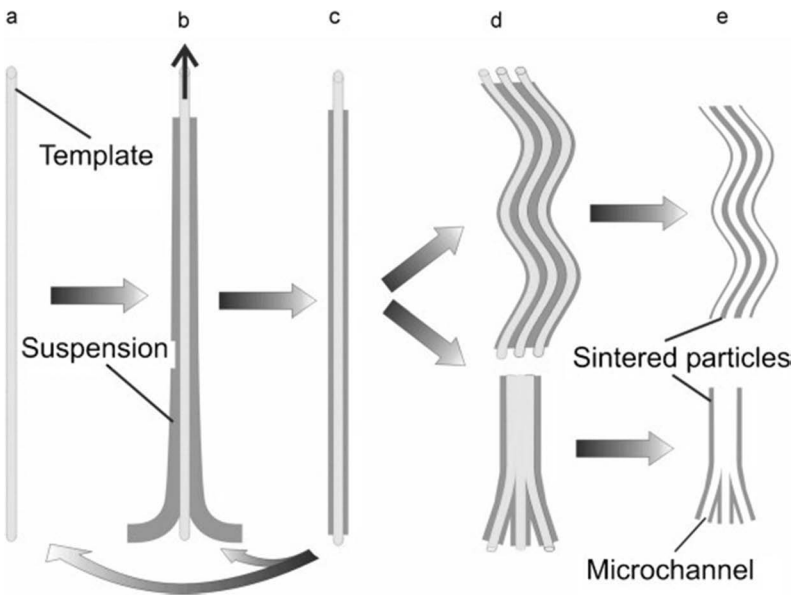

Figure 6.3: Preparation procedure of tubular porous microchannels by microtemplating: *(a)* microtemplate; *(b)* coating of the microtemplate with a suspension with sinterable particles; *(c)* microtemplate with coated layer; *(d)* reshaping and numbering-up and *(e)* sintering (and removal of the microtemplate)[1].

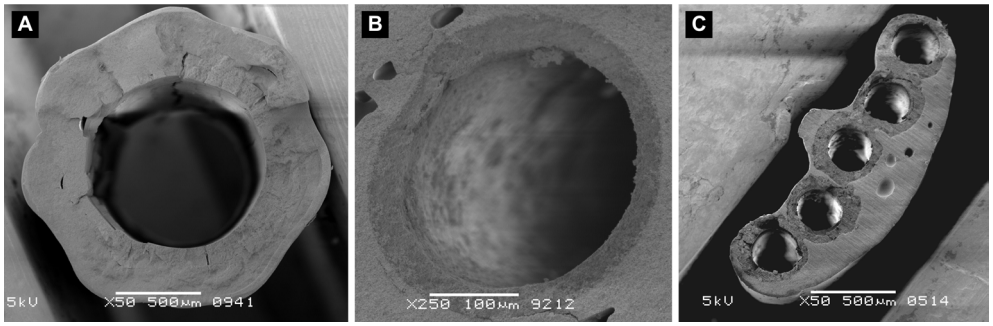

Figure 6.4: Porous ceramic microchannels fabricated by microtemplating: *(a)* single microchannel, *(b)* microchannel with multiple layers, *(c)* multiple microchannels with multiple layers (adapted from [1]).

Fabrication of tubular microchannels via templating has several advantages. With this method, microchannels with small inner diameters can be obtained (Figure 6.4), which are controlled by the outer diameter of the polymeric hollow fiber template. Furthermore, multilayered microchannels can be prepared by simply repeating the coating step with different suspensions (Figure 6.4.b). Multilayered hollow fibers are very relevant for heterogeneously catalyzed reactions, which require high catalytic surface area. In addition, internal numbering up can be easily performed by merging the coated hollow fibers in green state and then sintering them together (Figure 6.4.c). Within the scope of this thesis, we prepared porous ceramic (α-Al_2O_3) hollow fibers and tested them with a few explorative experiments using a model gas-liquid system [9]. The adsorption of CO_2 in water was chosen as a gas-liquid model reaction system. As can be seen in Figure 6.5, the water could be saturated with CO_2 in a very short time, thanks to the high surface to volume ratio of the fabricated tubular porous hollow fiber.

Besides the above-mentioned advantages, we must also remark that surface areas and interfaces of the fabricated hollow fibers are not as well-defined (see Figure 6.4) as hollow fibers fabricated by commercial extrusion or spinning methods. However, we can say that this micro-templating technique is very suitable for small-scale production and explorative research, thanks to its simplicity. This fabrication method

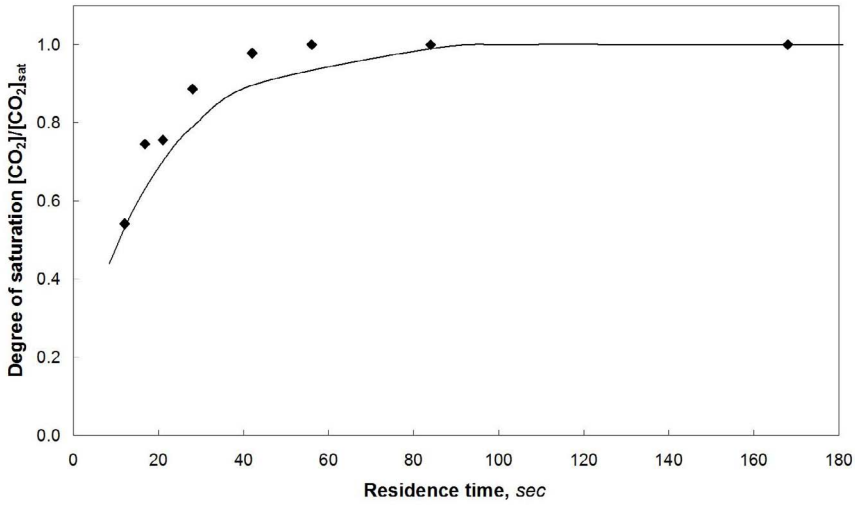

Figure 6.5: Gas-liquid contacting in a tubular porous ceramic microchannels fabricated by microtemplating (internal diameter≈750 μm): CO_2 absorption in water vs. liquid residence time in the porous channel. Solid lines represent results from numerical modeling(adapted from R. Groote[9]).

can be applied for the fabrication of ceramic hollow fibers in locations which do not have the facilities for spinning and extrusion processes.

6.2.2 Helical porous microreactors: Improved mass transfer by secondary flow

Due to the small characteristic length of the microchannels, laminar flow is dominant inside microfluidic devices. Therefore, the radial mass transfer in the liquid phase proceeds via diffusion. Even though this provides more control on the hydrodynamics in the microchannel, it can lead to mass transfer limitations in the case of a wall reaction process (e.g. heterogeneous catalyzed reaction). As an attempt for improving the liquid mass transfer properties (Chapter 3), we integrated biphasic flow (slug flow with inert gas bubbles) and observed significant improvement in catalytic reaction rate. Though it is a simple and efficient alternative, we must also note that in slug flow operation mode the possible coalescence of the phases creates uncertainty about

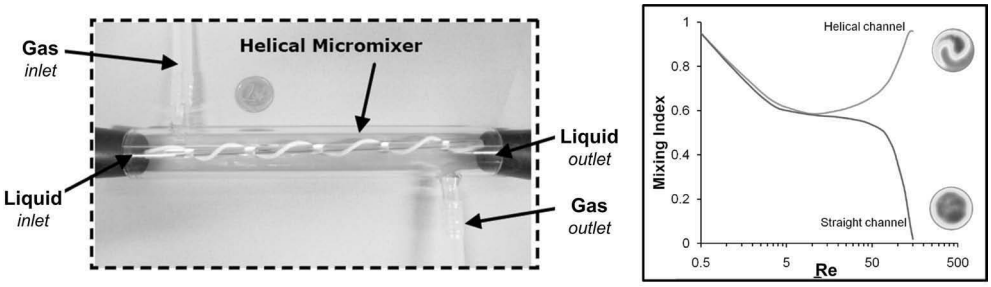

Figure 6.6: *(left)* Experimental setup used for O_2 uptake in water, *(right)* Mixing index vs. Re comparing helical microchannel with equivalent length of straight channel[15].

the actual flow pattern in the reactor channel. Furthermore, the scaling-up for this operation mode is less trivial than for single phase operation.

In literature, many mixing strategies for microreactors were intensively investigated. The micromixers are classified in two main types: active (by external energy input) or passive (by restructuring the flow) micromixers[10]. Besides slug flow[11], common examples for passive micromixers include zig-zag mixers[12], converging-diverging channels[13], hydrodynamic focusing[14] and chaotic advection[12].

Among these, chaotic advection can be created by the use of a helical geometry (inducing Dean vortices), which was already demonstrated for several membrane applications[15]. Within our project, Jani et al.[15] have recently published on a helical membrane microcontactor for the absorption of oxygen in water (gas-liquid model reaction). They reported improved mass transfer properties due to generation of secondary flow, which provides enhanced mixing in the microchannels and higher gas uptake in the liquid phase (Figure 6.6).

The application of this geometry would be of great interest for gas-liquid-solid processes in membrane reactors. As also mentioned in previous sections of this thesis, membrane reactors usually suffer from mass transfer limitations in the liquid phase. The formation of Dean vortices (secondary flows) in the liquid stream would improve the transport of the liquid reactant from the bulk phase to the reactor wall, where the catalyst is located. Moreover, the operation of this type of reactor is relatively

easy; no further precautions have to be taken in addition to a standard membrane reactor operation.

We must also remark that the generation of secondary flows is known to occur at relatively high Reynolds (Re) numbers (typically >50) and to obtain these numbers within microchannels, high liquid velocities are required[15]. Therefore, long reactor channels will be needed in order to obtain sufficient residence time for the liquid reactant. Furthermore, the fabrication of these reactors can be of concern in practice, depending on the chosen reactor material. The preparation for polymeric hollow fibers in helical geometry can be relatively easy thanks to the ductile properties of the material. However, fabrication of porous ceramic or metallic hollow fibers would be more challenging. Structuring of the hollow fiber would be needed already in the green state (before sintering) and precautions need to be taken that the helical structure should sustain during the sintering.

6.2.3 Non-aqueous gas-liquid-solid reactions

As demonstrated in this thesis, the use of porous medium is a promising concept for multiphase reactions in microreactors. Despite of the advantages of the concept, additional precautions need to be taken to prevent wetting of the porous structure by the liquid phase in order to obtain a stable gas-liquid interface. In this thesis, we applied the reactor concept to aqueous processes and in order to avoid wetting, we modified the surface properties of porous ceramic materials selectively (by hydrophobization).

Even though the hydrophobization of the surface is an efficient way for interface stabilization in aqueous systems, for organic solvents with lower surface tension (e.g. ethanol: $23{\cdot}10^{-3}$ N/m) than water ($72{\cdot}10^{-3}$ N/m) wetting of a porous medium cannot be prevented easily. Organic solvents are commonly used in microreactor technology, therefore two potential solutions are addressed, in order to overcome this drawback in our reactor concept.

Firstly, counterbalancing gas pressure (trans-membrane pressure) can be applied to avoid wetting and to position the G-L-S interface. With the excess pressure from

the gaseous side, the liquid can be pushed back to the inner side of the porous medium and the interface can be stabilized. This method is commonly used in conventional membrane reactors. Vospernik et al.[16] and Bercic et al.[17] demonstrated that the interface could accurately be positioned with this method. One drawback of this method is the requirement of additional equipment during the operation for the pressure regulation, which makes them technically demanding. Furthermore, the pressure drop along the channel length may differ for liquid and gas phases, depending on the length, diameter, flow rates and fluid properties. This could cause inaccuracy of the G-L-S interface along the reactor axis.

Secondly, the utilization of gas-permeable selective layers can be considered, as also demonstrated in Chapter 4 (PDMS). The addition of such a selective membrane layer (e.g. PEBAX, PDMS[18]) on the porous support would avoid the intermixing of the gas and liquid phases and stabilize the interface. Even though such membranes can cause additional mass transfer resistance, the coating layers can be made very thin to limit this problem for mass transfer from the gas phase.

6.2.4 Heat transfer in porous microreactors

Thanks to their improved heat and mass transfer characteristics, microreactors are very suitable to explore fast and exothermic reactions. In exothermic G-L and G-L-S reactions, such as hydrogenations and fluorinations, removal of the heat released by the reaction is very crucial. In the scope of this thesis, we mainly focused on the conceptual functionality and mass transfer properties of our microreactors, and did not investigate the heat transfer. We worked with low liquid phase reactant concentrations, in which the heat release with the reaction was not of big concern. Still, for future application of porous microreactors in highly exothermic processes, some recommendations for heat transfer are addressed below.

Heat transfer in porous microreactors is more complex than in conventional dense microreactors. In a dense reactor, heat transfer can simply proceed through the reactor wall. In our porous microreactors the reactor wall is used for the supply of

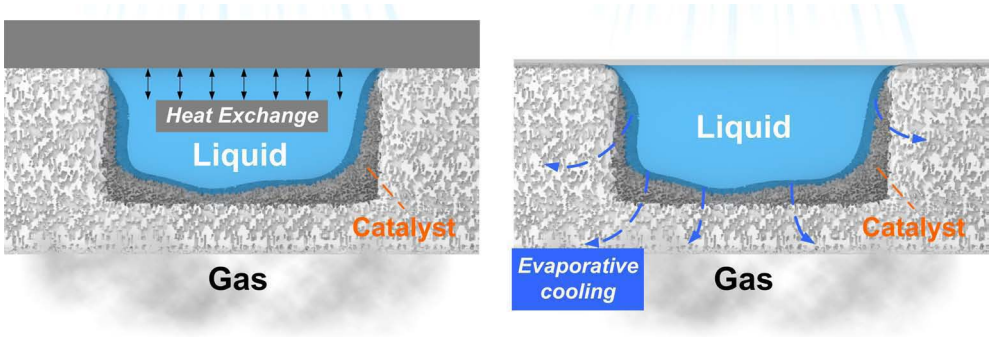

Figure 6.7: Possible ways of heat removal for porous microreactors in exothermic reactions: *(a)* Integration of a heat exchanging plate for planar geometry, *(b)* Evaporative cooling for removal of the generated heat in planar and tubular geometry.

the gaseous reactant. Therefore, other strategies need to be applied for heat removal. The reactor geometry (planar or tubular) is a critical factor in the choice of a strategy. In planar microreactors, a simple approach can be implemented in which the open porous microchannels can be covered with a heat exchanging plate (Figure 6.7.a). In this case, the heat exchange does not directly take place at the reaction interface. However, the small dimensions of the microchannels should make this strategy sufficient for the heat removal.

Evaporative cooling (Figure 6.7.b) is a good alternative for heat removal in exothermic reactions. This method can be applied for both planar and tubular microreactors. It is very suitable, especially in combination with a porous medium. In this method, the evaporation of the liquid solvent creates a cooling effect and this can be used for the removal heat generated with the exothermic reaction. The vapor can be instantly removed through the porous membrane. As an example, the enthalpy of reaction for hydrogenation of nitrite can be estimated as ∼450 kJ/mol (from enthalpies of formation[19]) and the evaporation enthalpy of water is ∼41 kJ/mol. In our study (low concentrations), the maximum reaction rate obtained was $22.7{\cdot}10^{-8}$ mol/min for a flow rate of 0.3 ml/min ($\sim 1.6{\cdot}10^{-2}$ mol/min). This means that with the evaporation of only 0.015% of the liquid stream the heat generated by the reaction can be removed. The advantage of this method is that the cooling takes place directly at the reaction

interface, where the heat is generated. Moreover, controlled amounts of evaporative solvent removal could be of advantage in the case in which the reaction product is located within the liquid phase, by increasing the concentration of the product in the solvent. However, accurate control of the process conditions is required to avoid operational problems for this concept. Excessive evaporation of the liquid solvent can lead to operational instabilities in the liquid phase and additional mass transfer limitations of the gas phase.
Other alternatives for heat removal can be the use of membranes with high thermal conductivities (e.g. palladium membrane [20,21]) or integration of external mass transfer concepts (e.g. loop reactors [22]).

6.3 Epilogue

The utilization of porous media and membrane technology for multiphase (gas-liquid-solid) contacting in microreactors is of great advantage. The gaseous reactant can efficiently be supplied to the reaction zone, gas and liquid phases meet directly at the catalyst surface, and their flow rates can independently be varied during operation. Porous ceramic and metallic microreactors offer stable interface with their simple reactor design.

Bibliography

[1] D. Salamon, Z. Chlup, L. Lefferts, and M. Wessling. Tailoring of free standing microchannels structures via microtemplating. *Materials Research Bulletin*, 46(4):505 – 511, 2011. 114, 117, 118

[2] M. Heule, S. Vuillemin, and L.J. Gauckler. Powder–based ceramic meso– and microscale fabrication processes. *Advanced Materials*, 15(15):1237–1245, 2003. 114

[3] J. de Jong, B. Ankone, R. G. H. Lammertink, and M. Wessling. New replication technique for the fabrication of thin polymeric microfluidic devices with tunable porosity. *Lab on a Chip*, 5:1240–1247, 2005. 114

[4] T. Rosqvist and S. Johansson. Soft micromolding and lamination of piezoceramic thick films. *Sensors and Actuators A: Physical*, 97-98:512 – 519, 2002. 115

[5] M. Bikel. *Fundamental aspects of phase separation microfabrication*. PhD thesis, Enschede, University of Twente, December 2009.

[6] L. Vogelaar, R.G. H. Lammertink, J.N. Barsema, W. Nijdam, L.A. M. Bolhuis-Versteeg, C.J. M. van Rijn, and M. Wessling. Phase separation micromolding: A new generic approach for microstructuring various materials. *Small*, 1(6):645–655, 2005. 114

[7] R.G.H. Lammertink. Porous ceramic and metallic microreactors. *NWO Vidi Grant*, 2006. 114, 115

[8] A. Roosen. Low–temperature/low-pressure lamination of green ceramic tapes. *Advanced Engineering Materials*, 2(6):374–376, 2000. 115

[9] R. Groote. Ceramic micro-membrane reactors for gas/liuid contacting in heterogeneously catalyzed reactions, November 2008. 118, 119

[10] V. Hessel, H. Lowe, and F. Schonfeld. Micromixers–a review on passive and active mixing principles. *Chemical Engineering Science*, 60(8-9):2479 – 2501, 2005. 120

[11] M. T. Kreutzer, F. Kapteijn, J. A. Moulijn, and J. J. Heiszwolf. Multiphase monolith reactors: Chemical reaction engineering of segmented flow in microchannels. *Chemical Engineering Science*, 60(22):5895 – 5916, 2005. 120

[12] S. Hardt, K. Drese, V. Hessel, and F. Schonfeld. Passive micro mixers for applications in the micro reactor and [micro sign]tas field. *ASME Conference Proceedings*, 2004(41642):45–55, 2004. 120

[13] A. M. Guzman and C. H. Amon. Dynamical flow characterization of transitional and chaotic regimes in converging-diverging channels. *Journal of Fluid Mechanics*, 321:25–57, 1996. 120

[14] T.T. Veenstra, T.S.J. Lammerink, M.C. Elwenspoek, and A. Berg van den. Characterization method for a new diffusion mixer applicable in micro flow analysis systems. *Journal of Micromechanics and Microengineering*, 9(2):199–202, 1999. 120

[15] J.M. Jani, M. Wessling, and R.G.H. Lammertink. Geometrical influence on mixing in helical porous membrane microcontactors. *Journal of Membrane Science*, In Press, Corrected Proof:–, 2011. 120, 121

[16] M. Vospernik, A. Pintar, G. Bercic, J. Batista, and J. Levec. Potentials of ceramic membranes as catalytic three-phase reactors. *Chemical Engineering Research and Design*, 82(5):659 – 666, 2004. 122

[17] G. Bercic, A. Pintar, and J. Levec. Positioning of the reaction zone for gas-liquid reactions in catalytic membrane reactor by coupling results of mass transport and chemical reaction study. *Catalysis Today*, 105(3-4):589 – 597, 2005. 122

[18] J. de Jong. *Application of membrane technology in microfluidic devices*. PhD thesis, Enschede, University of Twente, April 2008. 122

[19] D.R. Lide and W.M. Haynes (Eds.). *CRC Handbook of Chemistry and Physics, 90th ed.* CRC Press/ Taylor and Francis, 2010. 123

[20] V. M. Gryaznov, M. M. Ermilova, and N. V. Orekhova. Membrane–catalyst systems for selectivity improvement in dehydrogenation and hydrogenation reactions. *Catalysis Today*, 67(1-3):185 – 188, 2001. 124

[21] R. Dittmeyer, K. Svajda, and M. Reif. A review of catalytic membrane layers for gas/liquid reactions. *Topics in Catalysis*, 29:3–27, 2004. 124

[22] J.C. Middleton and K.J. Carpenter. *Loop Reactors*. Wiley–VCH Verlag GmbH & Co. KGaA, 2000. 124

Samenvatting

Het doel van het onderzoek in dit proefschrift is om nieuwe concepten te onderzoeken voor meerfase-microreactoren (gas-vloeistof-vast; afgekort als G-L-S) waarbij gebruik wordt gemaakt van membraantechnologie voor het met elkaar in contact brengen van deze fasen. Poreuze micro- en mesoreactoren, zijn ontwikkeld door middel van verschillende bereidingsstappen en getest voor G-L-S modelreacties. Hiertoe hebben we keramische (alumina, Al_2O_3) en metalen (roestvrij stalen) reactoren met vlakke of cilindrische geometrie ontwikkeld en gekarakteriseerd. Deze reactoren zijn gebruikt voor katalytische hydrogenering en fotokatalytische degradatie reacties in water. Uit de resultaten blijkt dat deze reactoren veelbelovend zijn voor toekomstige toepassingen in microreactortechnologie.

Hoofdstuk 1 geeft aan algemeen overzicht van microreactoren en reeds bestaande concepten voor het uitvoeren van meerfasereacties in deze reactoren. Daarnaast wordt een overzicht gepresenteerd van conventionele membraanreactoren, gevolgd door achtergrondinformatie over de modelreacties die in dit onderzoek zijn gebruikt. Tot slot worden het doel en de opzet van dit proefschrift gegeven worden.

Hoofdstuk 2 beschrijft de bereiding van poreuze keramische mesoreactoren en hun toepassing voor de katalytische hydrogenering van nitriet in water. Hiertoe zijn cilindrische reactoren gemaakt met verschillende fabricatietechnieken, oppervlaktemodificatie (om het oppervlak hydrofoob te maken) en methoden voor immobilisatie van katalysatoren. De zo verkregen reactoren hebben gecontroleerde eigenschappen met betrekking tot bevochtiging en katalytische activiteit. Het bevochtigingsgedrag van de waterige oplossing aan het katalysatoroppervlak en de positie van het gas-vloeistof (G-L) grensvlak konden worden beinvloed met behulp van oppervlaktemodificatie. Op deze manier werd een stabiel G-L-S-grensvlak verkregen voor het uitvoeren van heterogeen gekatalyseerde reacties. Reactoren

met gecontroleerde bevochtigingseigenschappen werden bereid waarbij het membraan hydrofoob werd gemaakt terwijl het dragermateriaal van de katalysator hydrofiel bleef. De reactoren die op deze manier verkregen werden, hadden een hoge katalytische activiteit voor de modelreactie, met nitrietconversies tot wel 80%. Bovendien bleven de prestaties van de reactoren constant, zelfs bij lage concentraties van de gasvormige reactant (H_2). Dit bewijst dat er een dusdanige goede aanvoer van H_2 is door het membraan dat de stofoverdracht ervan geen beperkende factor wordt.

In **hoofdstuk 3** hebben we de invloed van de geometrie en operationele parameters op de prestaties van de keramische (Al_2O_3) micro- en mesoreactoren bestudeerd. Hiertoe hebben we reactoren gemaakt met verschillende interne diameters, een gecontroleerde laagdikte van het dragermateriaal voor de katalysator (γ-Al_2O_3) en een actief oppervlak van Pd met vereiste bevochtigingseigenschappen. Daarnaast hebben we een inerte *slug flow* geintegreerd in deze poreuze membraanreactor. Hiermee konden we de voordelen van het gebruik van een gedispergeerde fase combineren met die van een continue fase. De zo verkregen reactoren werden getest voor de katalytische hydrogenering van nitriet onder verschillende operationele parameters. De resultaten toonden aan dat de prestatie van de reactor verbetert met toenemende laagdikte van het dragermateriaal voor de katalysator. Dit komt door een toenemende hoeveelheid Pd-katalysator aan het grensvlak waar de reactie plaatsvindt. Echter, de prestatie neemt niet evenredig toe met de toename van de hoeveelheid Pd aan het grensvlak. Dit wijst er op dat bij een toenemende laagdikte van het γ-Al_2O_3 de stofoverdracht een beperkende factor kan worden. Verder hebben reactoren met een kleinere interne diameter een betere prestatie vergeleken met reactoren met een grotere interne diameter. Dit bevestigt dat de prestaties van deze reactoren verbeteren als gevolg van de verbeterde stofoverdrachtseigenschappen bij miniaturisatie van de karakteristieke lengteschalen. Bovendien hebben we aangetoond dat de externe stofoverdracht verder verbeterd kan worden door de integratie van (inerte) *slug flow*.

Hoofdstuk 4 beschrijft het gebruik van poreuze roestvrij stalen holle vezels met koolstof nanovezels (*carbon nanofibers*, CNFs). Sterke en hoog poreuze roestvrij stalen holle vezels werden verkregen waarbij het mogelijk was om CNFs met een

hoog specifiek oppervlak te laten groeien aan het poreuze roestvrij stalen oppervlak. Deze microreactoren hadden een hoog specifiek oppervlak, goede mechanische eigenschappen en lieten een veelbelovende activiteit zien in de reductie van nitriet. De resultaten toonden aan dat de aanwezigheid van CNFs op het roestvrij stalen oppervlak de prestaties van de reactor aanzienlijk benvloedden. In reactoren waarop CNFs waren gegroeid, kon nitriet zelfs worden gereduceerd wanneer er geen H_2 en Pd aanwezig waren. Deze resultaten tonen aan dat het ontwikkelde reactormateriaal intrinsieke reducerende eigenschappen bezit.

Hoofdstuk 5 beschrijft het gebruik van poreuze microreactoren in fotokatalytische G-L-S systemen. Vlakke fotokatalytische membraanmicroreactoren met gecontroleerde oppervlakte-eigenschappen en fotokatalytische activiteit werden succesvol verkregen met behulp van microfabricagetechnieken (op poreus Al_2O_3), gevolgd door immobilisatie van de TiO_2 fotokatalysator en selectieve oppervlaktemodificatiestappen. Deze reactoren werden getest voor de (UV-geinduceerde) fotokatalytische degradatie van methyleenblauw en fenol in water, waarbij extra O_2 werd toegediend in de reactiezone. De reactor had een hoge fotokatalytische activiteit met tot wel 90% degradatie. Bovendien toonden deze resultaten aan dat de degradatiesnelheid in de reactor aanzienlijk hoger werd door membraangeassisteerde toevoer van O_2 gedurende het fotokatalytische proces. Deze laatste bevinding laat duidelijk de voordelen van het ontwikkelde concept zien.

Hoofdstuk 6 vat de resultaten samen die behaald zijn binnen het kader van dit onderzoek. Verder worden er aanbevelingen voor toekomstig onderzoek gegeven alsmede enkele afsluitende opmerkingen.

Het gebruik van poreuze media en membraantechnologie voor het in contact brengen van meerfasesystemen (gas-vloeistof-vast) in microreactoren biedt grote voordelen. In deze reactoren kan de gasvormige reactant efficient worden toegevoegd aan de reactiezone; de gas- en vloeistoffase ontmoeten elkaar direct aan het katalysatoroppervlak en gedurende het proces kunnen de verschillende stroomsnelheden onafhankelijk van elkaar worden gevarieerd. Poreuze keramische en metalen microreactoren combineren

stabiele grensvlakken met een simpel reactorontwerp.

Acknowledgements

It has been a bit more than 4 years and my PhD journey is almost over. This journey made me grow scientifically, learn many things and hopefully get a Dr. title. However, the thing that I most cared about it was that I met many people, made a lot of friends for life and had a lot of fun. With this section, I would like to thank you all for making my stay here so special. I am aware that this is the most popular section of my thesis, therefore I tried to write very careful and I hope I did not forget anyone. For those, whom I forgot, please let me know, I owe you a drink.

First, I would like to start with my promotor and supervisor (more a like a superdude) Prof. Dr. **Rob** Lammertink. Rob, as we first met 4.5 years ago for the job interview, you gave me very nice amazing first impression and after all these years, I can honestly say, I am very happy to have made the right choice and decided to do a PhD with you. You shared my enthusiasm when I could get good results. You cheered me up when I was down; you put me back on my feet when I was too much up. You helped, advised and improved me on scientific and personal level. You showed to me and everybody around you that hierarchy is unnecessary, as long as you know how to communicate. Of course, I cannot forget the fun factor, our trips to Japan, USA, parties that we had together, group events, beer motivation that we had, and many other things. I really appreciate it all; I am very proud and happy to have a supervisor, promoter and most importantly a friend like you. Thank you for everything. I wish you, **Cindy** and your children all the best in the future.

I would like to thank my co-promotor Prof Dr.-Ing. **Matthias** Wessling for his help and guidance in this project. Matthias, even though you could not be intensively involved in my project at the final part (due to your departure), you have been an inspiring person to me and most of the people in our group(s). You ideas, tips and tricks in our meetings were of great value and made me grow personally and scientifically. Thanks for all and I wish you great success in Aachen.

Another person that I would like to thank is Prof. Dr. Ir. **Leon** Lefferts. I really appreciated your contribution to this work. You and the entire CPM group were always open to collaborate, and at the end, I think we all benefited from that. In addition, your experience in catalysis and your critical view on the results was of great help. It was a great pleasure to work with you. I also would like to thank Prof. Dr. **Guido** Mul, for our great collaboration on photocatalysis (Chapter 5). It was a nice coincidence that at the time we decided to work on photocatalysis, you moved to Twente. Your input to the project was of great importance, which lead us to a nice piece of work. Thanks for all the valuable discussions and our nice chats on the corridor.

Furthermore, I would like to thank my other **committee members**, for taking part in the committee and Prof Dr. Han Gardeniers, for your feedbacks in the MCS-SFI seminars, Prof. Dr. Volker Hessel for the excellent reviews and books on every field of microreactors that made my adaptation to the microreactor world really fast, Prof. Dr. ir. Michiel Kreutzer for the inspiring lectures on national conferences, which lead to the work presented in the second part of Chapter 3. Also thanks to my **STW users committee members** R. Reintjens, M. Roelands, P.W. Hilberink, R.A. Terpstra, M. Wiegel, M. Blom, H. Leeuwis, for their positive and also critical feedback to the project.

Greet, our official and unofficial secretary, you are an amazing person and one of the people that I always envy. Even at your busiest times, you always have a smile on your face, ready to help, coming up with solutions to everyone on every possible aspect in a very fast way. Your enormous amount of help during this period is highly appreciated from all of us. Thank you very much!

Next, I would like to thank to my project partners (also co-authors). Every piece of work presented in this thesis was a result of intensive collaborations with you. **Jigar**, dear project and destiny partner, Mr. Euromembrane. As I told you many times, I am very happy to have shared this project with you. You are a real good friend, a great officemate, we supported each other always in the most stressful periods of our lives, and we had a lot of fun together, many parties (even in Japan), we will keep on doing that. I wish you, **Falguni** and your third almost-member of your family all the best. **David**, my half-time project partner, full-time friend. As we met, I was the optimistic and you were the pessimistic one. With time, we adapted to each other, we even changed roles in between. At the end, we even managed to get one paper out. Most importantly, I gained very good friend, standing behind me in the most stressful times of my PhD and also when my car did not start. Best luck to you with Yujie in Czech. **Joost vB**, thanks for helping me out, especially at the beginning of the project, when I had no idea what to do. I really appreciated your help and your company. Good luck with the final stage of your PhD. My friend **Kumar**, me meeting you was one the best things that happened to my project. Thanks to your helpful personality and hairy foams, I jumped in the catalysis world, which led to three chapters of this thesis. This collaboration made us develop a very cool friendship for good and bad days. Thanks a lot! **Sergio**, the Basque carbon nanofiber grower, after knowing you for 4 years, at the final stage of our PhDs, we realized that we could do something together and finally we could publish a paper together within couple of months. And we had a lot of fun, long discussions, exchanging weird e-mails with a humor that nobody else would understand. Take good care of yourself Basco de Gama. **Mieke** and **Nieck**, you guys were helping me out many times already, even though you had no direct connection to my project. Owing to your ability to fabricate those hollow fibers, a giant collaboration of 5 different research groups started and we have a very nice paper. Thanks for all the help! **Suleyman**, my last minute co-author, thanks for all the input in to our work to figure out a lot of mysteries in iron. Also, for the nice company, I wish a lot of luck in USA and also with Besiktas.

I wouldn't be able to finish my PhD without the technical support of the following people. I wanna thank **Bert**, for his helpful personality, designing the holder for my reactor, which worked enough to have 3 chapters written and his help with IC, **Karin**, for letting me freely work in the CPM labs and supporting me when I needed, **Louise** for all possible analysis techniques, and of course **John Heeks**, the rising star, most popular person of our group, for your patience, helpful attitude, for answering all our questions and being able to build everything. Thanks to you all!

Besides my project partners and technical support, I was also blessed with 4 young victims (my students) during my PhD. **Ramon**, for helping me out at the beginning of my PhD, finding out what cannot work :), writing the Dutch summary of this thesis and being a good friend of mine, **Tobias**, the surface modifier, for your great idea on selective hydrophobization, **Timon**, for awesomely photocatalyzing with P2M2, **Henk** for the flowing sluggy and creating the second part of Chapter 3. Guys, you all significantly contributed to this work, I am very happy to have met all of you, we are still in contact, let's keep it that way! Thanks!

Now it is time for my paranymphs: **Matias**, my half-Turkish, half-Argentinian brother, my first housemate, boob-de-boules rival, I am very grateful to you, I am very happy that I met you, (in your words) you formed my home away from being home. You are the person that I like to share my things with, such as waking you up in the middle of the night telling you that I met the women of my life. I had happy and sad moments during my stay in Holland, all these years, regarding work, personal life; you were always there for me standing by my side. I am very happy that you met a great person like **Gert** and I wish you both a bright future.

Here comes the other paranymph, my fully Turkish (actually Armenian) brother **Erman**. A person, that I met in the first days of university about 11 years ago, in physics class (which later I failed),

a person that taught me math, a very enthusiastic person like myself, a person that is always supporting me in complicated times, even when he is high (remember Amsterdam), a party dude, who falls asleep in the parties at 12 pm, but later wakes up and dances, a very important person to me. 10 numara adamsin kardesim.
Two other special people to me, who are of great meaning to me. **Kadir**, my brother, who left home with me 7 years ago to study Aachen in the same airplane, sleeping on the same air mattress (without air) with me on my first night at Cagri's house (bele iyi geliyo abi direk yerde yatmak), eating together uncooked bread from the supermarket, lunches and dinners at Chicken pont, visiting me 23 times in Netherlands, even though I never visited you in Stuttgart. I am very happy to have a friend like you! **Hakan**; you and **Tugba**'s support from the time I saw you was incredible to me, taking me to your house like your younger brother, feeding me, giving me money when I needed, giving advices to me at bad times, finishing those 2 bottles of Raki together. Your departure from the group and Enschede was and is still heavy to me. Thanks for everything, we still have great times to come, I wish you both and your new family member a great time.
Further, I would like to thank all the members of our new "Super Freaking Intelligent" SFI group, for the great times, that we had. **Zeynep** and **Aytac**, for being there for me from the first moment that I arrived to Enschede and for all the Raki that we drank with long conversations. **Elif**, being most original (or crazy) officemate that I ever had, not attacking me even though I tease you a lot, for our breaks and cooking kofte for my birthday, **Ineke**, for being my desk neighbor, your relaxing personality, for your great laughs that we have in the office, **Jigar**, you already were acknowledged don't ask for more, **Gor**, my goring Armenian friend, for being my first housemate (379), for your friendship during the most stressful periods of PhD, great dinners in your house and goring to breaks with me, **Sreenath**, for your awesome dances in the parties and our jokes on equipment finances (you still owe me a lot of money for all the borrowed equipment, I hope you will pay them back soon), **Damon** for your amazingly thick and dense chest hair, **Yali**, for joining our group and especially my new project (we are gonna rock), **Martin E.** for being a hot! embosser (do not press too much:)), **Lidy** and **Nienke**, for all the support and all the paper work you have done for us. I would like to thank also my old officemates from ME314 (which now is occupied by Rob forces), **Alisia**, **Srivatsa** and **Kishore**, for the nice ambiance and friendly talks.
I would like to thank some people, from good old times of MTG. **Katja**, for being such a caring friend at good and bad times, **Christoph**, for being forever 5 and keeping the childhood spirit together with me, **Maik**, for maiking it everytime and having an idea on every field of science, **Jens**, for introducing to me the red Schnaps and being the funniest Spalter, **Ikenna** for your weird humor and calling me Jun (Pshht!), **Joao** for being the talkative Portuguese b.st.rd, **Karina** (Ms. Euromembrane) for being strong in the tough times and staying 18 for many years, **Joerg** for lending me you tie, when I most needed it. You guys welcomed me to your group with very warmly and it made my adaptation very easy.
Current members of MTG, I had enormous fun inside and outside of the office, being for 3 years your official and 1.5 years unofficial colleague. Thanks for your all the good times. I wanna thank **Antoine** for being the best party dude ever, for all your crazy dances, the things that happen to you on your way back home after a Jagermeister session, **Olga** for accepting to take me if I am one day over 150 kg, for sharing HiCOM and ByeCOM enthusiasm with me, **Harro** for talking a lot and a lot, for your clean heart, keeping my secrets:), offering always your help, **Imre** for your help and great arrangement for the one of the most special days of my life, **Didi** for all the advises you gave me during the final part of my PhD and taking over the "Jun!" responsibility after Ikenna, **Enver** for the inappropriate conversations that we have in Turkish on the corridors, for having things to do every evening and feeding me every lunch time, **Nicolas** for your super fun, sportive and enthusiastic

character and that night in Amsterdam, **Mayur** sharing the PhD destiny with me, being 24/7 in the lab, listening to and solving my problems and our great night life start in Enschede, **Harmen**, for your relaxing personality and getting super drunk from the orange juice at our place, **Marlon**, for sharing the same musical taste with me (yes, Dio rules!), **Jeroen P.** for the 'box'es on the corridors, **Joris** for the 'box'-'kick' double combos, **Zandrie** for funny, but uncomfortable remarks combined with your laughter, **Wojciech** for being my table chief, but also my lab slave, **Jumeng** my Chinese buddy with a big laughter and great humor, **Szymon** for his politeness, the 24/7 smile on his face and for Bata and OSPT partnerships, **Anne Corine**, for going through hard-times, still being strong, fighting, for all the happy and sad times we shared, **Nieck**, for all the fun on the corridors and parties and our new project on interfacial ballimerization, **Marcel**(lo) for all the IT support and being a Catalan lover like myself, **John** for the funny (or crazy) sounds and remarks on the corridor, **Ana** Banana, for the many parties (ending up in me eating flowers) and talking incredibly a lot, **Gerard** (Halil Celal Cadafalch Gazquez) for talking even more than Ana and entering my office 45 times per day (on average), **Frank** for the intensive high and side 5s. I also would like to thank my other colleagues for all the fun inside and outside of the labs, **Jorrit**, **Sander**, **Bernke**, **Geraldine**, **Erik** (E.R=ik), **Erik vdV**, **Herman**, **Kitty**, **Wika**, **Emiel**, **Michiel**, **Marcel**, **Louis**, **Weihua**, **Martin W.**, **Giri** and all others.

Special words of thanks goes to all the members of the Think Tank: **Jordi** (I love you, too), **Joan** (life coaching: more than 3 times means girlfriend, bringing girlfriend to your mothers village means marriage), **Roma** (Catalan casanova, my temporary housemate and moving company), **Jeroen Nsync** (yo gangster yo, Ajax, yo yo yo). You people have ruled one period of my PhD, we had incredible amount of fun and we will have a lot more in the future. Our picture is still hanging on the wall of the student office. (As promised) I would also like to thank to **Dio**, **Lady Gaga** and **Katy Perry** for the inspiring songs, which made us bond together so strongly.

With this paragraph, I would like thank all the group members of CPM, for all their help during my PhD period. With their welcoming behavior, I felt like in my own group, could get a lot of work done. I would like to thank **Digvijay** for his support and tips for the thesis and the funny conversations that we had, **Chris** (the dawg) for his smart ideas, his mediocre reactor and acknowledging the awesomity of my microreactors, **Bert**, **Karin**, **Louise**, **Kumar**, **Sergio**, **Ruben**, **Berta**, **Arie**, **Marijana**, **Trionfetti**, **Davide**, **Cassia**, **Rao**, **Arturo** for all the help, fun conversations on the corridors, in the lab and also outside of the university. I also like to thank all the members of the PCS, inviting me for their borrels, dinners and other activities, especially, **Chieh-Chao** for their cheerful and helpful personality, **Engin** (Hoca!) for being the engine of his group, his incredibly high amount of scientific ideas and for all the fun in the breaks.

Within these 4 years, besides these groups I also met a lot of other cool people inside and outside of the university. I also wanna thank them: **Anil**, don't forget, we are gonna still gonna shake the scientific world with our superduper plasma membrane microreactor, **Janet**, a lot of parties, dancing and a lot of food, you were really missed here after your departure, **Denis**, you are a director (Janet's stukje) with great talent and humor, I think your value will be understood in 50 years from now, **Can**, for being the other Can, making people ask me if it is a common name, for being very close friend from the first time that we met in the sport center, for the long long breaks and Raki nights, **Burak**, cakma fizikci, you were my favorite proposal plans ruiner and military service postponing company, **Jose**, best "la bomba" performer, I ever knew, I expect some performance in my defense party, **Ferran**, the geek, but a very useful one, a good friend, thanks for making us keep the catalan traditions all these years, **Michael**, Mojito fetishist, New Zealander Gordon Ramsay, **Pavlina**, thank for your enthusiasm on drinking the sniper, b52, being the first blonde greek girl I ever met, introducing the sirtaki to every party and all the nice dinners and BBQs that we had together,

Dimitris, thanks for all your honesty, telling me about my surprise birthday party, introducing me the Kasteel Rouge, killer jokes (e.g. Sniper=Chinese rapist), **Guus** (eeeee), el inventor de Women Correction Device, muchos thankos for being like mios in manios aspectos, eating muchos meatios, drinking muchios, doing partios, when you are singulos, **RBK**, thanks for teaching Laura the art of doñaism:) **Greg**(ory), you were my best last year friend, a lot of dinners, movie nights, biggest "Naked Gun" fan after me, we were trying hard to get rid of PhD depression, **Daphne**, you are a background hero of this thesis, you gave me a lot support, and all your tips made me successfully go through this period, thanks a lot!

Also I cannot forget the fun that I had with a lot friends from Turkey, my land buddies, special thanks to **Erhan**, **Arzu**, **Cem**, **Berker**, **Esen**, **Feridun**, **Bilge**, **Hasan**, **Sertan**, **Ozlem**, **Fehmi** (oryantal), **Oya** and **Emre**.

Of course I cannot, forget my teammates from my volleyball team Harambee, that I was fighting together with on the volleyball field. **Dimitris**, my greek brother. I think I am the only one you did not threaten with "I'll kick your ass!", we should still play a game to decide who Cyprus belongs to, **Leon**, my dear friend who was always there for me for every problem I have, even eating a plastic flowers with me in parties if needed, **Jona**, tingler of my research images, exchanging shoes in the H1-van after parties, starting relationship at the same day as me, **Wim**, my robot friend (hot action!), you were my company at the day when I first met Laura in Lunatic, sharing a sleeping bag with me in Deldenhorst, **Jesper**, my setter competition and finally my co-coach, **Sander**, my Casanova friend with big heart, **Tjeerd**, knee wining person, competition for number 10, and also (according to the positions) **Wilco**, **Schoemmie**, **Tijmen**, **Tank**, **van Maanen**, **Jordi**, **Alink**, **Tjibbe**, **Brul**, **Bert**, **Aart**, **Hans**, **Bassie**, **Luuk**, **Demmer**, **Thor**, **Reinder**, **Jasper**, **Matthijs**, **Julian**, **Maxim**, **Lin**, **Rob** and **Sjaak**. We had a lot of wins, a lot of defeats, promotions, relegations, but also incredible parties. You people, were a very important part of my Enschede life. Also, my physios, trying to fix my old and injured body, **Rene**, **Johan** and **Nikki**.

I also want to thank **Werner** und **Sigi** (my German parents), for making my adaptation to Aachen and Germany very smooth, letting me be the only male student accommodating in your house, taking very good care of me at my first times living abroad, for the bike tours that we had, amazing food that Sigi cooks, for all the advices that you gave me during and after my stay in Germany.

Tambien me gustaria darle gracias a toda la familia **Garcia Alba**, en especial a **Angel**, **Dulce** y **Xavi**, por darme la bienvenida a su familia con los brazos abiertos. Estoy muy feliz de tener una segunda familia como vosotros, gracias por abrirme las puertas de vuestra casa, por tratarme como a un hijo, cuidando de mi, dandome de comer increibles cantidades de comida, por vuestro apoyo en el dia que le pedi a Laura en matrimonio, por todas las horchata, cenas de Navidad, chorizos, jamon y longanizas, por hacerme un fan del FC Barcelona y del Nastic! Gracias por todo!

I would like to give special thanks to my family for being there and supporting me all these years. All my uncles and aunts, my grandparents **Halil**, **Naci**, **Edibe** (I know you are all watching me) and **Nahide** and all cousins, for all the support. Special thanks to my uncle **Taner** for offering me his beautiful photograph for the cover of my thesis and my cousin **Cenk** for the cover design. I would also like to thank my sister **Elif** and her husband **Bugra**, my niece **Lale**, for being here with me in Netherlands, for the family support away from home and all the happy days we had together. Especially, I would like to thank to my parents **Ahmet** and **Necla** Aran. This thesis is dedicated to you because of all the support, inspiration and encouragement you have given me from the elementary school until the end of my PhD, but mentally and scientifically. You are the best parents one can ever have, sacrificing from yourself to make me feel happier, taking an airplane the same night, when you hear that I need help. You are the biggest part of who I am today, I am very proud to be your son. I hope that one day I can pay you back.

Last but by far not the least, comes the women of my life, my future-wife, Ms. Tarragona, a.k.a. Kleo(patra), the best thing that ever happened to me, **Laura** Garcia Alba. There are no words enough to describe my love to you, how much I need your presence, how much fun I have with you and how safe I feel when I wake up next to you. I love you, for loving me the way I am, for sharing my happiness, being there for me in my deepest moments when I fall weak, agreeing with the 15 kg of Bonus Can that I gained after meeting you, for your absolute honesty, sharing with me the head of your prawns, for forcing me to learn Spanish and not learning 10 words of Turkish, for the way that you love and take care of your family and my family, for the way you say "que asco", for making me dance salsa, for not letting me grow a moustache and threatening me to grow a moustache for yourself, for be being a feminist, for sharing over 100 songs together, and ∼2302 other things. Thank you, for being in Lunatic on that night, for deciding to go upstairs with me in my house, making me run after you for a month and finally, after 3.5 years agreeing to walk with me to the Mediterranean balcony and saying YES to me, when I asked you to. After almost 4 years of being you, still when I am driving alone in the car and listening to music, I am day-dreaming about all the great days we are gonna have in the future. Thanks for making me feel that way. ∞ x ∞ x ∞ x ∞ x ∞, no es sufficient com per descriure el meu amor per tu.

Can

The Author

Halil Can Aran was born in Istanbul (Turkey) on the 21st of February 1982. He graduated from *St. George's Austrian High School* in 2000. Afterwards, he started his bachelor study in Chemical Engineering at *Istanbul Technical University* and received his B.Sc. degree in 2004. He continued with a master study at *Rheinwestfaelische Technische Hochschule (RWTH) Aachen* in Germany. During his studies he worked on projects in close collaboration with industry: "Optimization of the cooling line of CONTIROD -Continuous casting and rolling plant for copper wire rod- of SMS Meer" (Mini-Thesis) supervised by Prof.Dr.-Ing. Thomas Melin and "Conceptual Process Design for Sustainable Raw Materials in corporation with Degussa AG" (Master-Thesis) supervised by Prof.Dr.-Ing Andreas Pfennig. He graduated in 2007 and started his PhD in the Membrane Technology Group at *University of Twente*. In 2010, he moved to the Soft matter, Fluidics and Interfaces group within the same university. During his PhD research, he worked on "Porous Ceramic and Metallic Microreactors", under supervision of Prof.Dr.ir. Rob Lammertink and Prof.Dr.-Ing. Matthias Wessling, as described in this thesis.